

MECHANISMS GOVERNING SPECIFICATION
OF PHOTORECEPTORS IN THE
MAMMALIAN RETINA

by
Kiara C. Eldred

A dissertation submitted to Johns Hopkins University in conformity with the requirements for
the degree of Doctor of Philosophy

Baltimore, Maryland
January 2020

©2020 Kiara C. Eldred
All rights reserved

Abstract

Human vision begins with detection of light by photoreceptors (PRs) in the retina, a thin layer of cells at the back of the eye. Cones are the primary daytime and color-detecting PRs that distinguish red, green, or blue light. These cells differentiate into three subtypes through a poorly understood two-step process: first, naïve PRs decide between blue and red/green fates, then between red and green fates. Despite decades of study, we know very little about the molecular mechanisms that generate cones in the human eye.

This thesis describes the findings that retinal organoids recapitulate human cone specification in developmental timing, gene expression, and morphology. A temporal switch in PR development was observed where blue cones are specified first, followed by red/green cones. Moreover, this regulation is controlled by thyroid hormone (TH) signaling, which is necessary and sufficient to control cone subtype fates through the nuclear hormone receptor thyroid hormone receptor β (Thr β). Expression of TH-regulating genes suggests that retina-intrinsic temporal control of TH levels and activity governs cone subtype specification. Interestingly, dysregulation of TH in premature infants is associated with color-vision defects, consistent with these findings. This work establishes human retinal organoids as a model system to study mechanisms of cell fate specification in developing human tissue (**Eldred** et al., *Science*, 2018).

Despite years of study, the mosaic of cone cell arrangement within the entire human

retina has not yet been characterized. To develop the tools necessary to image and analyze this large tissue, in this thesis we quantitatively characterized the distribution of PRs in the mouse retina. We then modeled their generation based on interactions between Thrb and TH gradients (**Eldred** et al., under review PLOS Computational Biology). These studies provide a detailed map of cone subtype patterning in the mouse retina, and suggest mechanisms for its development and maintenance. These software and analysis tools will be applied to the human retina to provide the first map of human cones.

Primary Reader and Advisor: Robert Johnston

Secondary Reader: Haiqing Zhao

Acknowledgments

I would like to start by thanking my family for always believing in me, and supporting me to pursue my dreams. I have always asked many questions, and I am so grateful to my parents and grandparents for putting up with all of them, and being honest when they did not know the answer. I specifically want to thank my Grandfather Duane for encouraging me to start pursuing my career interests at an early age. He pushed me to not only want to be a researcher, but to *do* research, and helped me establish the connections to do so during high school at ZymoGenetics. There I was mentored by Pallavur Sivakumar, who encouraged me and gave me the confidence in myself that I could continue in science, which is very important for a young female in science.

Next I would like to thank Richard Palmiter for inviting me to work in his lab during my undergraduate studies at the University of Washington. I would like to thank Richard specifically for pushing me to attend Johns Hopkins University. I told him I didn't know if I should go to JHU or to the University of Michigan. He said "Ok, let's flip a coin.... Looks like your going to Michigan!". In that moment I realized I was hoping for it to flip to Hopkins, and that meant that was the school I needed to go to.

I cannot thank my mentor, Robert Johnston, enough for taking a big risk with accepting me as a student and having the faith in me to pursue a crazy new project in his lab. Throughout the process of learning a new system, bringing it to his lab, and pushing forward with the project, he never wavered in his support and faith in me. There were many times when I thought this system was impossible and that I would not be able to get anything to work again, but Bob always told me it would all work out. He has taught me to dream big, and not to be afraid of trying crazy experiments.

I am eternally grateful to Donald Zack for inviting me to work in his lab and learn how to grow retinas. His generosity is truly amazing, and I aspire to keep the same open collegiality that he has shown me as I progress in science. In the same vein I am enormously grateful to Karl Whalin, Don's former post-doc, for teaching me how to grow retinas. He took many hours out of his day to teach me the intricacies of stem cell maintenance and retinal organoid development.

I would also like to thank all the members of the Johnston lab. Specifically Caity Anderson and Kayla Viets, for being amazing friends and colleagues, I am so grateful for their support. I am also very grateful to the ladies of the human side of the lab, Sarah Hadyniak, and Katarzyna Hussey. These two have spent many hours feeding my retinas and caring for my cells so that I can visit my family, go to conferences, and take much needed mental breaks out of the city. I would also like to thank all the other past and present lab members who have made my every day fun and full of laughter, including Lukas Voortman, Liz Urban, ANF, Akin Sogunro, Heather Johnson, India Reiss, Cyrus Zhou, Sang Tran, Mini Yuan, Jenny Yan, and Chaim Chernoff.

I would like to thank my roommate Kevin DeLong, for being an amazing support throughout my graduate school career. He has been an incredible friend, and has helped

immensely with my R coding problems. I also want to thank Ashley Beitel for being an amazing friend and support for me during this process.

Finally I want to thank Matthew Wooten for being the best person in the world. Has been a wonderful support to me throughout graduate school, from taking care of Stella to helping me get through rough days, he always makes me laugh when I need it the most. Also thanks to Stella the trash puppy for her snuggles and smelly tongue.

Table of Contents

Abstract	ii
Acknowledgments	v
List of Tables	ix
List of Figures	x
Chapter I: Introduction	1
Mechanisms of Photoreceptor Patterning in Vertebrates and Invertebrates..	2
Figures	21
Summary of Thesis	34
Chapter II: Thyroid hormone signaling specifies cone subtypes in human retinal organoids	36
Abstract	37
Introduction	37
Results	38
Discussion	44
Figures	46
Materials and Methods	53
Supplemental Figures	62
Chapter III: Modeling binary and graded cone cell fate patterning in the mouse Retina	67

Abstract	68
Author Summary	69
Introduction	70
Results	73
Discussion	80
Figures	84
Materials and Methods	99
Supplementary Material	102
References	128
Curriculum Vitae	159

List of Tables

Chapter I

Table 1. PR Proteins with Functional, But Not Sequence-Level, Homology ...	14
Table 2. PR Proteins with Sequence-Level, But Not Functional, Homology ...	15
Table 3. PR Proteins with Functional and Sequence-Level Homology	15

Chapter III

Table 1. Homology arm primers	14
Table 2. gRNA primers	15
Table 3. Genotyping Primers	15

Chapter III

Table S1: Retina image names and genotypes	111
Table S2: Comparison of hand (H) and computer © segmented retinal sections	98
Table S3: Parameters used in the microenvironmental model	111

List of Figures

Chapter I

Figure 1. Retinas Are Patterned in Stochastic/Regionalized, Regionalized, and Ordered Mosaics	21
Figure 2. The Gene Regulatory Networks Controlling PR Specification	25
Figure 3. Gradients of Signaling Molecules Determine Regionalized Retinal Development	28
Figure 4. Retinal Development Proceeds Through Waves of Differentiation ...	30
Figure 5. Looping of DNA Elements Regulates Cone Subtypes	32
Supplementary Figure 1: The gene-regulatory network controlling PR specification in <i>Gallus gallus domesticus</i>	33

Chapter II

Fig. 1. S and L/M cone generation in human retinal organoids	46
Fig. 2. Human cone subtype specification is recapitulated in organoids	48
Fig. 3. Thyroid hormone signaling is necessary and sufficient for the temporal switch between S and L/M fate specification	50
Fig. 4. Dynamic expression of thyroid hormone signaling regulators during development	52
Supplemental Figure 1. CRX expression precedes S-opsin and L/M-opsin Expression	62

Supplemental Figure 2. T3 signals through Thr β to suppress S fate and promote L/M fate	63
Supplemental Figure 3. Expression of thyroid hormone regulators in developing human retinas	64
Supplemental Figure 4. Differentiation protocol for retinal organoids	65
Supplemental Figure 5. Histogram of expression values used to identify the inflection point in the heat map of transcript expression	66

Chapter III

Figure 1. Analysis of opsin expression intensity the mouse retina	84
Figure 2. Identification of cone subtypes	86
Figure 3. Spatial Distribution of M- and S-opsins in cone cells.	87
Figure 4. S- and M-opsin intestines in cones	88
Figure 5. Intensity of M- and S-opsins in cones	90
Figure 6. Model for cone cell fate specification	91
Figure 7. Simulated cone mosaic produced by the quantitative model	93
Figure 8. D-V cone patterning in simulated and experimental data	95
Figure 9. Correlation between CEC fate and S-opsin transitions	97
Figure 10. ThrB2 KO mouse intensity plots	99
Figure S1: Fitting of cell expression data	114
Figure S2: Comparison of D-V profiles between retinas	115
Figure S3: S-only cell fraction	116
Figure S4: Correlation between S- and M-opsin in retinal cells	117

Figure S5: Correlation between S- and M-opsin in retinal cells regionally ..	117
Figure S5: Expression of S- and M-opsin in retinal cells	119
Figure S6: Fitting of cell expression intensity data	120
Figure S8: Expression in modeled cell populations	121
Figure S9: Opsin concentrations in modeled cells	122
Figure S10: Correlation between S- and M-opsin in modeled cells	123
Figure S11: Analysis of pixel intensities in images of THRB2 KO cells	124
Figure S12: Expression of S-opsin in THRB2 KO retinal cells	125
Figure S13: Mean retina description	126
Figure S14: Best fit parameterization	127

Chapter I

Introduction

This chapter is divided into two sections. The first section is a comprehensive review of the mechanisms of photoreceptor patterning across species, focusing on fly, zebrafish, chicken, mouse, and human photoreceptor mosaics. This review was published in *Trends in Genetics*, 32: 638-659 (2016). Kayla Viets and I worked together to publish this review as equal authors. My role in this work included a literature review of chick, mouse, and human photoreceptor patterning, and the comparison of these mechanisms across all species described. Kayla Viets completed a literature review of the fly and the zebrafish retina, and contributed equally to the comparison of photoreceptor specification mechanisms across all species described. The second section in Chapter I, “Summary of Thesis” outlines the content of this thesis, and describes the major findings of each chapter.

Mechanisms of photoreceptor patterning in vertebrates and invertebrates

Kayla Viets*, Kiara Eldred*, and Robert J Johnston Jr.†

Department of Biology, Johns Hopkins University, 3400 N. Charles Street
Baltimore, MD 21218-2685 USA

* Equal authors

†Corresponding Author.

Keywords: photoreceptor, retina, mosaic, human, *Homo sapiens*, mouse, *Mus musculus*, fruit fly, *Drosophila melanogaster*, chick, *Gallus gallus domesticus*, zebrafish, *Danio rerio*, regulatory network, eye, color vision, evolution, motion-detecting, color-detecting, cone, rod, inner photoreceptor, outer photoreceptor, stochasticity, regionalization, gene network

Abstract

Across the animal kingdom, visual systems have evolved to be uniquely suited to the environments and behavioral patterns of different species. The visual acuity and color perception of organisms depend on the distribution of photoreceptor subtypes within the retina. Retinal mosaics can be organized into three broad categories: stochastic/regionalized, regionalized, and ordered. Here, we describe the retinal mosaics of flies, zebrafish, chickens, mice, and humans and the gene regulatory networks controlling proper photoreceptor specification in each. By drawing parallels in eye development between these divergent species, we identify a set of conserved organizing principles and transcriptional networks that govern photoreceptor subtype differentiation.

Introduction

Evolution has produced highly tuned opsin proteins that enable organisms to detect wavelengths of light specific to their environments. For instance, humans can differentiate colors most precisely in the yellow to red range of the color spectrum, which corresponds to the colors of ripening fruit (Julius and Nathans, 2012; Osorio and Vorobyev, 2005, 2008), while flies are sensitive to polarized light, which assists in navigation during flight (Mazzoni et al., 2008; Weir and Dickinson, 2012; Wernet et al., 2012). In this review, we describe the patterns of photoreceptor (PR) mosaics and the gene regulatory networks that lead to diverse PR subtype fates across several commonly studied organisms: fruit flies, zebrafish, chickens, mice, and humans. The retinal mosaics of these organisms can be grouped into three classes: stochastic/regionalized, regionalized, and ordered. These species share numerous similarities in retinal development, revealing surprising conservation in the gene regulatory mechanisms and developmental patterns that form diverse visual systems.

Retinas are patterned in stochastic/regionalized, regionalized, and ordered mosaics

*The stochastic/regionalized mosaic of the *Drosophila melanogaster* retina*

The *Drosophila melanogaster* (fruit fly) retina is composed of approximately 800 ommatidia (i.e. unit eyes) each of which contains eight PRs, R1-R8 (**Fig. 1A2**). These PRs can be divided into two groups: the outer PRs, R1-R6, and the inner PRs, R7 and R8. The outer PRs encircle the inner PRs, and the R7 is located above the R8 relative to the apical surface of the retina (**Fig. 1A2**) (Wolff and Ready, 1991). A rhabdomere, a series of thousands of microvilli containing a high concentration of photopigment, extends the full length of each PR cell body (**Fig. 1A2**) (Pichaud, 2014; Ready, 1993).

All outer PRs express the motion-detecting photopigment Rhodopsin 1 (Rh1) (**Fig. 1A3-A6, A8**) (O'Tousa et al., 1985; Zuker et al., 1985). Expression of different Rhodopsins in the inner PRs defines four subtypes of ommatidia: **pale** (**Fig. 1A3**), **yellow** (**Fig. 1A4**), **dorsal third yellow** (**Fig. 1A5**), and **dorsal rim** (**Fig. 1A6**) (Bell et al., 2007; Chou et al., 1996; Chou et al., 1999; Fortini and Rubin, 1990; Mazzoni et al., 2008; Montell et al., 1987; Papatsenko et al., 1997; Tomlinson, 2003; Wernet et al., 2003; Zuker et al., 1987). In **pale** ommatidia, **pR7s**

express UV-detecting Rhodopsin 3 (Rh3) and **pR8s** express blue-detecting Rhodopsin 5 (Rh5) (**Fig. 1A3, A9-A10**)(Bell et al., 2007; Chou et al., 1996). In **yellow** ommatidia, **yR7s** express UV-detecting Rhodopsin 4 (Rh4) and **yR8s** express green-detecting Rhodopsin 6 (Rh6)(Bell et al., 2007; Chou et al., 1996) (**Fig. 1A4, A9-A10**). PRs in the ventral two-thirds of the retina are arranged in a stochastic mosaic: **pale** and **yellow** ommatidia in this region are randomly patterned in a ratio of 35:65(Bell et al., 2007) (**Fig. 1A1 and A7**). Specialized ommatidial subtypes occur in the dorsal region of the retina. In the **dorsal third** of the retina, Rh3 is co-expressed with Rh4 in stochastically distributed **yR7s**(Mazzoni et al., 2008) (**Fig. 1A1, A5, A11**). **Dorsal rim** ommatidia are found only at the extreme dorsal edge of the retina and express Rh3 in both R7s and R8s (**Fig. 1A1, A6, A12**)(Wernet et al., 2003).

An ordered array of cones and rods in the retina of Danio rerio

As in flies, *Danio rerio* (zebrafish) PRs contain a ciliated region with a high concentration of photopigment (**Fig. 1B2**)(Allison et al., 2010; Raymond and Barthel, 2004). In zebrafish, this region is known as the outer segment and is located at the apical end of the PR (**Fig. 1B2**). Outer segments connect to the ellipsoid, which refracts light onto the outer segment (**Fig. 1B2**)(Hoang et al., 2002; MacNichol et al., 1978; Raymond and Barthel, 2004; Tarboush et al., 2014; Wheeler, 1982). The ellipsoid is joined to the myoid region, which contracts to extend and retract PRs in response to changes in light (**Fig. 1B2**)(Ali, 1975; Nagle, 1983; Troutt and Burnside, 1988). Below the myoid lies the cell soma, which contains the nucleus (**Fig. 1B2**)(Raymond and Barthel, 2004; Wheeler, 1982).

Zebrafish retinas contain four PR classes: rods, which express motion-detecting rhodopsin (RH1); short single cones, which express UV opsin (SWS1); long single cones, which express blue opsin (SWS2); and double cone pairs, in which one cone expresses red opsin (LWS) and the other cone expresses green opsin (RH2) (**Fig. 1B2**)(Branchek and Bremiller, 1984; Nawrocki et al., 1985; Raymond et al., 1993; Vihtelic et al., 1999). Zebrafish PRs are arranged in a repetitive pattern throughout the retina(Raymond and Barthel, 2004). Rows of double cones alternate with rows of interdigitated UV and blue cones (**Fig. 1B1, B4**). Within double cone rows, each red-green pair is turned 180 degrees with respect to the previous double cone (**Fig. 1B1, B4**). Each row of double cones is shifted one half cycle with respect to the previous row, so

each UV cone is flanked by two green cones and each blue cone is flanked by two red cones (**Fig. 1B1, B4**). Rods are interspersed evenly between the rows of cones, forming a square pattern around UV cones (**Fig. 1B1, B5**)(Allison et al., 2010; Branchek and Bremiller, 1984; Engstrom, 1963; Fadool, 2003; Larison and Bremiller, 1990; Raymond, 1995a).

Within this highly ordered mosaic, regionalized expression of two subtypes of LWS (LWS-1 and LWS-2) and four subtypes of RH2 (RH2-1, RH2-2, RH2-3, and RH2-4) in double cones defines distinct areas of the zebrafish retina. In the **inner central/dorsal** area, double cones expressing LWS-2 and RH2-1 are interspersed with double cones expressing LWS-2 and RH2-2 (**Fig. 1B3**). The **outer central/dorsal** area surrounds the **inner central/dorsal** area, and all double cones in this region express LWS-2 and RH2-2 (**Fig. 1B3**). The next ring of expression, the **inner periphery/ventral** area, contains double cones expressing LWS-1 and RH2-3 (**Fig. 1B3**). Finally, double cones in the **outer periphery/ventral** area express LWS-1 and RH2-4 (**Fig. 1B3**)(Chinen et al., 2003; Takechi and Kawamura, 2005).

Overlapping regular spacing of PR subtypes forms a semi-random mosaic in the Gallus gallus domesticus retina

Similar to zebrafish, the *Gallus gallus domesticus* (chicken) retina contains Rh1-expressing rods, specialized for night vision, and multiple single and double cone types. The four single cone types in the chicken retina are sensitive to red, green, blue, and violet wavelengths of light (expressing LWS, Rh2, SWS2, and SWS1 opsins respectively)(**Fig. 1C2**)(Bruhn and Cepko, 1996; Govardovskii and Zueva, 1977). These cone types have been identified chiefly by differently colored oil droplets located between the inner and outer segments, which may act as a filter for specific wavelengths of light, as well as focusing photons onto the outer segment(Hart, 2001; Kram et al., 2010; Meyer and May, 1973; Wilby et al., 2015) (**Fig. 1C2**). Two morphologically different sets of double cones in chickens are sensitive to long wavelengths of light(Wai et al., 2006). In the more common double cone pair, both cones have an oil droplet(Araki et al., 1990; Wai et al., 2006) (**Fig. 1C2, Type B**). In the other pair, only the larger (primary) cone contains an oil droplet (**Fig. 1C2, Type A**)(Hart, 2001; Wai et al., 2006). These double cones may be specialized for motion detection rather than color vision, as they appear to

contain the same photopigments and synapse on one another (Campenhausen and Kirschfeld, 1998; Osorio and Vorobyev, 2005; v. Campenhausen and Kirschfeld).

Double cones cover about 40% of the chicken retina, with a majority positioned ventrally (Kram et al., 2010). Green and red single cones each comprise about 20% of total cone cells. Blue and violet cones make up the remaining 12 and 8%, respectively, and are more abundant dorsally (Kram et al., 2010). Each cone in the chicken retina is positioned at a regular distance from other cones of the same subtype (ex: each red cone is at a specific distance from its neighboring red cone cell) (Kram et al., 2010). However, the relative positions of different cone cell subtypes (ex: red vs. green) are not regular. Thus, the final retinal pattern in chickens is semi-random (**Fig. 1C1, C3, 4D**), rather than the perfectly ordered pattern seen in zebrafish (**Fig. 1B1**) (Kram et al., 2010).

Chickens and other birds have an afoveate structure, meaning the most central part of the retina is densely packed with cones and lacks rods (Bruhn and Cepko, 1996; Morris, 1982) (**area centralis, Fig. 1C1**). Further from the foveal center, cone packing becomes less dense (Bueno et al., 2011; Headington et al., 2011; Kram et al., 2010; Wilby et al., 2015). In addition to the **area centralis**, rod numbers are reduced in a lateral stripe through the center of the retina (Bruhn and Cepko, 1996) and in the dorsal retina (**central meridian** and **dorsal rod free zone, Fig. 1C1**). The rod population has a pattern distinct from cones, forming a ventral to dorsal gradient (Bruhn and Cepko, 1996) (**dorsal rod free zones, Fig. 1C1**).

*Regionalized patterning of cones in the retina of *Mus musculus**

The *Mus musculus* (mouse) retina has fewer PR types than zebrafish and chickens, containing motion-detecting rods that express rhodopsin and three subtypes of color-detecting cones that express S-opsin (UV-detecting), M-opsin (green-detecting), or both S- and M-opsins (**Fig. 1D2-D5**). These PRs are patterned in a regionalized mosaic, with cones arranged in opposing dorsal to ventral gradients (**Fig. 1D1, D6**). M-opsin is expressed most highly in the dorsal third, and S-opsin is expressed in the ventral two thirds (Lukats et al., 2005; Szel et al., 1996) (**Fig. 1D1, D6**). In the region in which these opposing gradients meet, single cone cells have varying levels of M- and S-opsin co-expression (Lukats et al., 2005; Rohlich et al., 1994) (**Fig. 1D1, D6**). A subset of S-opsin expressing cones appears to be stochastically arranged

throughout the retina(Applebury et al., 2000) (**Fig. 1D1**). These cones may be part of a primordial S-cone color system that synapses onto a dedicated population of bipolar cells(Haverkamp et al., 2005). Rods are evenly interspersed throughout the retina and vastly outnumber cones, making up about 97% of the PR population(Jeon et al., 1998) (**Fig. 1D1, D7**).

Stochastic/regionalized patterning of cones and rods in the Homo sapiens retina

The human retinal mosaic contains four types of PRs: rods for night vision, and blue (S-opsin), red (L-opsin), and green (M-opsin) cones for color and daytime vision(Deeb, 2005; Hunt, 2001; Kainz, 1998; Nathans, 1999; Nathans et al., 1986) (**Fig. 1E2-E5**). Human retinal patterning is mostly random, with a few areas of organization. Similar to chickens, the central area of the human retina is densely packed with cones(Hendrickson, 1992) (**Fig. 1E1**). This area can be divided into three regions: the **foveola**, the **fovea**, and the **macula** (**Fig. 1E1**). The **foveola** contains only L- and M-opsin-expressing cones arranged in a stochastic pattern(Roorda et al., 2001; Roorda and Williams, 1999) (**Fig. 1E1**). S-cones become integrated into the mosaic outside the **foveola** within the **fovea** and the **macula** (**Fig. 1E1, E6**)(Curcio et al., 1991). It is unclear whether the S-cone mosaic is also random(Curcio et al., 1991), or if it is distributed in a lattice pattern, separate from the L/M-cone cell pattern(Ahnelt, 1998; Cornish et al., 2004; Curcio et al., 1991). Cones in the **foveola** and **fovea** are smaller than those found in the **macula** and in the **posterior pole**(Curcio et al., 1990) (**Fig. 1E1**). Rods are integrated into the mosaic starting in the **macula** region(Curcio et al., 1991) (**Fig. 1E1**). The **posterior pole** of the retina is rod-dominated, with a random pattern of L-, M-, and S-cones scattered throughout (Hofer et al., 2005) (**Fig. 1E1, E7**). One other densely packed cone region exists along the **peripheral rim** of the retina(Williams, 1991) (**Fig. 1E1**).

L- and M-cones are so similar that until very recently it was almost impossible to distinguish between the two(Gowdy and Cicerone, 1998; Hofer et al., 2005; Li and Roorda, 2007; Otake et al., 2000; Roorda et al., 2001; Roorda and Williams, 1999; Rossi et al., 2011; Williams, 2011). It is widely believed that the only difference between L- and M-cones is the opsin expressed. However, evidence from monkeys suggests that the two populations have different numbers of synapses between the cone and the midget bipolar cell(Calkins et al., 1994). S-cones are easily distinguished by their short, stubby outer segments, while L/M-cones produce

long, skinny outer segments(Ahnelt, 1998; Ahnelt et al., 1987; Curcio et al., 1991; Mustafi et al., 2009). S- and L/M-cones also have distinct patterns of connectivity with other retinal cell types(Ahnelt, 1998).

The unique retinal patterning of different organisms has evolved to suit their environments and behaviors

Evolution has optimized stochastic/regionalized, regionalized, and ordered retinal patterns to fit the needs of diverse organisms. For example, regionalization of specialized ommatidia within an overall stochastic mosaic provides the fly with the optimal light-detecting abilities to respond to its environment. The **dorsal rim** ommatidia detect polarized light to allow proper navigation during flight, while the coexpression of Rh3 and Rh4 in **dorsal third yR7s** may assist in detecting the location of the sun(Mazzoni et al., 2008; Weir and Dickinson, 2012; Wernet et al., 2012). The evolutionary advantage of a stochastic rather than patterned distribution of PRs remains unclear. Random placement of **yellow** and **pale** ommatidia that results in similar 65:35 ratios throughout the eye may be the simplest evolutionary mechanism to ensure that all regions of the retina detect multiple wavelengths of light with the same efficiency.

The ordered distribution of zebrafish cones is uniquely suited to its aquatic environment, preventing under- or over-sampling of specific light wavelengths in different areas of the retina(Fadool, 2003). The ability to detect such a broad spectrum of light wavelengths may allow the zebrafish to see efficiently when light conditions vary due to water turbidity, seasonal changes, and fluctuations in water microorganism and mineral content(Wheeler, 1982).

The semi-random mosaic of the chicken retina is tuned to perceive many wavelengths of light with high visual acuity. The chicken's cone-rich retina and densely packed **area centralis**, which also has a greater ganglion cell density (Ehrlich, 1981; Straznicky and Chohade, 1987), likely provides high-acuity color vision in daylight to allow identification of prey and predators. Different bird species display different ratios of cone subtypes. For example, sea birds generally have fewer long-wavelength opsin cones compared to blue and green, possibly because long wavelengths are filtered out by water(Hart, 2001; Lythgoe, 1979). This implies that genetic mechanisms governing cone subtype specification are highly tunable to the environmental niche that an avian species inhabits.

Because the regionalized mouse retina contains two color-detecting opsins that are mostly separated into the dorsal third and ventral retina, mouse vision is believed to be largely monochromatic. Ventral expression of S-opsin and dorsal expression of M-opsin allows the mouse to maximize sampling of ultraviolet (sky) and terrestrial light sources with the most appropriate PRs. In the center of the retina, where S- and M-opsin expression converges, differing levels of opsin coexpression between neighboring cells may give the mouse dichromatic vision(Baden et al., 2013; Chang et al., 2013).

The random distribution of the three human cone types allows for efficient spectral sampling of the visual field and maximizes contrast sensitivity(Julius and Nathans, 2012; Osorio and Vorobyev, 2005, 2008). The dense packing of cones in the fovea provides maximal visual acuity in the daylight, and the rod-dominated retina outside of the macula allows for efficient night vision.

The gene-regulatory networks controlling PR specification share functional and sequence-level homologs

The gene-regulatory networks controlling PR specification are extremely complex and in many cases are still being elucidated. Here, we provide simplified networks to highlight the proteins that play conserved roles in PR fate at either the functional or sequence level, focusing mainly on flies, zebrafish, and mice, whose gene-regulatory networks are better characterized than those of chickens and humans. PR differentiation occurs in four basic decision steps (**Fig. 2A**): 1) PR vs. non-PR fate; 2) Rod vs. cone fate; 3) Cone subtype; and 4) Opsin subtype.

Step 1: PR vs. non-PR fate choice

Step 1 of PR specification involves the expression of factors that distinguish differentiating PRs from other cell fates. In flies, the zinc finger transcription factor Glass plays this role(Moses et al., 1989) (**Fig. 2B, Step 1**). Vertebrate PR differentiation involves a core set of conserved transcription factors, including Cone-Rod Homeobox (Crx), the Orthodenticle Homeobox proteins (Otx2 and Otx5), and the Retinal homeobox proteins (Rx1, RaxL, Rax)(Akagi et al., 2005; Bovolenta et al., 1997; Chen and Cepko, 2002; Chen et al., 1997; Chuang et al., 1999; Emerson and Cepko, 2011; Emerson et al., 2013; Freund et al., 1997;

Furukawa et al., 1997a; Furukawa et al., 1997b; Furukawa et al., 1999; Furukawa et al., 2000; Gamse et al., 2002; Hennig et al., 2008; Jacobson et al., 1998; Li et al., 2015; Liu et al., 2001; Muranishi et al., 2011; Nelson et al., 2008; Nelson et al., 2009; Nishida et al., 2003; Ochi et al., 2004; Omori et al., 2011; Ragge et al., 2005; Rivolta et al., 2001; Shen and Raymond, 2004; Slavotinek et al., 2015; Sohocki et al., 1998; Swain et al., 1997; Takagi et al., 2015; Vincent et al., 2014; Wang et al., 2014) (**Fig. 2C-F, Step 1**). Species-specific inputs have emerged to regulate these conserved factors. In zebrafish, the Hippo pathway transcriptional activator Yes-associated protein (Yap) represses these core transcription factors (**Fig. 2C, Step 1**), while in mice, the Notch-1 transmembrane receptor plays this role (**Fig. 2E, Step 1**) (Asaoka et al., 2014; Jadhav et al., 2006; Yaron et al., 2006). The core PR factors are also activated by species-specific inputs: in zebrafish, the signaling molecule Sonic hedgehog (Shh) and the transcription cofactor Lbh-like activate Rx1 and Otx2, respectively (**Fig. 2C, Step 1**) (Li et al., 2015; Stenkamp et al., 2002). The network topology between these conserved factors varies between organisms; in mice, Rax activates Otx2 (Muranishi et al., 2011) (**Fig. 2E, Step 1**), while in zebrafish, no link between Rx1 and Otx2 has been established (**Fig. 2C, Step 1**) (Chuang et al., 1999; Furukawa et al., 1997a; Furukawa et al., 2000; Li et al., 2015; Muranishi et al., 2011; Nelson et al., 2009). In both mice and zebrafish, Otx2 likely activates Crx (**Fig. 2C, E, Step 1**) (Hennig et al., 2008; Li et al., 2015). Other regulators complement these core factors: for example, in zebrafish, Crx activates the species-specific Otx homolog Otx5 to drive PR fate (**Fig. 2C, Step 1**) (Asaoka et al., 2014; Gamse et al., 2002; Liu et al., 2001; Shen and Raymond, 2004).

Step 2: Rod vs. cone fate choice

In Step 2, PR precursors select either rod or cone fate. In *Drosophila*, outer PRs (rods) are specified by the presence of the homeodomain protein Defective Proventriculus (Dve), which represses the expression of color-detecting Rhodopsins (**Fig. 2B, Step 2**) (Johnston et al., 2011). In zebrafish, mice, and humans, the bZIP transcription factor Neural retina leucine zipper protein (Nrl) and the orphan nuclear receptor Nuclear Receptor Subfamily 2 Group E Member 3 (Nr2e3) play important roles in rod fate (**Fig. 2C, E-F, Step 2**) (Bessant et al., 1999; Chen et al., 2005; DeAngelis et al., 2002; Haider et al., 2006; Haider et al., 2000; Haider et al., 2001; Jacobson et al., 2004; Kitambi and Hauptmann, 2007; Liu et al., 2001; Mears et al., 2001; Milam et al., 2002;

Mitton et al., 2000; Montana et al., 2011; Nelson et al., 2008; Nishiguchi et al., 2004; Oh et al., 2007; Rehemtulla et al., 1996; Roger et al., 2010; Swain et al., 2001; Wright et al., 2004; Yoshida et al., 2004). Nrl activates Nr2e3 in mice and may play a similar role in humans and zebrafish (**Fig. 2E-F, Step 2**)(Hao et al., 2012; Oh et al., 2008). In zebrafish and possibly chickens, Retinoic acid (RA) signaling is also involved in rod development (**Fig. 2C-D, Step 2**); in zebrafish, RA signals through the RAR α receptor and possibly the RXR γ receptor to specify rods (**Fig. 2C, Step 2**)(Hyatt et al., 1996; Stevens et al., 2011). Additionally, the growth factor glial cell line-derived neurotrophic factor (GDNF) is expressed specifically in rods in both chickens and mice and may also play a role in zebrafish (**Fig. 2D-E, Step 2**)(Frasson et al., 1999; Lucini et al., 2007; Ogilvie et al., 2000; Rothermel and Layer, 2003; Volpert et al., 2007). Two non-conserved factors, the SUMO-E3 ligase/transcription factor Pias3 and the orphan nuclear receptor Ror β , are also involved in rod fate in mice (**Fig. 2E, Step 2**)(Kautzmann et al., 2011; Montana et al., 2011; Onishi et al., 2010; Onishi et al., 2009). Recent evolutionary studies suggest that mammalian S-cone and rod PRs may have similar lineages, and may temporally switch from S-cone precursors to rods(Kim et al., 2016).

In *Drosophila*, the zinc finger transcription factor Spalt (Sal) drives inner PR (“cone”) fate by repressing Dve (**Fig. 2B, Step 2**)(Johnston et al., 2011). In an additional step, not conserved in higher organisms, inner PR “cones” differentiate further into two types: R7s, specified by the homeodomain transcription factor Prospero (Pros) and the transcription factor subunit Nf-yc, and R8s, specified by the zinc finger transcription factor Senseless (Sens)(**Fig. 2B, Step 2**)(Cook et al., 2003; Morey et al., 2008; Xie et al., 2007).

In zebrafish, the BMP family ligand Gdf6a induces the transcription factor Tbx2b to repress rod fate and allow cone development (**Fig. 2C, Step 2**)(Alvarez-Delfin et al., 2009; Duval et al., 2014; Raymond et al., 2014). Tbx2b does not appear to play a conserved role in cone specification; it is involved in dorsal-ventral retinal development in chickens, mice, and humans, but its expression is not restricted to cones(Gibson-Brown et al., 1998; Sowden et al., 2001). In chickens and mice, RA signaling through the Rxr γ receptor may be important for cone fate (**Fig. 2D-E, Step 2**) (Hoover et al., 1998; Kelley et al., 1995; Mori et al., 2001; Roberts et al., 2005). Additionally, Thr β 2 receptor plays a role in cone specification in chickens, mice, and humans (**Fig. 2D-F, Step 2**)(Applebury et al., 2007; Cakir et al., 2015; Gibson-Brown et al.,

1998; Liu et al., 2007; Ng et al., 2001; Ng et al., 2011; Roberts et al., 2006; Shibusawa et al., 2003; Sjöberg et al., 1992; Trimarchi et al., 2008; Weiss et al., 2012; Yanagi et al., 2002; Zhou et al., 2015).

Step 3: Cone subtype choice

In Step 3, cone precursors are specified into subtypes, marked by expression of specific color-detecting opsins. Interestingly, several of the proteins required for cone subtype selection in flies are conserved in vertebrate PRs, though they have been adapted to play different roles. Selection between **yellow** and **pale** ommatidial subtypes in *Drosophila* is based on the stochastic expression of the PAS-bHLH transcription factor Spineless (Ss) in 65% of R7s (Wernet et al., 2006). In **yR7s**, Ss activates expression of Rh4 and Dve, which represses Rh3 (**Fig. 2B, Step 3**) (Johnston et al., 2011; Wernet et al., 2006). In **pR7s** lacking Ss, Rh4 and Dve are not expressed, leading to activation of Rh3 by Sal and Orthodenticle (Otd), a homolog of vertebrate Crx, Otx2, and Otx5 (**Fig. 2B, Step 3**) (Tahayato et al., 2003; Wernet et al., 2006). Intriguingly, the mammalian homolog of Sal, Sall3, has been conserved at both the sequence and functional levels; it also activates opsins in mice (**Fig. 2E, Step 3**) (de Melo et al., 2011).

In **yR7s**, Ss represses an unknown signal to R8s (**Fig. 2B, Step 3**). In the absence of this signal, the Warts (Wts) serine/threonine kinase is activated, causing repression of the transcriptional coactivator Yorkie (Yki), a homolog of zebrafish Yap, in **yR8s** (**Fig. 2B, Step 3**). Repression of Yki induces activation of Rh6 and loss of Rh5 (**Fig. 2B, Step 3**) (Chou et al., 1996; Chou et al., 1999; Jukam and Desplan, 2011; Mikeladze-Dvali et al., 2005; Wernet et al., 2006). In **pR7s**, the unknown signal activates the PH domain-containing protein Melted (Melt), which represses Wts to allow Yki activation and Rh5 expression in **pR8s** (**Fig. 2B, Step 3**) (Jukam and Desplan, 2011; Mikeladze-Dvali et al., 2005). Additionally, Otd acts permissively in **pR8s** to activate Rh5 (**Fig. 2B, Step 3**) (Johnston et al., 2011).

In **dorsal third yR7s**, reduced Ss and Dve levels, combined with activation by the Iroquois complex of transcription factors (IroC), induces co-expression of Rh3 with Rh4 (**Fig. 2B, Step 3**) (Johnston et al., 2011; Mazzoni et al., 2008; Thanawala et al., 2013). In the **dorsal rim**, high local concentrations of the diffusible morphogen Wingless (Wg) act with IroC to drive expression of the homeodomain transcription factor Homothorax (Hth) in R7s and R8s (**Fig. 2B,**

Step 3, Fig. 3A)(Tomlinson, 2003; Wernet et al., 2003). Hth represses Ss in R7s and Rh5, Rh6, and Sens in R8s, causing Rh3 expression in R7s and R8s (**Fig. 2B, Step 3**)(Johnston, 2013; Tomlinson, 2003; Wernet et al., 2003).

In zebrafish, mice, and humans, T3 thyroid hormone signals through the $\text{tr}\beta\text{2}/\text{Thr}\beta\text{2}$ receptor to drive expression of specific opsins. In zebrafish, T3 activates LWS opsin, in mice, it activates M-opsin and represses S-opsin, and in humans, it may select L/M-opsins over S-opsin (**Fig. 2C, E-F, Step 3**)(Applebury et al., 2007; Cakir et al., 2015; Gibson-Brown et al., 1998; Liu et al., 2007; Ng et al., 2001; Ng et al., 2011; Roberts et al., 2006; Shibusawa et al., 2003; Sjoberg et al., 1992; Suzuki et al., 2013; Trimarchi et al., 2008; Weiss et al., 2012; Yanagi et al., 2002; Zhou et al., 2015). RA signaling through the $\text{RXR}\gamma\text{a}/\text{RXR}\gamma$ receptor also controls opsin expression in vertebrates; in zebrafish, RA signaling activates LWS opsin and represses SWS1 and SWS2 opsins, while in mice, it may repress S-opsin (**Fig. 2C, E, Step 3**)(Mitchell et al., 2015; Prabhudesai et al., 2005; Roberts et al., 2005).

Since T3 and RA are also involved in earlier steps of PR specification, additional factors likely work with them to specify cone subtypes. In mice, Pias3, BMP, and COUP-TFII work with T3 to activate M-opsin (**Fig. 2E, Step 3**)(Onishi et al., 2010; Roberts et al., 2006; Satoh et al., 2009). BMP and COUP-TFII may also assist RA and T3 in repressing mouse S-opsin (**Fig. 2E, Step 3**)(Satoh et al., 2009).

Additional factors have been implicated in vertebrate opsin expression, though it is currently unclear if they are conserved between species. In zebrafish, Gdf6a drives SWS2 expression and works in combination with Tbx2b to activate SWS1 (**Fig. 2C, Step 3**)(Alvarez-Delfin et al., 2009; Duval et al., 2014; Raymond et al., 2014). Additionally, the fish-specific transcription factor *Sine oculis homeobox homolog 7* (Six7) drives activation of RH2 (**Fig. 2C, Step 3**)(Ogawa et al., 2015). In mice, Shh signaling may activate Sall3, which acts with Ror β to activate S-opsin (**Fig. 2E, Step 3**) (de Melo et al., 2011; Kawakami et al., 2009; Srinivas et al., 2006).

Step 4: Opsin subtype choice

In zebrafish and humans, a final choice further differentiates cone subtypes based on opsin subtype expression (**Fig. 2C, F, Step 4**). Zebrafish red- and green-detecting cones select

between multiple LWS and RH2 opsin subtypes, respectively (**Fig. 5B**)(Tsujimura et al., 2007; Tsujimura et al., 2010; Tsujimura et al., 2015). RA, potentially acting through RXR γ a, directs expression of LWS-1 over LWS-2 (**Fig. 5B**)(Mitchell et al., 2015). Human L/M cones select between the closely related L- and M-opsins (**Fig. 5C**)(Wang et al., 1992). In both zebrafish and humans, locus control regions (LCRs) have evolved to regulate opsin subtype choice at the *cis* level (see below; **Fig. 5**)(Tsujimura et al., 2007; Tsujimura et al., 2010; Tsujimura et al., 2015).

Functional and sequence-level homology

The proteins controlling PR specification can be divided into three main categories based on their functional and/or sequence-level homology. The first category involves factors that serve similar developmental roles but share no sequence homology (Table 1). A second category includes factors that are conserved on the sequence level but perform unique roles in different organisms (Table 2). The third category contains factors with functional and sequence-level homology (Table 3). In some cases, factors in this category may drive further, species-specific processes in addition to their conserved role.

Table 1: PR proteins with functional, but not sequence-level, homology

Function	Fly	Zebrafish	Mouse
PR fate	Glass	Lbh-like	N/A
Rod fate	Dve	N/A	Pias3, Ror β
Cone fate	Pros, Nf-yc, Sens	Tbx2b, Gdf6a	N/A
Opsin choice	Ss, Dve, IroC, Wg, Hth	Gdf6a, Tbx2b, Six7	COUP-TFII, Pias3, BMP, Ror β

Table 2: PR proteins with sequence-level, but not functional, homology

Gene	Fly	Zebrafish	Chicken	Mouse	Human
Otd/Otx2/ Otx5	Opsin choice	PR fate	PR fate	PR fate	Retinal cell fate
Yki/Yap	Opsin choice	PR fate repression	N/A	N/A	N/A
Shh	N/A	PR fate	N/A	Retinal regionalization	N/A

Table 3: PR proteins with functional and sequence-level homology

Gene	Fly	Zebrafish	Chicken	Mouse	Human
Crx	N/A	PR fate	PR fate	PR fate	PR fate
Otx2/Otx5	N/A	PR fate	PR fate	PR fate	N/A
Rx1/RaxL/ Rax	N/A	PR fate	PR fate	PR fate	N/A
Nrl	N/A	Rod fate	N/A	Rod fate	Rod fate
Nr2e3	N/A	Rod fate	N/A	Rod fate	Rod fate
RA	N/A	Rod fate, opsin choice, opsin subtype choice	Rod fate, cone fate	Cone fate, opsin choice	N/A
GDNF	N/A	Rod fate (?)	Rod fate	Rod fate	N/A
Sal/Sall3	Cone fate, opsin choice	N/A	N/A	Opsin choice	N/A
trβ2/Thrβ2	N/A	Opsin choice	Cone fate	Cone fate, opsin choice	Cone fate, opsin choice

Gradients of signaling molecules determine regionalized retinal development

In addition to conserved gene-regulatory networks, diverse organisms share a common mechanism for delineating retinal regions, involving gradients of signaling molecules. Two models exist for how such gradients are established. The first, more traditional model suggests that gradients arise from diffusion of signaling molecules from a specific source. This occurs in *Drosophila*, where Wg is secreted from a stripe called the dorsal margin to create a dorsal-to-ventral gradient in the larval eye disc that specifies the location of dorsal rim ommatidia in adults (**Fig. 3A**)(Legent and Treisman, 2008; Tomlinson, 2003).

An alternative “gradient-free” model proposes that enzymes that produce or degrade signaling molecules are expressed in a regionalized pattern, regulating local levels of small molecules to create a gradient throughout the tissue(Hernandez et al., 2007). This gradient-free mechanism may establish ventral to dorsal gradients of RA involved in retinal development and patterning in zebrafish, chickens, and mice(Bruhn and Cepko, 1996; Hyatt et al., 1996; McCaffery et al., 1993; Mey et al., 1997; Perz-Edwards et al., 2001; Prabhudesai et al., 2005; Roberts et al., 2006; Stevens et al., 2011). In the developing chicken and mouse retina, the dorsally-expressed aldehyde dehydrogenase AHD2 produces low RA, and the ventrally-expressed aldehyde dehydrogenase V1 produces high RA, creating regional “gradients” of RA in the retina (**Fig. 3B-C**)(McCaffery et al., 1992; McCaffery et al., 1999a, b; McCaffery et al., 1993; Mey et al., 1997). In the chick, the ventral-to-dorsal gradient of RA mirrors the rod gradient, suggesting that regionalized RA processing enzymes drive gradients of PR subtypes (**Fig. 3C**)(Mey et al., 1997; Nicotra et al., 1994; Stenkamp et al., 1993). In the mouse, an additional enzyme, the oxidase CYP26, causes RA degradation and a potential breakdown in the gradient in the central retina (**Fig. 3B**)(Mey et al., 1997; Sakai et al., 2004). Together, these conserved patterns delineate different retinal regions during development.

Interestingly, in adult retinas of both chick and mouse, ventral V1 dehydrogenase expression is lost, leaving dorsal AHD2 as the only RA synthesizing enzyme and causing a reversal of the gradient to higher RA levels in the dorsal retina (**Fig. 3B-C**)(McCaffery et al., 1993; Mey et al., 1997). In mice, this reversal may promote ventral S-opsin repression after postnatal day 8 by activation of RXR γ (**Fig. 3B**)(Mey et al., 1997; Niederreither et al., 1997;

Roberts et al., 2005). In the chicken, it is unclear how this reversal affects PR fate specification (**Fig. 3C**).

Deiodinases play a similar role in thyroid hormone gradient formation. They are expressed in regionalized areas and/or at different time points in the chick (Trimarchi et al., 2008), mouse (Corbo et al., 2007; Ng et al., 2010), and zebrafish retinas (Bagci et al., 2015; Guo et al., 2014; Thisse et al., 2003). In mice, Deiodinase 2 (Dio2), which converts thyroid hormone from the inactive T4 to the active T3 form, is expressed at higher levels in the dorsal retina (Bedolla and Torre, 2011; Corbo et al., 2007) and likely establishes a T3 gradient (Dentice et al., 2013) (**Fig. 3B**). High dorsal T3 signaling promotes expression of M-opsin and repression of S-opsin (Glaschke et al., 2011; Onishi et al., 2010; Roberts et al., 2005; Roberts et al., 2006; Shibusawa et al., 2003) (**Fig. 3B**). Low T3 signaling in the ventral retina allows expression of S-opsin (**Fig. 3B**) (Roberts et al., 2006).

Dorsal-ventral BMP gradients and ventral-dorsal Shh gradients in the mouse retina activate M- and S-opsin, respectively, but the sources of these gradients are still unclear (**Fig. 3B**) (de Melo et al., 2011; Inoue et al., 2010; Kawakami et al., 2009; Satoh et al., 2009).

Retinal development proceeds through waves of differentiation

Despite significant differences in morphology, regionalization, and sensitivity between organisms, retinal development in many species involves waves of differentiation. Within the developing fly eye-antennal disc, a wave of differentiation known as the morphogenetic furrow moves from the posterior to the anterior of the retina (**Fig. 4A**), driven partially by the signaling molecule Hedgehog (Hh) and the bHLH transcription factor Atonal (Ato) (Heberlein et al., 1993; Jarman et al., 1994; Jarman et al., 1995; Ma et al., 1993; Ready et al., 1976; Wolff and Ready, 1991). Undifferentiated PR precursors lie anterior to the furrow, whereas posterior to the furrow, PRs differentiate in a specific order (**Fig. 4A**) (Ready et al., 1976; Wolff and Ready, 1991). The R8 PR serves as a “founder” cell, recruiting undifferentiated PR precursors and driving their stepwise differentiation into a complete ommatidium via multiple signaling pathways (well-reviewed in (Baonza et al., 2001; Freeman, 1994, 1996; Pichaud, 2014; Quan et al., 2012; Tio et al., 1994; Tomlinson and Ready, 1987; Treisman, 2013)). The initial differentiation of R2, R5, R3, and R4 is followed by the second mitotic wave (**Fig. 4A**), after which R1, R6, and R7

sequentially differentiate(Ready et al., 1976; Tomlinson and Ready, 1987; Wolff and Ready, 1991).

Though separated by over 800 million years of evolution, zebrafish retinal differentiation shares much in common with the processes observed in flies. As in flies, a wave of neural differentiation driven in part by Hedgehog signaling and *ath5*, a zebrafish homolog of *Ato*, spreads across the developing retina (**Fig. 4B**)(Masai et al., 2000; Neumann and Nüsslein-Volhard, 2000). In zebrafish, PRs differentiate from an initial patch(Hu and Easter, 1999; Raymond, 1995b; Schmitt and Dowling, 1996). Cones spread from this patch in a wave resembling an opening fan, with differentiation sweeping from ventral-nasal to dorsal-temporal(Raymond and Barthel, 2004; Raymond, 1995b; Schmitt and Dowling, 1996) (**Fig. 4B**). A mitotic wave follows the initial fan gradient to complete cone differentiation(Hu and Easter, 1999; Raymond, 1995b). Early-differentiating red cones may act similarly to R8 PRs in *Drosophila*, functioning as “founders” to recruit undifferentiated cone precursors and drive their differentiation(Raymond and Barthel, 2004). While rods are also found initially in the ventral patch, they differentiate separately from cones. Clusters of rod precursors scattered throughout the retina undergo multiple rounds of mitosis before differentiating into rods and migrating to their final positions around UV cones(Fadool, 2003; Johns and Fernald, 1981; Raymond, 1995b; Schmitt and Dowling, 1996).

The chicken retina is similar to the zebrafish in that differentiation begins at a central patch, the area centralis(Bruhn and Cepko, 1996; Trimarchi et al., 2008; Wai et al., 2006). Sequential waves of transcription factor expression emanate from the center to the periphery to drive cell differentiation and retinal patterning (**Fig. 4C**). First, a wave of cone precursor transcription factors is expressed, including *Thrb2* and *Otx2*(Trimarchi et al., 2008). Individual cone subtypes then express opsins in temporal waves. Green and red opsins are expressed first, followed by blue and violet(Bruhn and Cepko, 1996) (**Fig. 4D**). An additional wave of differentiation sweeps linearly across the retina from the ventral to dorsal region to pattern rods (**Fig. 4E**)(Bruhn and Cepko, 1996).

Although mice do not have a fovea, retinal differentiation follows the same central to peripheral pattern that is seen in chickens (**Fig. 4C**)(Carter-Dawson and LaVail, 1979; Young,

1985). Generation of different retinal cell types is coincident with temporal waves, and this phenomenon has been used to identify important factors in retinal generation(Dinet et al., 2011).

The developmental pattern of the human and other primate retinas closely resembles the chick and mouse retina, with differentiation following sequential waves emanating from the optic disk, near the fovea, outward(Cornish et al., 2005; Hendrickson et al., 2008; La Vail et al., 1991) (**Fig. 4C**). S-cones are seen first in the foveal area followed by L/M-cones, and later rods outside of the fovea (Hendrickson et al., 2008; Xiao and Hendrickson, 2000). The fetal fovea is not packed as tightly as the adult fovea(Hendrickson, 1992), suggesting that differentiated cones migrate toward the central fovea later in development to create a densely packed array(Cornish et al., 2004; Diaz-Araya and Provis, 1992; Packer et al., 1990).

Looping of DNA elements regulates cone subtypes

Beyond retina-wide signaling gradients and waves of differentiation, conserved mechanisms control retinal development at an individual PR level. Looping of regulatory DNA elements plays a critical role in opsin choice across organisms. In *Drosophila*, DNA looping may regulate the stochastic expression of *ss*, the key determinant of R7 (“cone”) subtype fate. The *ss* locus contains an enhancer, which activates *ss* in 100% of R7s, and two silencers, which randomly repress *ss* in 35% of R7s (**Fig. 5A**)(Johnston and Desplan, 2014). Because the two silencers are located at a significant distance from the *ss* promoter, it is likely that they regulate *ss* through a looping-based mechanism. An enticing hypothesis is that the enhancer and silencers compete for looping to the *ss* promoter, resulting in activation or repression of *ss* and regulation of downstream Rhodopsins (**Fig. 5A**).

In a striking example of convergent evolution between zebrafish and humans, DNA elements known as locus control regions (LCRs) likely regulate opsin expression through looping-based mechanisms. In both cases, ancestral enhancers that regulated the expression of a single opsin gene were adapted in response to an opsin gene duplication(Bowmaker, 2008; Brainard, 2000; Hofmann and Carleton, 2009; Nathans, 1999; Trezise and Collin, 2005; Tsujimura et al., 2007; Tsujimura et al., 2010; Tsujimura et al., 2015).

Zebrafish opsin genes are regulated by two LCRs, one that selects between LWS subtypes and one that selects between RH2 subtypes (**Fig. 5B**)(Tsujimura et al., 2007; Tsujimura

et al., 2010; Tsujimura et al., 2015). LCR-mediated regulation of opsin subtypes is controlled in a temporal progression (Takechi and Kawamura, 2005; Tsujimura et al., 2007; Tsujimura et al., 2010). RH2-1, RH2-2, and LWS-2 are expressed earliest and are present in the central and dorsal regions of the zebrafish retina, which develop first (**Fig. 1B3, Fig. 5B**) (Takechi and Kawamura, 2005). RH2-3, RH2-4, and LWS-1 are expressed later and thus localize to the later-developing retinal periphery (**Fig. 1B3, Fig. 5B**) (Takechi and Kawamura, 2005).

Human opsin genes are regulated by one LCR that selects between L- and M- opsin expression (**Fig. 5C**) (Nathans et al., 1989). It is hypothesized that the LCR loops randomly to the promoter of either the L- or M-opsin gene to drive opsin expression (Nathans et al., 1986; Peng and Chen, 2011; Smallwood et al., 2002). Alternatively, the human LCR might activate opsins in a temporal progression, after which L- and M-opsin-expressing cones might migrate to their final, random positions in the human retina (Diaz-Araya and Provis, 1992; Packer et al., 1990).

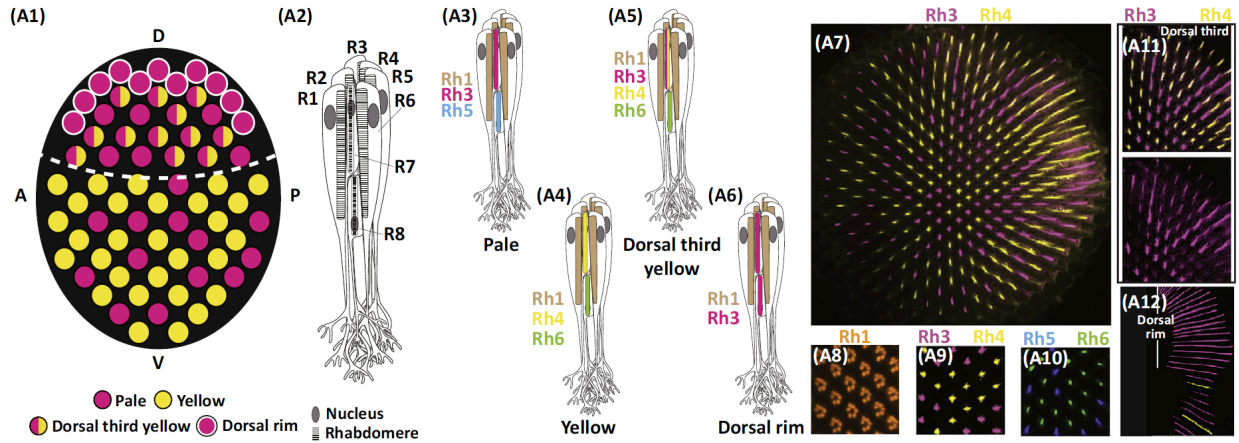
The zebrafish and human LCRs are all about 0.5 kb in size, perhaps reflecting a common sequence length that is required for robust activation of opsin expression (Nathans et al., 1989; Smallwood et al., 2002; Tsujimura et al., 2007; Tsujimura et al., 2010). Despite their common sizes, the RH2, LWS, and human LCRs have little sequence similarity other than shared binding sites for the transcription factor Crx (Tsujimura et al., 2007; Tsujimura et al., 2010).

Conclusion

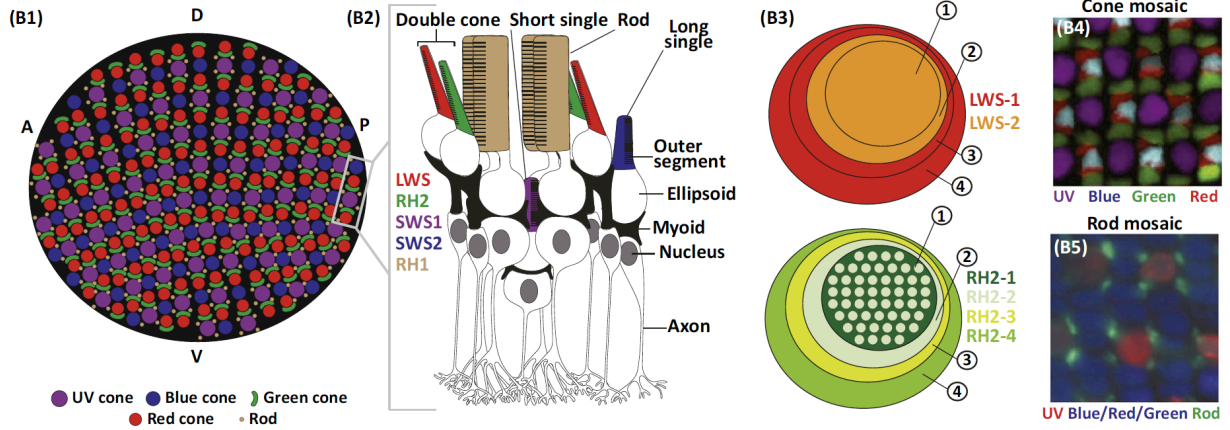
Many questions about the gene-regulatory and evolutionary mechanisms governing retinal development remain unanswered (see “Outstanding Questions” box). Further study of PR development and maintenance will provide insight into the evolutionary advantages of different retinal mosaics and uncover additional conserved and species-specific gene-regulatory networks required for retinal patterning. A deeper understanding of these mechanisms may ultimately lead to new treatments for many developmental disorders of the visual system and the development of effective PR regenerative therapies.

Chapter I Figures:

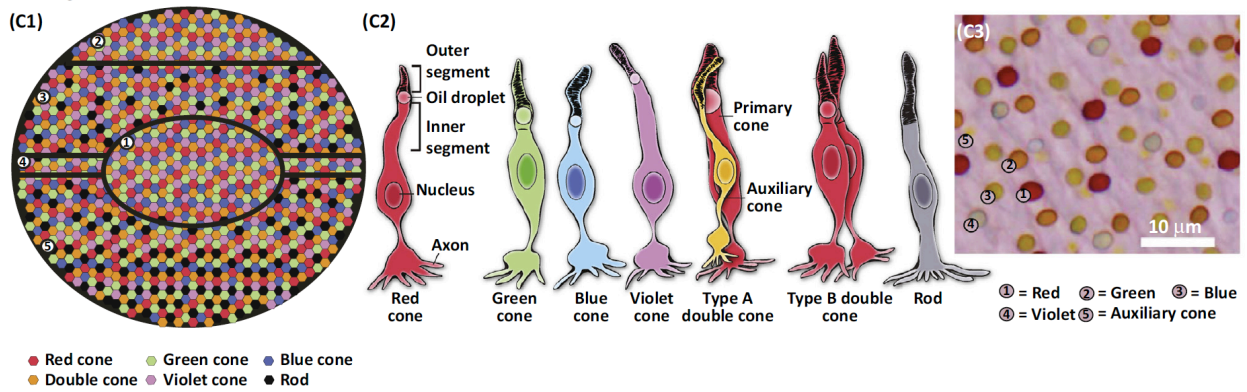
Drosophila melanogaster



Danio rerio



Gallus gallus domesticus



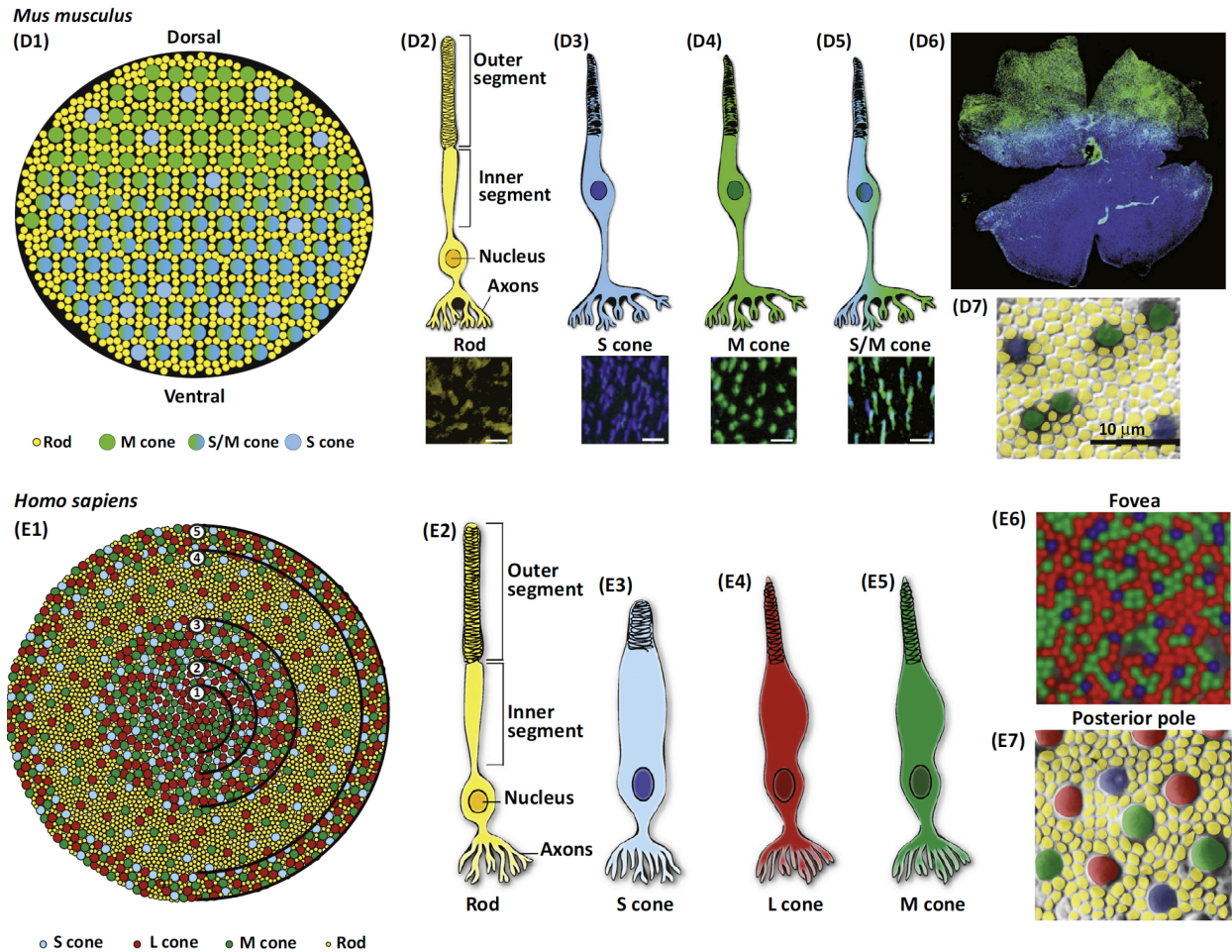


Figure 1: Retinas are patterned in stochastic/regionalized, regionalized, and ordered mosaics.

A1) Schematic of the *Drosophila melanogaster* (fruit fly) PR mosaic (not to scale). D: Dorsal, V: Ventral, A: Anterior, P: Posterior.

A2) Schematic of a *Drosophila* ommatidium.

A3) Schematic of a pale ommatidium.

A4) Schematic of a yellow ommatidium.

A5) Schematic of a dorsal third yellow ommatidium.

A6) Schematic of a dorsal rim ommatidium.

A7) Whole-mount immunostain of a *Drosophila* retina showing the stochastic distribution of ommatidial subtypes.

A8) Immunostain showing Rhodopsin 1 (Rh1) expression in the outer PRs.

- A9)** Immunostain showing the stochastic patterning of Rh3 and Rh4 in a section of the *Drosophila* retina.
- A10)** Immunostain showing the stochastic patterning of Rh5 and Rh6 in a section of the *Drosophila* retina.
- A11)** Immunostain of the dorsal third of the *Drosophila* retina, showing coexpression of Rh3 and Rh4 in dorsal third yR7s.
- A12)** Immunostain of the dorsal rim of the *Drosophila* retina, showing expression of Rh3 in R7s and R8s.
- B1)** Schematic of the *Danio rerio* (zebrafish) PR mosaic (not to scale). D: Dorsal, V: Ventral, A: Anterior, P: Posterior.
- B2)** Schematic side view of a single unit of the zebrafish retinal pattern.
- B3)** Schematic showing the overlapping, regionalized expression patterns of zebrafish LWS and RH2 opsin subtypes (not to scale). 1: Inner central/dorsal area, 2: Outer central/dorsal area, 3: Inner periphery/ventral area, 4: Outer periphery/ventral area.
- B4)** Immunostain of a section of the zebrafish cone mosaic. Reprinted from *Progress in Retinal and Eye Research*, Volume 42, M. Hoon, H. Okawa, L. Della Santina, R.O. Wong, Functional architecture of the retina: Development and disease, Pages 44-84, Copyright (2014), with permission from Elsevier.
- B5)** Immunostain of a section of the zebrafish rod mosaic. Reprinted from *Developmental Biology*, Volume 258, J.M. Fadool, Development of a rod photoreceptor mosaic revealed in transgenic zebrafish, Pages 277-290, Copyright (2003), with permission from Elsevier.
- C1)** Schematic of the *Gallus gallus domesticus* (chicken) PR mosaic (not to scale). 1: area centralis, 2: dorsal rod free zone, 3: dorsal rod zone, 4: central meridian, 5: ventral rod rich zone.
- C2)** The chicken has five different types of cone cells: red, green, blue, violet, and double cones. Type A double cones contain an auxiliary cone lacking an oil droplet. Type B double cones both have oil droplets. Images adapted from Wai *et al.*, 2006 and Santiago Ramon y Cajal, 2000(Santiago Ramon, 2000; Wai *et al.*, 2006).
- C3)** Light microscope image of oil droplets in the chicken retina. Adapted from Figure 1b from Kram *et al.*, 2010(Kram *et al.*, 2010).
- D1)** Schematic of the *Mus musculus* (mouse) PR mosaic (not to scale).

D2-D5) Labeled depiction and immunostaining of mouse PRs. Rods shown in yellow (D2), S-cones in blue (D3), M-cones in green (D4), and S/M-cones in blue/green (D5).

D6) Immunostain of a whole-mount mouse retina. Green: M-opsin. Blue: S-opsin.

D7) Pseudocolored DIC section of whole-mount mouse retina, showing cone and rod distribution. Rods shown in yellow. Blue and green are arbitrarily chosen to represent S- and M-cones, respectively, but each cell could express S-opsin only, M-opsin only, or both S- and M-opsins. Adapted from Jeon et al. 1998 (Jeon et al., 1998). Copyright 1998, <http://www.jneurosci.org/content/18/21/8936.long>, under Creative Commons Attribution 4.0 International Public License and Disclaimer of Warranties (<http://creativecommons.org/licenses/by/4.0/legalcode>).

E1) Schematic of the *Homo sapiens* (human) PR mosaic (not to scale). 1: foveola, 2: fovea, 3: macula, 4: posterior pole, 5: peripheral rim.

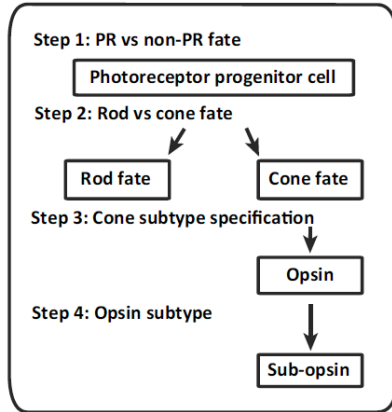
E2-E5) Labeled depiction of human PRs. E2: rod, E3: S-cone, E4: L-cone, E5: M-cone.

E6) Pseudocolored adaptive optics image of the human fovea. Blue: S-cones, Red: L-cones, Green: M-cones. Adapted from Figure 8B of Williams et al., 2011 (Williams, 2011). Copyright 2011, <http://www.ncbi.nlm.nih.gov/pmc/articles/PMC3189497/>, DOI 10.1016/j.visres.2011.05.002, under Creative Commons Attribution 4.0 International Public License and Disclaimer of Warranties (<http://creativecommons.org/licenses/by/4.0/legalcode>).

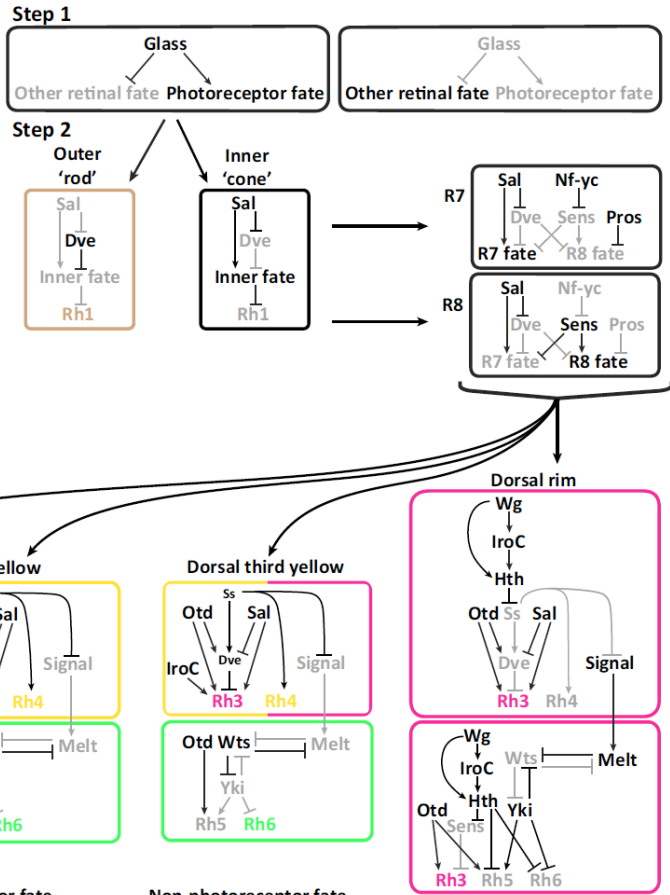
E7) Pseudocolored image of human cones in the posterior pole. Yellow: rods, Blue: S-cones. Red and green are arbitrarily chosen to represent L- and M- cones, respectively, but each cell could be either red or green. Adapted from Curcio et al., 1991 (Curcio et al., 1991). Copyright 1991, <http://onlinelibrary.wiley.com/doi/10.1002/cne.903120411/abstract>, DOI 10.1002/cne.903120411, under Creative Commons Attribution 4.0 International Public License and Disclaimer of Warranties (<http://creativecommons.org/licenses/by/4.0/legalcode>).

Note: In *Danio rerio* and *Mus musculus*, the optic disc is located temporal to the central retina, and in *Gallus gallus domesticus* and *Homo sapiens* retinas, it is located temporal to the foveal center. This area is devoid of photoreceptors and is not represented in the included mosaics.

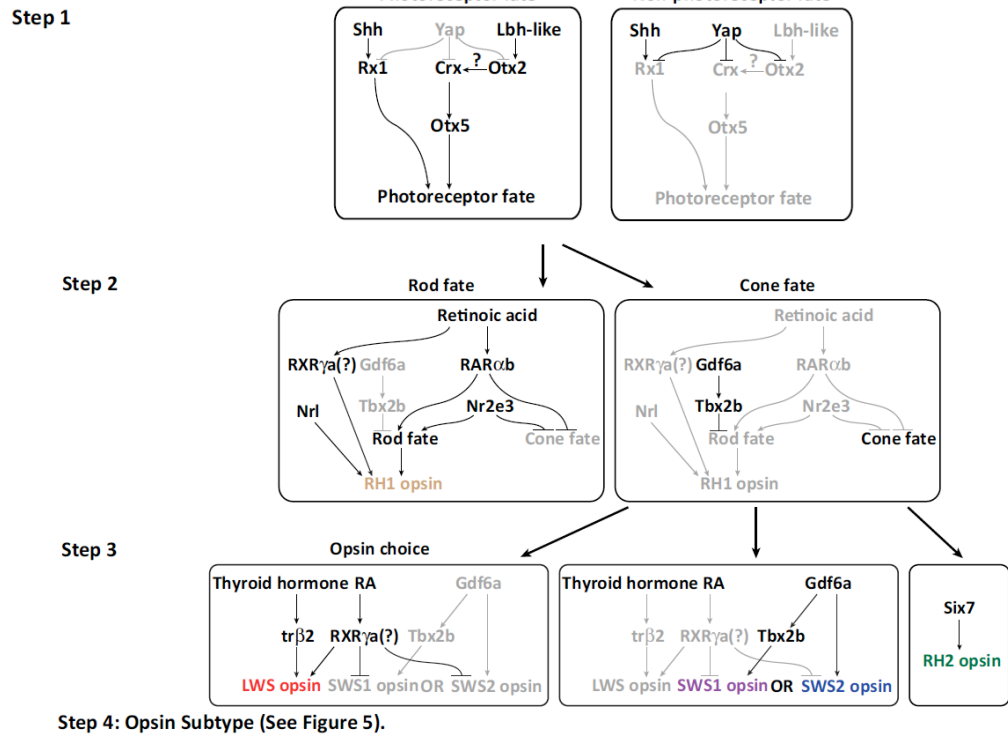
(A) Basic photoreceptor specification logic



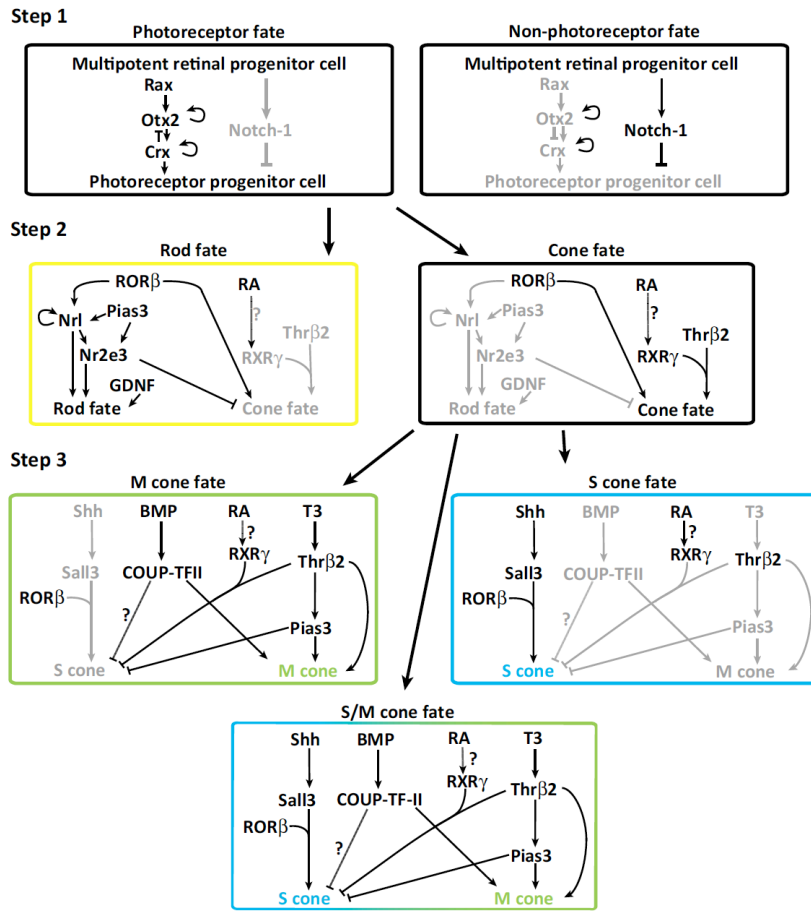
(B) *Drosophila melanogaster*



(C) *Danio rerio*



(D) *Mus musculus*



(E) *Homo sapiens*

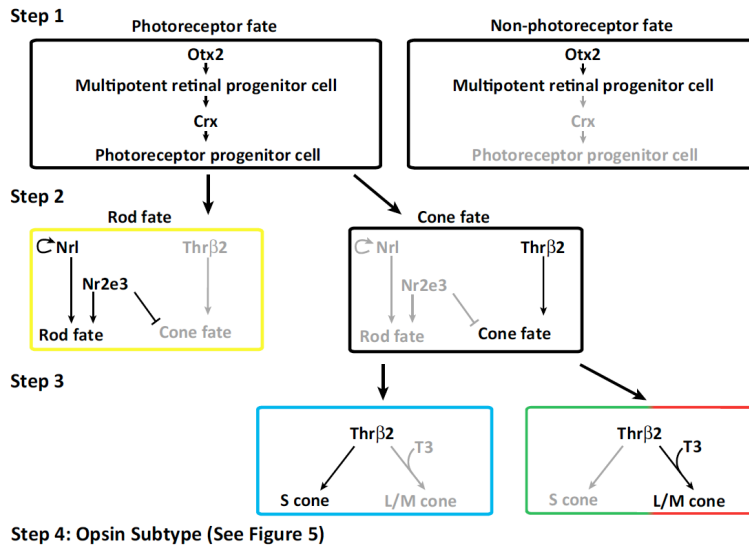


Figure 2: The gene-regulatory networks controlling PR specification. All gene-regulatory networks have been simplified to emphasize PR factors that are conserved between species.

Arrows within gene networks solely represent our current understanding of network relationships and do not imply genetic mechanisms such as direct or indirect transcriptional regulation.

A) The basic steps of PR differentiation, which are largely conserved between organisms.

B) *Drosophila melanogaster*.

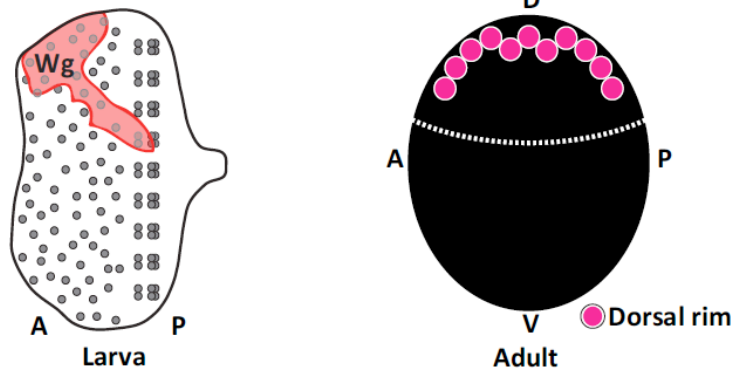
C) *Danio rerio*.

D) *Gallus gallus domesticus*.

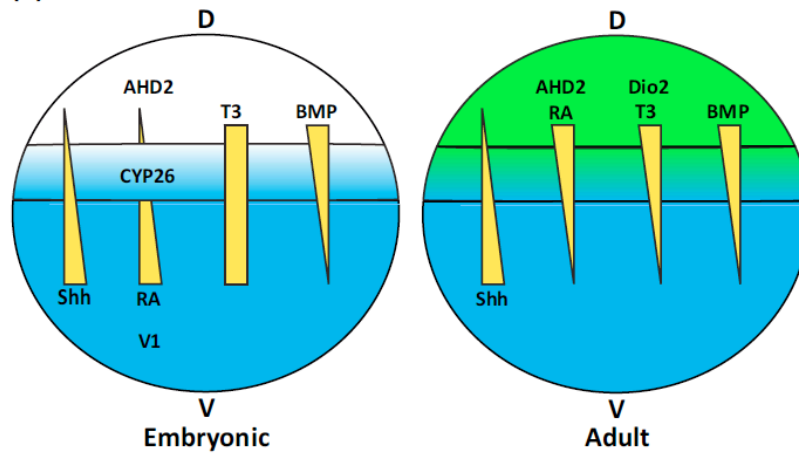
E) *Mus musculus*.

F) *Homo sapiens*.

(A) *Drosophila melanogaster*



(B) *Mus musculus*



(C) *Gallus gallus domesticus*

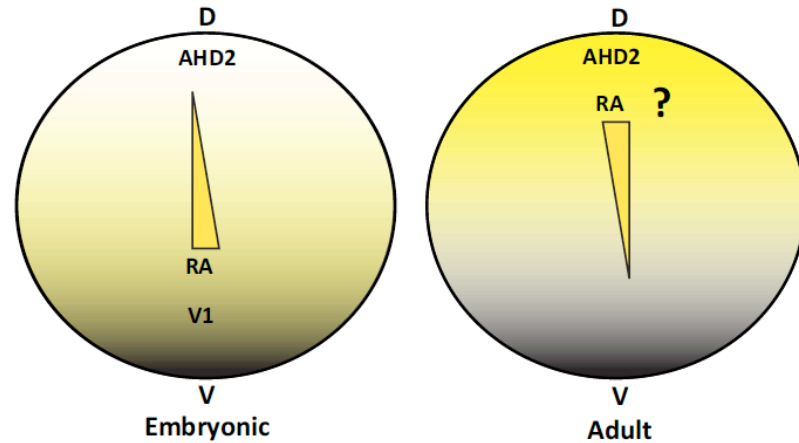


Figure 3: Gradients of signaling molecules determine regionalized retinal development.

For A-C, D: dorsal, V: ventral, A: anterior, P: posterior.

A) In *Drosophila*, the diffusible morphogen Wg is expressed in a dorsal patch of the larval eye disc, beginning the signaling cascade leading to expression of Rh3 in the **dorsal rim** in the adult (See **Fig. 2B**).

B) Gradients of signaling molecules in the mouse retina leading to M (green) and S (blue) opsin expression. Sonic Hedgehog (Shh) is expressed in a ventral to dorsal gradient in both the embryo and the adult. Retinoic acid (RA) is expressed in a ventral to dorsal gradient at embryonic stages, and is produced by the enzymes V1 (ventral, high enzymatic activity) and AHD2 (dorsal, low enzymatic activity). CYP26 degrades RA in a strip through the middle of the retina. In the adult neither V1 nor CYP26 are expressed, so RA is present in a dorsal to ventral gradient. Thyroid hormone (T3) is present throughout the embryonic retina. In the adult, T3 is present in a dorsal to ventral gradient, presumably governed by the presence of the T3 synthesizing enzyme Dio2. BMP is present in a dorsal to ventral gradient in both the embryonic and adult mouse retina.

C) In the chicken, RA is expressed in a ventral to dorsal gradient at embryonic stages and is produced by V1 and AHD2, as in mice. This mirrors the ventral to dorsal gradient of rods (black) within the chick retina. In the adult, V1 is not expressed, so RA is present in a dorsal to ventral gradient.

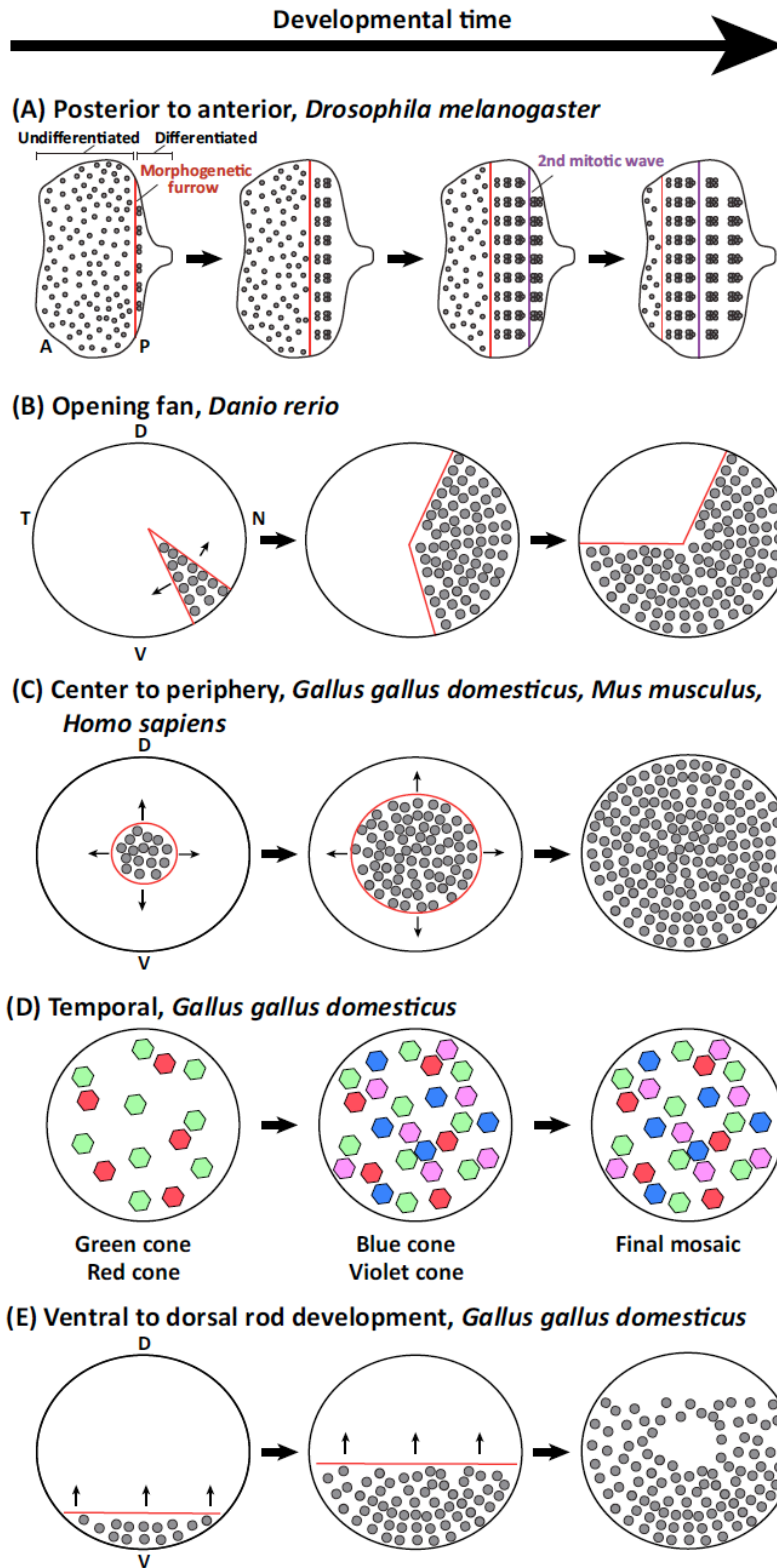


Figure 4: Retinal development proceeds through waves of differentiation.

For A-E, A: anterior, P: posterior, D: dorsal, V: ventral, N: nasal, T: temporal.

A) In *Drosophila*, waves of differentiation and mitosis move from posterior to anterior.

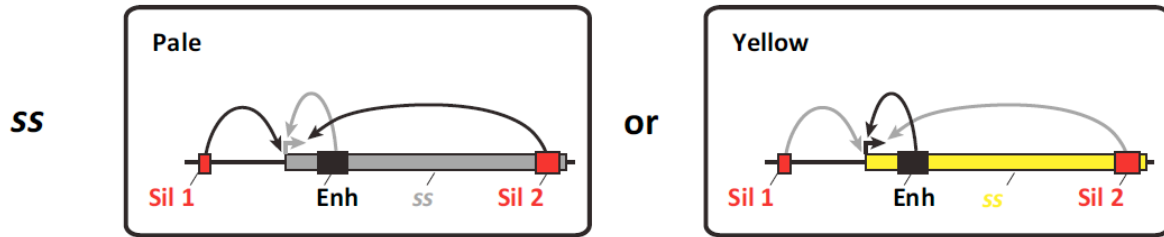
B) In zebrafish, differentiation proceeds from ventral-nasal to dorsal-temporal in a wave resembling an opening fan.

C) In chickens, mice, and humans, differentiation begins in the center of the retina and expands towards the periphery.

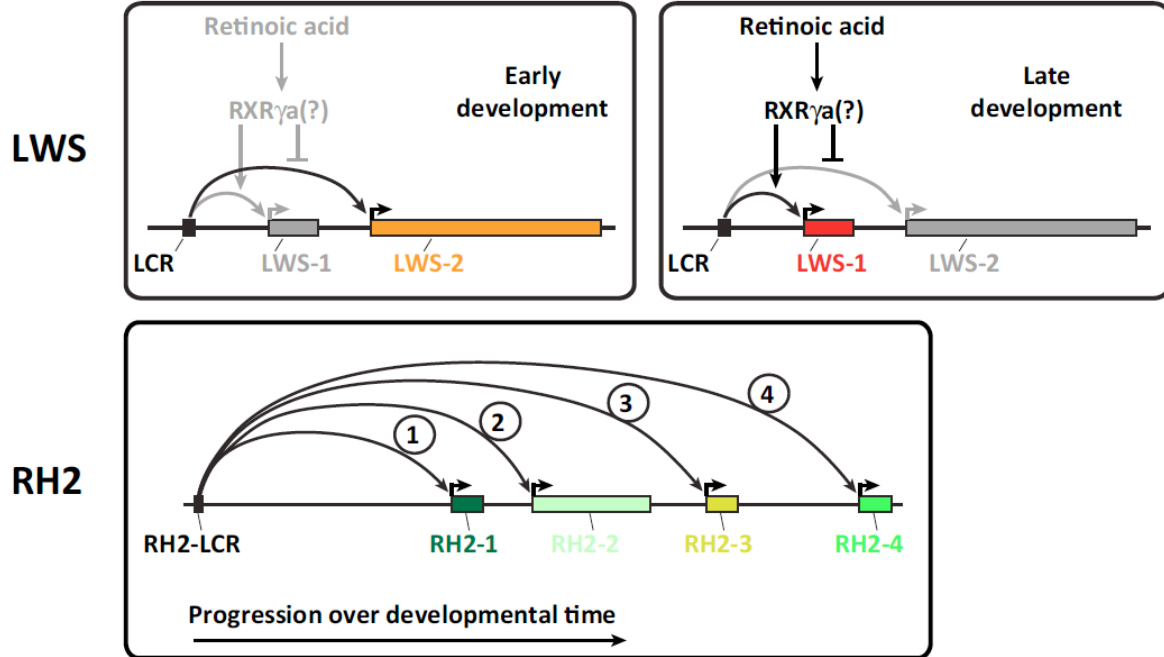
D) Chicken retinal development also involves a temporal wave of cone maturation. Green and red cones are the earliest to mature, followed by blue and violet cones.

E) A ventral-to-dorsal wave of differentiation patterns rods in the chicken retina in a density gradient, excluding the **area centralis**.

(A) *Drosophila melanogaster*



(B) *Danio rerio*



(C) *Homo sapiens*

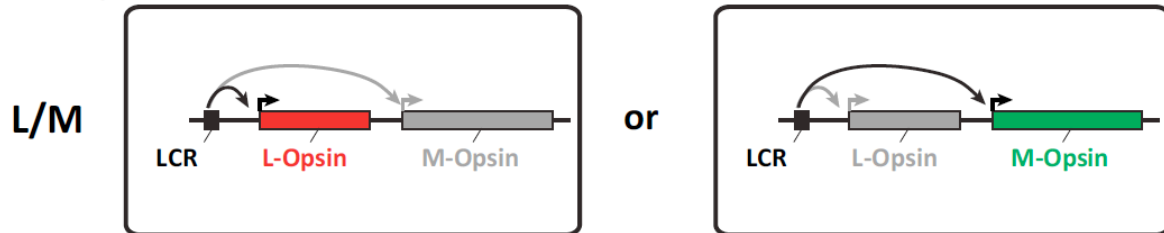


Figure 5: Looping of DNA elements regulates cone subtypes.

A) In *Drosophila*, looping of regulatory elements may cause activation or repression of *ss*, the key determinant of R7 subtype fate. Sil1: Silencer 1, Enh: Enhancer, Sil2: Silencer 2.

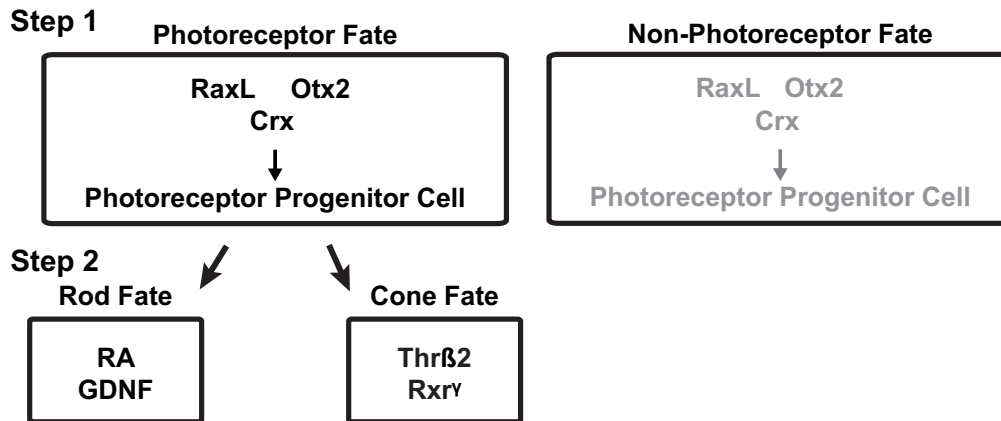
B) RA signaling and LCR looping select between opsin subtypes in zebrafish. Numbers in RH2 box indicate the temporal order of RH2 subtype expression.

C) LCR looping selects between L- and M-opsin for expression in human L/M-cones.

Supplemental Figure 1

A

Gallus gallus domesticus



Supplemental Figure 1: The gene-regulatory network controlling PR specification in *Gallus gallus domesticus*. The gene-regulatory network has been simplified to emphasize PR factors that are conserved between species. Arrows within gene networks solely represent our current understanding of network relationships and do not imply genetic mechanisms such as direct or indirect transcriptional regulation.

Summary of Thesis

Human vision begins with detection of light by photoreceptors in the retina, a thin layer of cells at the back of the eye. Cones are the primary daytime and color-detecting photoreceptors that distinguish red, green, or blue light. These cells differentiate into three subtypes through a poorly understood two-step process: first, naïve photoreceptors decide between blue and red/green fates, then between red and green fates. Despite decades of study, we know very little about the molecular mechanisms that generate cones in the human eye. This thesis investigates the mechanisms of photoreceptor speciation in the human and the mouse retina. In order to study human photoreceptors, I learned and further developed a system to differentiate retinal organoids from stem cells. The ability to generate functional human retinal tissue in a dish holds promise for regenerative therapies for debilitating diseases such as retinitis pigmentosa and macular degeneration, which currently affect over 2 million US residents. Controlled generation of specific photoreceptor types will be critical for transplants to restore vision (Artero Castro et al., 2018; Reh, 2016).

After this introductory Chapter I, Chapter II describes my findings that retinal organoids are similar to human retinas in developmental timing, gene expression, and morphology. I observed a temporal switch in photoreceptor development where blue cones are specified first, followed by red/green cones. Based on previous studies (Ng et al., 2001; Roberts et al., 2006), I hypothesized that thyroid hormone signaling could play a role in regulating this temporal switch. I found that organoids supplemented with thyroid hormone differentiated only red/green cones, whereas organoids with mutations that knock out Thyroid hormone receptor β (Thr β) generated only blue cones, even when grown with excess thyroid hormone. From these data, my studies demonstrate that thyroid hormone signaling is necessary and sufficient for specifying red/green cones. By examining gene expression using RNA-seq over 250 days of development in collaboration with Sarah Hadyniak, and Boris Brenerman, we observed temporally dynamic levels of thyroid hormone-degrading and -activating proteins in organoids. My studies indicate that the retina itself controls thyroid hormone levels, ensuring low thyroid hormone signaling early to specify blue cones and high thyroid hormone signaling later to produce red/green cones. Interestingly, dysregulation of thyroid hormone in premature infants is associated with color-

vision defects, consistent with my findings (Rovet and Simic, 2008; Simic et al., 2010; Yassin et al., 2018). My work establishes human retinal organoids as a model system to study mechanisms of cell fate specification in developing human tissue (Eldred et al., 2018).

Chapter III of this thesis describes the cone photoreceptor mosaic of the mouse retina, and proposes a model for how these cone fates could be specified based on a single gradient of thyroid hormone. This section explores the different cell fate decision processes that take place in the mouse retina: a graded response of co-expressing cells that have variable amounts of S and M opsins depending on the levels of thyroid hormone they are exposed to, and a population of cells that expresses only S opsin in a binary manner. Cameron Aviles and Elijah Roberts wrote the software program to identify cones from immunofluorescence images, and Elijah Roberts further analyzed the data and defined the model, and contributed to writing the manuscript. We also describe the mosaic in a Thr β 2-null mutant, in which the cells cannot respond to the thyroid hormone gradient. Despite years of study, the mosaic of cone cell arrangement within the entire human retina has not yet been characterized. These software and analysis tools will be applied to the human retina to provide the first map of human cones. This chapter is written in the form of a manuscript soon to be submitted to eLife.

My work has established organoids as a model system to study human development, and opened new doors for regenerative therapies through our ability to generate specific cone populations. The Johnston lab is now collaborating with doctors to transplant healthy lab-grown organoids into model organisms with vision-impaired retinas, aiming to restore vision and eventually treat debilitating diseases such as retinitis pigmentosa and macular degeneration.

Chapter II

Thyroid Hormone Signaling Specifies Cone Subtypes in Human Retinal Organoids

This chapter describes the retinal organoid system in which human retinal tissue is differentiated from stem cells. I show here that retinal organoids recapitulate human development, and that thyroid hormone signaling is necessary and sufficient for L/M cone fate specification. Sarah Hadyniak assisted in growing and processing retinal samples for a number of the RNA-seq time points described in this manuscript. Katarzyna Hussey performed the RNAi experiments. Boris Brenerman assisted in analysis of the RNA-seq data. Ping-Wu Zhang created the inducible Cas9 cell line that I used to create the *Thrb* mutant stem cell lines. Xitiz Chamling, Valentin M. Sluch, and Derek S. Welsbie contributed to creating the vectors that I used to create the *Thrb* mutant stem cell lines. This manuscript was published in *Science* 362:eaau6348 (2018).

Thyroid hormone signaling specifies cone subtypes in human retinal organoids

Kiara C. Eldred, Sarah E. Hadyniak, Katarzyna A. Hussey, Boris Brenerman, Ping-Wu Zhang, Xitiz Chamling, Valentin M. Sluch, Derek S. Welsbie, Samer Hattar, James Taylor, Karl Wahlin, Donald J. Zack, and Robert J. Johnston Jr.

One sentence summary: Cone specification in human retinal organoids

Abstract

The mechanisms underlying specification of neuronal subtypes within the human nervous system are largely unknown. The blue/S, green/M and red/L cones of the retina enable high-acuity daytime and color vision. To determine the mechanism controlling S vs. L/M fates, we studied the differentiation of human retinal organoids. Organoids and retinas have similar distributions, expression profiles, and morphologies of cone subtypes. S cones are specified first, followed by L/M cones, and thyroid hormone signaling controls this temporal switch. Dynamic expression of thyroid hormone-degrading and activating proteins within the retina ensures low signaling early to specify S cones and high signaling late to produce L/M cones. This work establishes organoids as a model for determining mechanisms of human development with promising utility for therapeutics and vision repair.

Key words: human retina, organoid, photoreceptor, cone cell, opsin, thyroid hormone receptor beta, Thr β , T3, T4, CRISPR/Cas9, DIO2, DIO3

Introduction

Cone photoreceptors in the human retina enable daytime, color, and high acuity vision (Viets et al., 2016b). The three subtypes of human cones are defined by the visual pigment that they express: blue- (short-wavelength/S), green- (medium-wavelength/M), or red- (long-wavelength/L) opsin (Nathans et al., 1986). Specification of human cones occurs in a two-step

process. First, a decision occurs between S vs. L/M cone fates (**Fig. 1A**). If the L/M fate is chosen, a subsequent choice is made between expression of L- or M-opsins (Smallwood et al., 2002; Vollrath et al., 1988; Wang et al., 1992; Wang et al., 1999). Mutations affecting opsin expression or function cause various forms of color blindness and retinal degeneration (Ladekjaer-Mikkelsen et al., 1996; Nathans et al., 1989; Patterson et al., 2016). Great progress has been made in our understanding of the vertebrate eye through the study of model organisms. However, little is known about the developmental mechanisms that generate the mosaic of mutually exclusive cone subtypes in the human retina. Here, we study the specification of human cone subtypes using human retinal organoids differentiated from stem cells (**Fig. 1D-K**).

Human retinal organoids generate photoreceptors that respond to light (Kaewkhaw et al., 2015; Nakano et al., 2012; Phillips et al., 2018; Wahlin et al., 2017; Zhong et al., 2014). We find that human organoids recapitulate the specification of cone subtypes observed in the human retina, including the temporal generation of S cones followed by L and M cones. Moreover, we find that this regulation is controlled by thyroid hormone signaling, which is necessary and sufficient to control cone subtype fates through the nuclear hormone receptor Thyroid Hormone Receptor β (Thr β). Expression of thyroid hormone-regulating genes suggests that retina-intrinsic temporal control of thyroid hormone levels and activity governs cone subtype specification. While retinal organoids have largely been studied for their promise of therapeutic applications (Artero Castro et al., 2018), our work demonstrates that human organoids can also be used to reveal fundamental mechanisms of human development.

Results

Specification of cone cells in organoids recapitulates development in the human retina

We compared features of cone subtypes in human organoids to adult retinal tissue. Adult human retinas and organoids at day 200 of differentiation displayed similar ratios of S to L/M cones as indicated by expression of S- or L/M-opsins (adult: S=13%, L/M=87%; organoid: S=29%, L/M=71%)(**Fig. 1B-C, S1A**). The difference in the ratio is likely due to the immaturity of the organoid at ~6 months compared to the terminally differentiated adult retina. We examined L/M cones with an antibody that recognizes both L- and M-opsin proteins due to their extremely high similarity. Both S and L/M cones expressed the cone-rod-homeobox transcription

factor (CRX), a critical transcription factor for photoreceptor differentiation (**Fig. 2A, E**)(Chen et al., 1997; Freund et al., 1997; Furukawa et al., 1997b), indicating proper fate specification in organoids. Additionally, cones in organoids and retinas displayed similar morphologies, with L/M cones that had longer outer segments and wider inner segments than S cones (**Fig. 2B-D, F-H**)(Curcio et al., 1991). The outer segments of cones were shorter in organoids than in adult retinas, consistent with postnatal maturation (**Fig. 2D, H**)(Hendrickson and Drucker, 1992). Thus, cone subtypes in human retinal organoids displayed distributions, gene expression patterns, and morphologies similar to cones of the human retina.

We next examined the developmental dynamics of cone subtype specification in organoids. In the human retina, S cones are generated during fetal weeks 11-34 (days 77-238), whereas LM cones are specified later during fetal weeks 14-37 (days 98-259)(Curcio et al., 1990; Xiao and Hendrickson, 2000). We tracked the ratios and densities of S and L/M cones in organoids by antibody staining over 360 days of differentiation. A significant number of cones expressing S-opsin were first observed at day 150 (**Fig. 2I, L-M**). The density of S cones leveled off at day 170 (**Fig. 2M**), at the timepoint when cones expressing L/M-opsin began to be observed (**Fig. 2J-M**). The population of L/M cones increased dramatically until day 300 (**Fig. 2K-M**) when they reached a steady-state density. Remarkably, the 20-day difference between S- and L/M-opsin expression onset in retinal organoids is similar to the 20-day difference observed in the appearance of S- and L/M- cones in the fetal retina (Xiao and Hendrickson, 2000). These observations show a temporal switch from S cone specification to L/M cone specification during retinal development.

We next conducted RNA-Seq through 250 days of iPSC-derived organoid development. We found that *S-opsin* RNA was expressed first at day 111 and leveled off at day 160, while *L/M-opsin* RNA was expressed at day 160 and remained steady after day 180, consistent with the timeline of photoreceptor maturation in organoids and fetal retinas (**Fig. 2N, Fig S1B**). Moreover, *CRX* RNA and CRX protein were expressed before opsins in organoids, similar to human development (Hoshino et al., 2017) (**Fig. 2N, Fig. S1B-G**). Thus, human organoids recapitulate many aspects of the developmental timeline of cone subtype specification observed in human retinas, providing a model system to uncover the mechanisms of these developmental changes.

Thyroid hormone signaling is necessary and sufficient for the temporal switch between S and L/M fate specification

Seminal work in mice identified thyroid hormone receptor $\beta 2$ ($Thr\beta 2$) as a critical regulator of cone subtype specification: *Thr\beta 2* mutants display a complete loss of M-opsin expression and a complete gain of S-opsin expression in cone photoreceptors (Applebury et al., 2007; Ng et al., 2001; Roberts et al., 2006). Similar roles for *Thr\beta 2* have been characterized in other organisms with highly divergent cone patterning (Sjoberg et al., 1992; Suzuki et al., 2013; Trimarchi et al., 2008). Additionally, rare human mutations in *Thr\beta 2* are reported to alter color perception, indicative of a change in the S to L/M cone ratio (Weiss et al., 2012). To directly test the role of *Thr\beta 2* in human cone subtype specification, we used CRISPR/Cas9 in human embryonic stem cells (ESCs) to generate a homozygous mutation resulting in early translational termination in the unique first exon of *Thr\beta 2* (**Fig. S2A**). Surprisingly, organoids derived from these mutant stem cells displayed no differences in cone subtype ratio from genotypically wild-type organoids (wild-type: S=62%, L/M=38%; *Thr\beta 2* KO: S=59%, L/M=41%; P=0.83). The S to L/M ratio is high for both wild-type controls and *Thr\beta 2* KO organoids likely due to variability in organoid differentiation. Thus, unlike previous suggestions based on other species, *Thr\beta 2* is dispensable for cone subtype specification in humans (**Fig. 3A-C**).

Since *Thr\beta 2* alone is not required for human cone subtype specification, we reexamined data from Weiss *et. al* (Weiss et al., 2012) and found that missense mutations in exons 9 and 10 affected both *Thr\beta 2* and another isoform of the human *Thr\beta* gene, *Thr\beta 1* (**Fig. S2A**). Thus, we asked whether *Thr\beta 1* and *Thr\beta 2* together are required for cone subtype specification in humans. To completely ablate $Thr\beta$ function (i.e. $Thr\beta 1$ and $Thr\beta 2$), we used CRISPR/Cas9 in human ESCs to delete a shared exon that codes for part of the DNA-binding domain (DBD) of *Thr\beta* (**Fig. S2A**). *Thr\beta* null mutant retinal organoids displayed a complete conversion of all cones to the S subtype (wild-type: S=27%, L/M=73%; *Thr\beta* KO: S=100%, L/M=0%; P<0.0001) (**Fig. 3D-E, H**). In these mutants, all cones expressed S-opsin and had the S cone morphology (**Fig. 3I-J**). Thus, $Thr\beta$ is required to activate L/M and to repress S cone fates in the human retina. $Thr\beta$ binds with high affinity to triiodothyronine (T3), the more active form of thyroid hormone, to regulate gene expression (Samuels et al., 1974). Depletion or addition of T3 alters the ratios of

S to M cones in rodents (Glaschke et al., 2010; Glaschke et al., 2011; Roberts et al., 2006). Since L/M cones differentiate after S cones, we hypothesized that T3 acts through Thr β late in retinal development to induce L/M cone fate and repress S cone fate. One prediction of this hypothesis is that addition of T3 early in development will induce L/M fate and repress S fate. To test this model, we added 20nM T3 to ESC- and iPSC-derived organoids starting from days 20-50 to day 200 of differentiation. We observed a dramatic conversion of cone cells to L/M fate (wild-type: S=27%, L/M=73%; wild-type + T3: S=4%, L/M=96%; P<0.01) (**Fig. 3F, H, Fig. S2B**). Thus, early addition of T3 is sufficient to induce L/M fate and suppress S fate.

To test whether T3 acts specifically through Thr β to control cone subtype specification, we differentiated *Thr β* mutant organoids with early T3 addition. *Thr β* mutation completely suppressed the effects of T3, generating organoids with only S cones (wild-type + T3: S=4%, L/M=96%; *Thr β* KO + T3: S=100%, L/M=0%; P<0.0001) (**Fig. 3F-H**). We conclude that T3 acts through Thr β to promote L/M cone fate and suppress S cone fate.

We confirmed the regulation of L/M-opsin expression through thyroid hormone signaling in a retinoblastoma cell line, which expresses L/M-opsin when treated with T3 (**Fig. S2C-D**) (Liu et al., 2007). T3-induced activation of *L/M-opsin* expression was suppressed upon RNAi knock down of *Thr β* (**Fig. S2E-F**), similar to the suppression observed in human organoids. Interestingly, in organoids, early T3 addition not only converted cone cells to L/M fate but also dramatically increased cone density (**Fig. 3F, K**). Moreover, T3 acts specifically through Thr β to control cone density (**Fig. 3G, K**). Early T3 addition may increase cone density by advancing and extending the temporal window of L/M cone generation.

Together, these results demonstrate that T3 signals through Thr β to promote L/M cone fate and repress S cone fate in developing human retinal tissue.

Dynamic expression of thyroid hormone-regulating genes during development

Our data suggest that temporal control of thyroid hormone signaling determines the S vs. L/M cone fate decision, whereby low signaling early induces S fate and high signaling late induces L/M fate. Thyroid hormone exists largely in two states: Thyroxine (T4), the most abundant circulating form of thyroid hormone, and T3, which binds thyroid hormone receptors with high affinity (Samuels et al., 1974; Schroeder et al., 2014). Since the culture media contains

low amounts of T3 and T4, we hypothesized that the retina itself could modulate and/or generate thyroid hormone to control subtype fates.

Conversion of T4 to T3 occurs locally in target tissues to induce gene expression responses (Darras et al., 2015; Dentice et al., 2013). Deiodinases, enzymes that modulate the levels of T3 and T4, are expressed in the retinas of mice, fish, and chicken (Bagci et al., 2015; Bonezzi et al., 2018; Bruhn and Cepko, 1996; Guo et al., 2014; Ng et al., 2010; Trimarchi et al., 2008). Therefore, we predicted that T3- and T4-degrading enzymes would be expressed during early human eye development to reduce thyroid hormone signaling and specify S cones, while T3-producing enzymes, carriers, and transporters would be expressed later in human eye development to increase signaling and generate L/M cones.

To test these predictions, we examined gene expression across 250 days of organoid development. The expression patterns of thyroid hormone-regulating genes were grouped into three classes: changing expression (**Fig. 4A**), consistent expression (**Fig. 4B**), or no expression (**Fig. 4C**). Interestingly, Deiodinase 3 (*DIO3*), an enzyme that degrades T3 and T4 (Dentice et al., 2013), was expressed at high levels early in organoid development but at low levels later (**Fig. 4A**). Conversely, Deiodinase 2 (*DIO2*), an enzyme that converts T4 to active T3 (Dentice et al., 2013), was expressed at low levels early but then dramatically increased over time (**Fig. 4A**). We examined RNA-Seq data from Hoshino *et. al* (Hoshino et al., 2017) and found that developing human retinas display similar temporal changes in expression of *DIO3* and *DIO2* (**Fig. S3A**). Deiodinase 1 (*DIO1*), which regulates T3 and T4 predominantly in the liver and kidney (Bianco et al., 2002), was not expressed in organoids or retinas (**Fig. 4C, S3C**). Thus, the dynamic expression of *Dio3* and *Dio2* supports low thyroid hormone signaling early in development to generate S cones and high thyroid hormone signaling late to produce L/M cones.

Consistent with a role for high thyroid hormone signaling in the generation of L/M cones later in development, expression of transthyretin (*TTR*), a thyroid hormone carrier protein, increased during organoid and retinal development (**Fig. 4A, S3A**)(Hoshino et al., 2017). In contrast, albumin (*ALB*) and thyroxine-binding globulin (*SERPINA7*), other carrier proteins of T3 and T4, were not expressed in organoids or retinas (**Fig. 4C, S3C**)(Hoshino et al., 2017).

T3 and T4 are transported into cells via membrane transport proteins (Sharlin et al., 2011). The T3/T4 transporters *SLC7A5* and *SLC7A8* increased in expression during organoid

differentiation (**Fig. 4A**). Additionally, two T3/T4 transporters, *SLC3A2* and *SLC16A2*, were expressed at high and consistent levels throughout organoid development (**Fig. 4B**). Other T3/T4 transporters (*SLC16A10*, *SLCO1C1*, *SLC5A5*) were not expressed in organoids (**Fig. 4C**), suggesting tissue-specific regulation of T3/T4 uptake. We observed similar expression patterns of T3/T4 transporters in human retinas (**Fig. S3A-C**)(Hoshino et al., 2017).

We next examined expression of transcriptional activators and repressors that mediate the response to thyroid hormone. Consistent with *Thrb* expression in human cones (Lee et al., 2006), expression of *Thrb* in organoids increased with time as cone cells were specified (**Fig. 4A**). Expression of thyroid hormone receptor α (*Thra*) similarly increased with time (**Fig. 4A**). Thyroid hormone receptor cofactors, co-repressor *NCoR2* and co-activator *MED1*, were expressed at steady levels during organoid differentiation (**Fig. 4B**). Similar temporal expression patterns were observed in human retinas (**Fig. S3A-B**)(Hoshino et al., 2017). Thus, our data suggest that expression of *Thrb* and other transcriptional regulators enables gene regulatory responses to differential thyroid hormone levels.

A complex pathway controls production of thyroid hormone. Thyrotropin-releasing hormone (TRH) is produced by the hypothalamus and other neural tissue. TRH stimulates release of thyroid-stimulating hormone α (CGA) and thyroid-stimulating hormone β (TSH β) from the pituitary gland. CGA and TSH β bind the thyroid-stimulating hormone receptor (TSHR) in the thyroid gland. T3 and T4 production requires Thyroglobulin (TG), the substrate for T3/T4 synthesis, and Thyroid Peroxidase (TPO), an enzyme which iodinates tyrosine residues in TG (Barrett, 2012). Interestingly, *TRH* was expressed in organoids and retinas but the other players were not (**Fig. 4A-C, S3A-C**)(Dubovy et al., 2017; Hoshino et al., 2017; Martino et al., 1980), suggesting that the retina itself does not generate thyroid hormone, rather it modulates the relative levels of T3 and T4 and expresses TRH to signal for thyroid hormone production in other tissues.

Therefore, the temporal expression of thyroid hormone signaling regulators supports our model that the retina intrinsically controls T3 and T4 levels, ensuring low thyroid hormone signaling early to promote S fate and high thyroid hormone signaling late to specify L/M fate (**Fig. 4D**).

Discussion

Organoids provide a powerful system to determine the mechanisms of human development. Model organism and epidemiological studies generate important hypotheses about human biology that are often experimentally intractable. This work shows that organoids enable direct testing of hypotheses in developing human tissue.

Our studies identify temporal regulation of thyroid hormone signaling as a mechanism controlling cone subtype specification in humans. Consistent with our findings, preterm human infants with low T3/T4 have an increased incidence of color vision defects (Dowdeswell et al., 1995; Rovet and Simic, 2008; Simic et al., 2010; Yassin et al., 2018). Moreover, our identification of a mechanism that generates one cone subtype while suppressing the other is critical for developing organoid-based transplant therapies to treat diseases such as color blindness, retinitis pigmentosa, and macular degeneration (Barnea-Cramer et al., 2016; Lamba et al., 2009; Pearson et al., 2012; Tucker et al., 2011).

Acknowledgements:

We thank Alex Kolodkin, Jeremy Nathans, and members of the Johnston lab for helpful comments on the manuscript.

Funding: KCE was a Howard Hughes Medical Institute Gilliam Fellow and was supported by the National Science Foundation Graduate Research Fellowship Program under Grant No. 1746891. RJJ was supported by the Pew Scholar Award 00027373.

Author Contributions: KCE: conception, data acquisition, new reagent contribution, data analysis, data interpretation, drafted and revised manuscript

SEH: data acquisition, data interpretation

KAH: data acquisition, data analysis, data interpretation

BB: data analysis, data interpretation

PWZ: new reagent contribution

XC: new reagent contribution

VMS: new reagent contribution

DSW: new reagent contribution

SH: data interpretation

JT: data analysis, data interpretation

KW: data acquisition, new reagent contribution

DJZ: data acquisition, new reagent contribution

RJJr: conception, data interpretation, drafted and revised manuscript

Competing interests: None.

Data and materials availability: RNA-seq data are available on GEO. All other data and methods are in the Supplemental Materials.

Chapter II Figures:

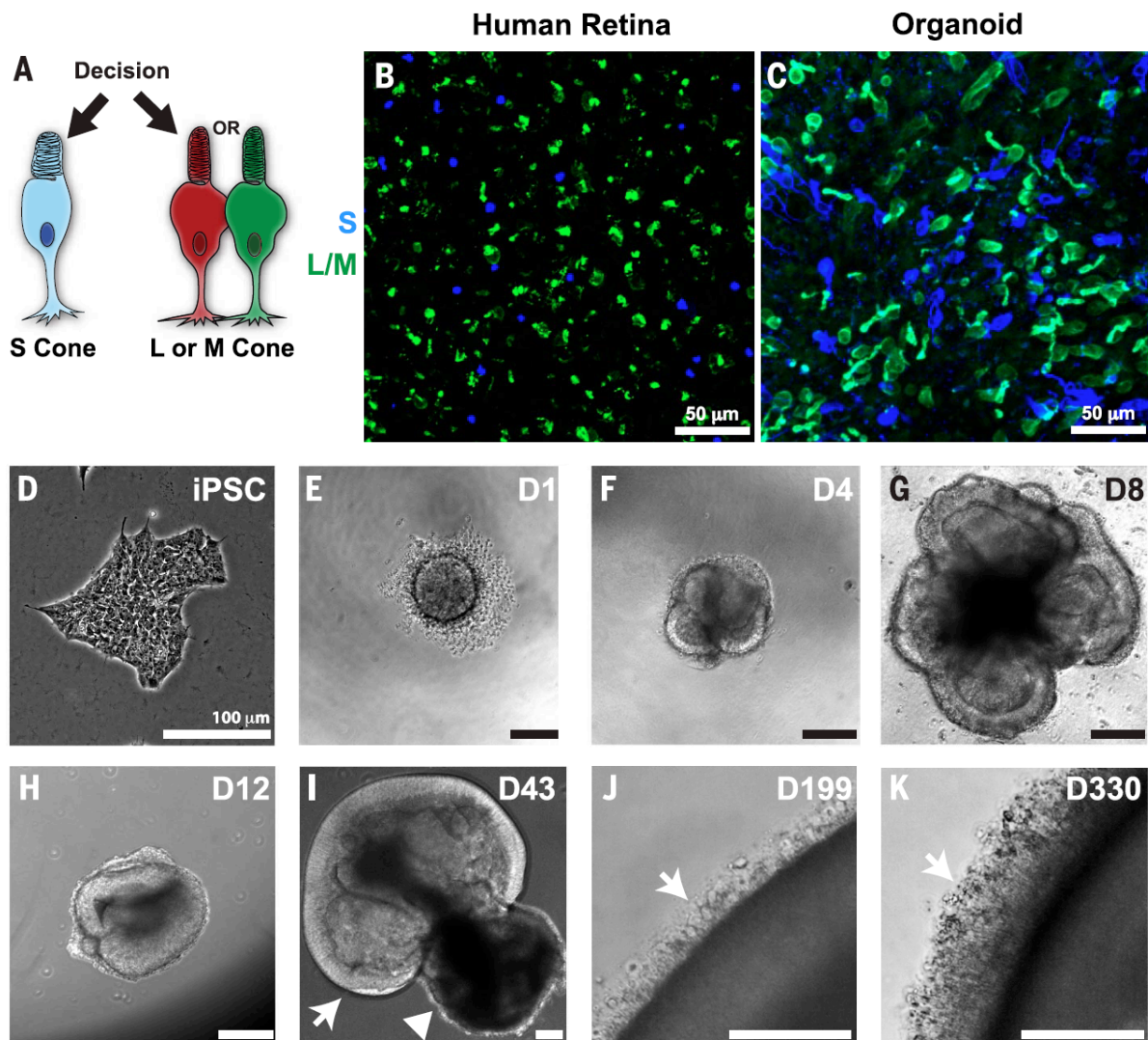


Figure 1. S and L/M cone generation in human retinal organoids

A) Decision between S and L/M cone subtype fate.

B-C) S-opsin (blue) L/M-opsin (green).

B) Human adult retina age 53.

C) iPSC-derived organoid, day 200 of differentiation.

D-K) Bright field images of organoids derived from iPSCs.

D) Undifferentiated iPSCs.

E) Day 1: aggregation.

F) Day 4: formation of neuronal vesicles.

G) Day 8: differentiation of retinal vesicles.

H) Day 12: manual isolation of retinal organoid.

I) Day 43: arrow indicates developing retinal tissue, arrowhead indicates developing retinal pigment epithelium (RPE).

J) Day 199: arrow indicates outer segments.

K) Day 330: arrow indicates outer segments.

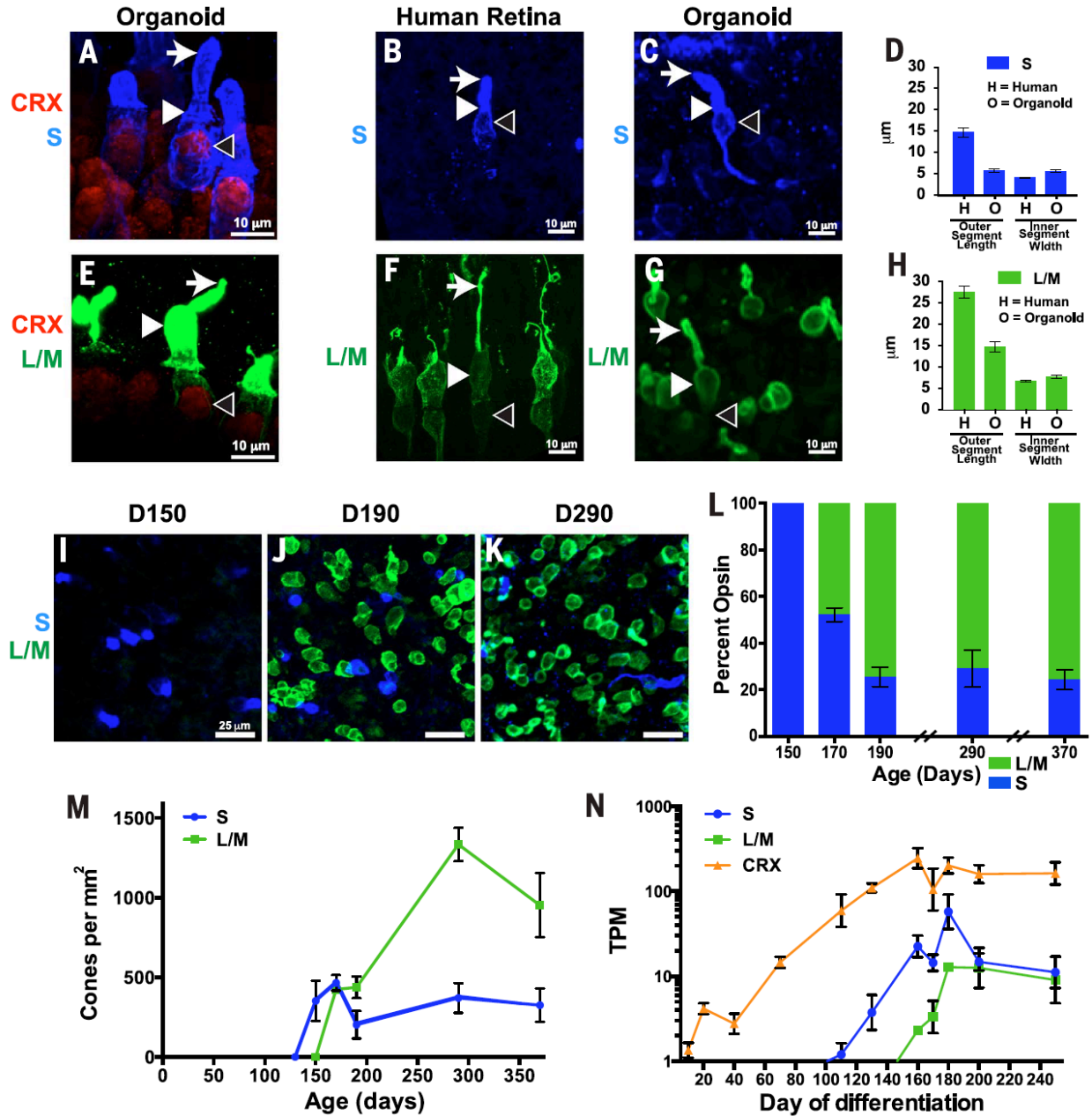


Figure 2. Human cone subtype specification is recapitulated in organoids

A-K) S-opsin (blue) and L/M-opsin (green) were examined in human iPSC-derived organoids (2A, C-E, G-M) and human retinas (2B, D, F, H).

A-C, E-G) Arrows indicate outer segments, full arrowheads indicate inner segments, empty arrowheads indicate nuclei.

A,E) CRX (a general marker of photoreceptors) is expressed in S cones and L/M cones.

B-D) S cones display short outer segments and thin inner segments in both human retinas and organoids.

F-H) L/M cones display long outer segments and wide inner segments in both human retinas and organoids.

D,H) Quantification of outer segment lengths and inner segment widths (adult retina: L/M, n=13, S, n=10; organoid: L/M, n=35, S, n=42).

I-N) S cones are generated before L/M cones in organoids.

L) Ratio of S:L/M cones during organoid development.

M) Density of S and L/M cones during organoid development.

N) *S-opsin* expression precedes *L/M-opsin* expression in human iPSC-derived organoids. *CRX* expression starts before opsin expression. TPM=Transcripts per Kilobase Million.

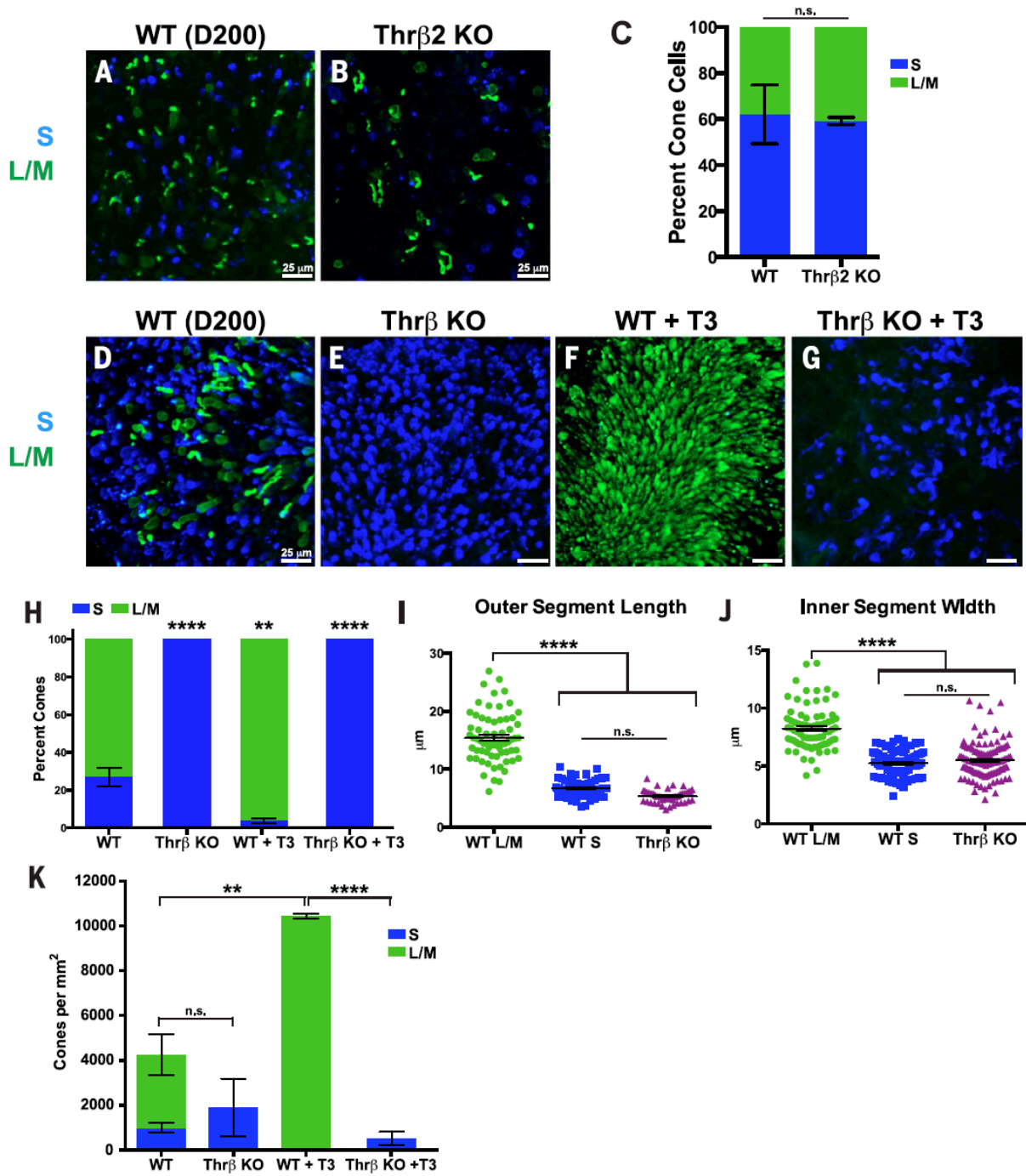


Figure 3. Thyroid hormone signaling is necessary and sufficient for the temporal switch between S and L/M fate specification

A-K) S-opsin (blue) and L/M-opsin (green) were examined in human ESC-derived organoids.

A) Wild-type (WT)

B) *Thrβ2* early termination mutant (*Thrβ2* KO).

- C)** Quantification of A-B (WT n=3, *Thrb*² KO n=3)
- D)** Wild-type (WT)
- E)** *Thrb* Knockout (*Thrb* KO)
- F)** WT treated with 20 nM T3 (WT + T3).
- G)** *Thrb* KO treated with 20 nM T3 (*Thrb* KO + T3).
- H)** Quantification of D-E (WT, n=9; *Thrb* KO, n=3; WT + T3, n=6; *Thrb* KO + T3, n=3. Tukey's multiple comparisons test comparisons test: WT vs *Thrb* KO, P<0.0001; WT vs WT + T3, P < 0.01; WT + T3 vs *Thrb* KO + T3, P<0.0001).
- I)** Length of outer segments (WT, L/M n=66 cells, WT, S n=66 cells, *Thrb* KO, n=50 cells. Tukey's multiple comparisons test: WT L/M vs. WT SW, P<0.0001; WT L/M vs. *Thrb* KO, P<0.0001; WT S vs. *Thrb* KO, not significantly different).
- J)** Width of inner segments (WT, L/M n=78 cells; WT, S n=78 cells; *Thrb* KO, n=118 cells. Tukey's multiple comparisons test: WT L/M vs. WT SW, P<0.0001; WT L/M vs. *Thrb* KO, P<0.0001; WT S vs. *Thrb* KO, not significantly different).
- K)** T3 acts through *Thrb* to increase total cone number. Quantification of density of S and L/M cones. (WT, n=6; *Thrb* KO, n=3; WT + T3, n=3; *Thrb* KO + T3, n=3. Tukey multiple comparisons test between total cone numbers: WT vs. *Thrb* KO, not significantly different; WT vs WT + T3, P<0.01; WT + T3 vs *Thrb* KO + T3, P<0.0001).

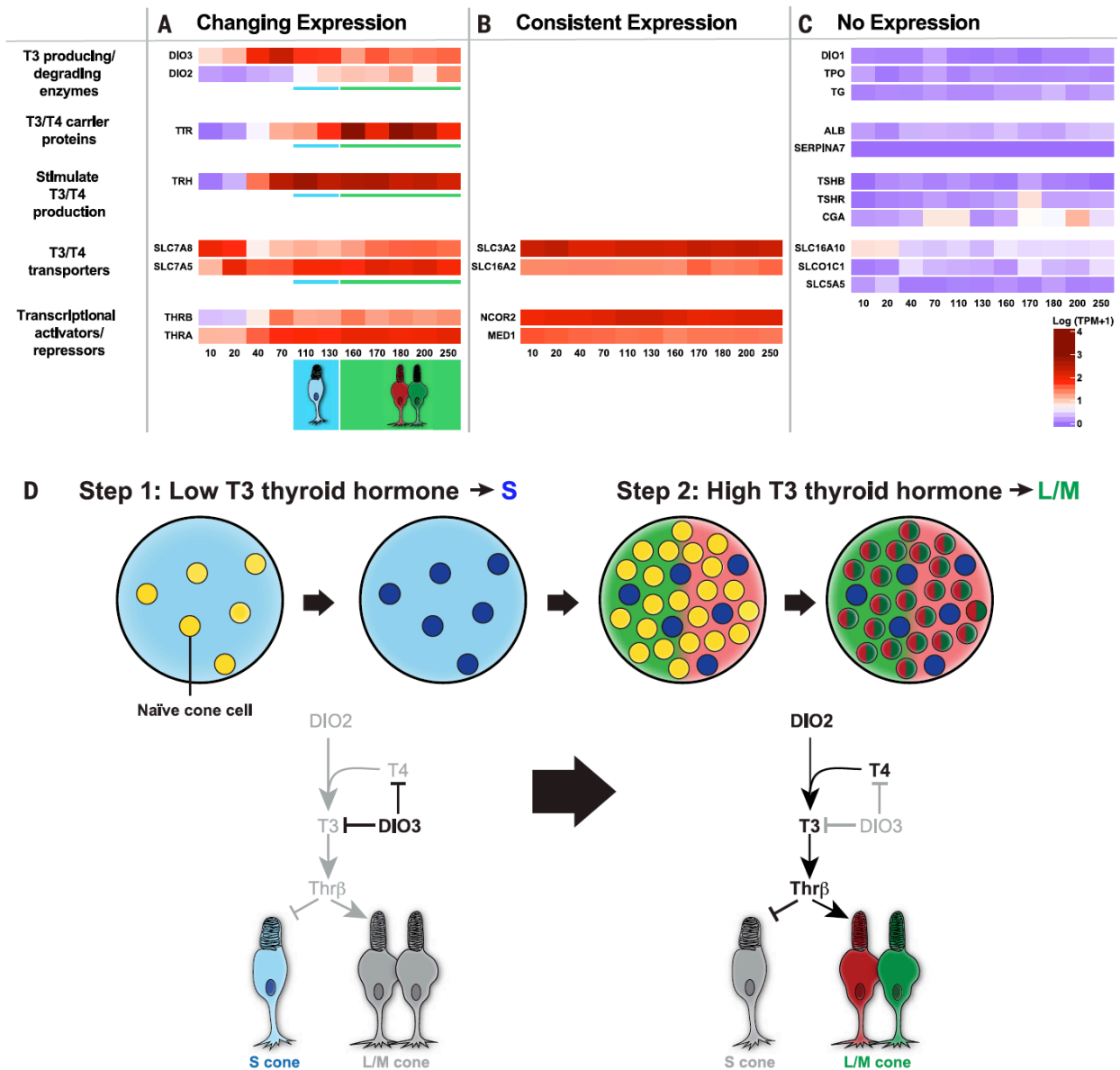


Figure 4. Dynamic expression of thyroid hormone signaling regulators during development
A-C) Heat maps of Log(Transcripts per Kilobase Million (TPM) + 1) values for genes with (A) changing expression, (B) consistent expression, and (C) no expression. Numbers at the bottom of heat maps indicate organoid age in days.

D) Model of the temporal mechanism of cone subtype specification in humans. For simplicity, only the roles of DIO3 and DIO2 are illustrated. In step 1, expression of DIO3 degrades T3 and T4 leading to S cone specification. In step 2, expression of DIO2 converts T4 to T3 to signal Thrβ to repress S and induce L/M cone fate.

Materials and methods

Cell Lines

H7 ESC (WA07, WiCell) and episomal-derived EP1.1 iPSC lines were used (Bhise et al., 2013). Pluripotency of EP1.1 was evaluated previously with antibodies for NANOG, OCT4, SOX2, SSEA4 (Wahlin et al., 2017). Stem cells were maintained in mTeSR1 (Stem Cell Technologies) on 1% (vol/vol) Matrigel-GFR™ (354230, BD Biosciences) coated dishes and grown in a 37°C HERAcell 150i incubator at 10% CO₂ and 5% O₂ incubator (Thermo Fisher Scientific). Cells were passaged every 3-6 days according to confluence as in Wahlin *et. al* (Wahlin et al., 2017). Cells were passaged with Accutase (SCR005, Sigma) for 7–10 minutes and dissociated to single cells. Cells in Accutase were added 1:2 to mTeSR1 plus 5 μM Blebbistatin (Bleb; B0560, Sigma), pelleted at 80 g for 5 minutes, and suspended in mTeSR1 plus Bleb and plated at 5,000 cells per well in a 6 well plate. After 48 hours, cells were fed with mTeSR1 (without Bleb) every 24 hours until the next passage. To minimize cell stress, no antibiotics were used.

WERI-Rb1 retinoblastoma cells were obtained from ATCC and maintained in RPMI + supplement media. Cells were grown in a 37°C HERAcell 150i 5% CO₂ incubator (Thermo Fisher Scientific) and passaged every 3-4 days at $\sim 1 \times 10^5 - 2 \times 10^6$ cells/mL in uncoated flasks. Cells were routinely tested for mycoplasma using MycoAlert (LT07, Lonza).

Cell Culture Media

Stem Cell media: mTeSR1 (StemCell Technologies)

E6 supplement: 970 ug/mL Insulin (11376497001, Roche), 535 ug/mL holo-transferrin (T0665, Sigma), 3.20 mg/mL L-ascorbic acid (A8960, Sigma), 0.7 ug/mL sodium selenite (S5261, Sigma).

BE6.2 media for early retinal differentiation: 2.5% E6 supplement (above), 2% minus vitamin A (12587010, Gibco), 1% Glutamax (35050061, Gibco), 1% NEAA (11140050, Gibco), 1mM Pyruvate (11360070, Gibco), and 0.87 mg/mL NaCl in DMEM (11885084, Gibco).

LTR (Long-Term Retina) media: 25% F12 (11765062, Gibco) with 2% B27 (17504044, Gibco), 10% heat inactivated FBS (16140071, Gibco), 1mM Sodium Pyruvate, 1% NEAA, 1% Glutamax and 1 mM taurine (T-8691, Sigma) in DMEM (11885084, Gibco)

RPMI + supplement media: 10% heat inactivated FBS, 2.5% penicillin (30-002-CI, Corning) in RPMI Medium 1640 (Gibco).

Thyroid hormone treatment: For organoids, 20 nM T3 (T6397, Sigma) in LTR. This concentration is based on T3 treatment levels for mouse retinal explant experiments (Roberts et al., 2006). For WERI-Rb1 cells, 100 nM T3 (T6397, Sigma) in RPMI + supplement media, similar to previous experiments inducing L/M opsin expression in this cell line (Liu et al., 2007).

Organoid differentiation

Organoids were differentiated from H7 WA07 ESCs or EP1.1 iPSCs as described in (Wahlin et al., 2017) with minor variations (**Fig. S4**).

Pluripotent stem cells were well-maintained, and only cultures with minimal to no spontaneous differentiation were used for aggregation. To aggregate, cells were passaged in Accutase at 37°C for 13 min to ensure complete dissociation. Cells were seeded in 50 ul of mTeSR1 at 3,000 cells/well into 96-well ultra-low adhesion round bottom Lipidure coated plates (51011610, NOF). Cells were placed in hypoxic conditions (10% CO₂ and 5% O₂) for 24 hours to enhance survival. Cells naturally aggregated by gravity over 24 hours.

On day 1, cells were moved to normoxic conditions (5% CO₂). On days 1-3, 50 uLs of BE6.2 media containing 3 μM Wnt inhibitor (IWR1e: 681669, EMD Millipore) and 1% (v/v) Matrigel were added to each well. On days 4-9, 100 uLs of media were removed from each well, and 100 uLs of media were added. On days 4-5, BE6.2 media containing 3 μM Wnt inhibitor and 1% Matrigel was added. On days 6-7, BE6.2 media containing 1% Matrigel was added. On days 8-9, BE6.2 media containing 1% Matrigel and 100 nM Smoothed agonist (SAG: 566660, EMD Millipore) was added.

On day 10, aggregates were transferred to 15 mL tubes, rinsed 3X in DMEM (11885084, Gibco), and resuspended in BE6.2 with 100 nM SAG in untreated 10 cm polystyrene petri dishes. From this point on, media was changed every other day. Aggregates were monitored and manually separated if stuck together or to the bottom of the plate.

On days 13-16, LTR media with 100 nM SAG was added.

Between days 11 and 16, retinal vesicles were manually dissected using sharpened tungsten needles. After dissection, cells were transferred into 15 mL tubes and washed 2X with 5 mLs of DMEM.

On days 16-20, cells were maintained in LTR and washed 2X with 5 mLs of DMEM, before being transferred to new plates to wash off dead cells.

To increase survival and differentiation, 1 μ M all-trans retinoic acid (ATRA; R2625; Sigma) was added to LTR medium from days 20-130. 10 μ M Gamma-secretase inhibitor (DAPT; 565770, EMD Millipore) was added to LTR from days 28-42.

Organoids were grown at low density (10-20 per 10 cm dish, 2-3 per well in 6 well plate) to reduce aggregation.

CRISPR mutations

Cell line: All mutations were generated in H7 ESCs. Cells were modified to express an inducible Cas9 element. First, the puromycin-Cas9 donor plasmid was modified. The *Puromycin* N-acetyl transferase gene (puromycin-resistance gene) was replaced with Blasticidin S deaminase gene (blasticidin-resistance gene) using Xba I-Xho I restriction enzyme sites in the plasmid puromycin-Cas9 donor (58409, Addgene). This plasmid is referred to as the blast-Cas9 donor plasmid.

The integration of the targeting vectors into a previously genetically modified H7 human ESC line (Sluch et al., 2017) was performed as follows: 0.25 million H7^{Brn3B::tdTomato} ES cells at 50% confluence were transduced using a DNA-In Stem kit (MTI-Globalstem, USA) with three plasmids (1 μ g each): Blast-Cas9 donor, M2rtTA donor (AAVS1-neo-M2rtTA: 60843, Addgene), and pSpCas9 (BB) plasmid (px459 v2.0: 62988, Addgene). gRNA sequences are listed below in the gRNA primer table. Cells were treated with Blasticidin (5 μ g/ml) and Geneticin (200 μ g/ml) for 5 days. Individual clones with both Blasticidin and Neomycin resistance survived, and were picked using sterile pipette tips and transferred to 96-well plates for clone identification. Positive clones carrying the correct insertion in both alleles were confirmed by PCR. Genotyping primers are listed below. Doxycycline induction was confirmed by qPCR and the verified clone iCas9 H7^{Brn3B::tdTomato-24} was used for further experiments.

Table 1. Homology Arm Primers

Primers for Cas9	Primer Name	Primer Sequence
Left arm	Left_ARM_F2	GGCCCTGGCCATTGTCACTT
	Cas9_Blast_R1	AGCAATTCACGAATCCCAAC
Right arm	Cas9_RARM_R1	CACCTTGTACTCGTCGGTGA
	Right_ARM_R1	GGAACGGGGCTCAGTCTGT
Primers for rtTA		
Left arm	Left_ARM_F2	GGCCCTGGCCATTGTCACTT
	rtTA_Neo_R1	GGCCATTTTCCACCATGATA
Right arm	rtTA_RARM_F2	GCTGATTATGATCCTGCAAGC
	Right_ARM_R1	GGAACGGGGCTCAGTCTGT

Cloning gRNA plasmids: Plasmids for gRNA transfection were generated using pSpCas9(BB)-P2A-Puro plasmid modified from the pX459_V2.0 plasmid (62988, Addgene) by replacing T2A with a P2A sequence. gRNAs were cloned into the vector following the Zhang Lab protocol:

https://media.addgene.org/cms/filer_public/e6/5a/e65a9ef8-c8ac-4f88-98da-3b7d7960394c/zhang-lab-general-cloning-protocol.pdf

Table 2. gRNA Primers

gRNA Primer Name	Primer Sequence
ThrB2_St_gRNA1_F	caccgAAAATACGCGTAATAATCAG
ThrB2_St_gRNA1_R	aaacCCTGATTATTACGCGTATTTTc
ThrB2_exon5_gRNA_F	caccGATACAGCGGTAGTGATACCCGG
ThrB2_exon5_gRNA_R	aaacCCGGGTATCACTACCGCTGTATC
AAVS1_gRNA_F	caccGGGGCCACTAGGGACAGGAT
AAVS1_gRNA_R	aaacATCCTGTCCCTAGTGGCCCc

Transfection and mutation identification

iCas9 stem cells were passaged in Accutase at 37°C for 13 min to ensure complete dissociation. Cells were seeded at 4×10^5 in 24 well plates for 24 hours in mTeSR with 5 μ M Bleb. After 24 hours, media was removed and mTeSR was added. Cells were transfected with 2.5 μ l DNA-In Stem (GST-2130, Life Technologies), 250 ng gRNA plasmid PX459v2 containing the gRNA and Cas9-p2a-puromycin-resistance genes in 50 μ l of Opti-MEM (31985062, Gibco). Cells were incubated for 24 hours, then media was removed and mTeSR and 1 μ g Doxycycline (D9891, MilliporeSigma) were added. After 24 hours, media was removed and mTeSR, 1 μ g Doxycycline, and 0.3-1 μ g of puromycin were added. After 24 hours, media was removed, and cells were washed 1X with mTeSR, and mTeSR was then added to the well. Surviving cells were passaged at single cell density, individual colonies were isolated, and mutations were confirmed by PCR sequencing. Gene diagrams of deletions are displayed in **Fig. S2A**.

Table 3. Genotyping Primers

Primer Name	Primer Sequence
ThrB2_St_295_F	GTGCTTGGAAATCTTGATGTTTAC
ThrB2_St_296_R	GGTGGTGTATTATTCATCTTCCCTT
ThrB2_St_293_F	ATGTTTACAGAGTCCTTCAATCAC
ThrB2_St_297_R	CTGAACCAGGGAAACAAAATGAAC
ThrB2_exon5_285_F	GAAAACAGCCTGTGGTAGAGTAAA
ThrB2_exon5_287_R	GGTGTGAGCTATTTCTAAGGCATT
ThrB2_exon5_284_F	CTGTCTCCTCCAACACTGTAGATA
ThrB2_exon5_289_R	GAAATCCTGGGCCTATGTTAACTC
ThrB2_exon5_286_F	TTGCAGAAGTAAAGAAACCAGACA

Immunohistochemistry

Retinal organoids: Retinal organoids were fixed in fresh 4% formaldehyde and 5% sucrose in PBS for 1 hour. Tissue was rinsed 3X in 5% sucrose in PBS, then incubated at 4°C in 6.75% sucrose in PBS for 30 min, 12.5% sucrose in PBS for 30 min, and 25% sucrose for 2 hours-

overnight. Organoids were incubated for 2 hours in blocking solution (0.2-0.3% Triton X-100, 2-4% donkey serum in PBS). Organoids were incubated with primary antibodies in blocking solution for 16-36 hours at 4°C. Organoids were washed 3X for 30 min in PBS, and then incubated with secondary antibodies in blocking solution for 2 hours at room temperature. Organoids were incubated in 300 nM DAPI in blocking solution for 10 min and washed 3X for 15 min in PBS. At the end of staining, organoids were mounted for imaging in slow fade (S36940, Thermo Fisher Scientific).

Retinas: Human retinas were obtained from the National Disease Research Interchange (NDRI). Human retinal tissue was fixed by the NDRI in 10% formalin within 12 hours post-mortem and stored at 4°C until dissection. Retinas were dissected and whole-mounted, then rinsed 3X in PBS for 20 min, and blocked for 48 hours at 4°C in 0.3% Triton X-100 and 4% donkey serum. Retinas were stained with the same protocol as detailed above for organoids.

WERI-Rb1 cells: WERI-Rb1 cells were adhered to 0.01% w/v Poly-L-lysine slides for 1-2 hours at 37°C and 5% CO₂ and then washed 1X in PBS. WERI-Rb1 cells were fixed in fresh 4% formaldehyde for 20 min. Slides were washed with PBS 3X, and then incubated for 2 hours in blocking solution. Primary antibodies were added at 4°C overnight. Slides were washed 3X in PBS and incubated in secondary antibodies for 2 hours at room temperature in blocking solution.

Antibodies

Primary antibodies were used at the following dilutions: goat anti-SW-opsin (1:200 for organoids, 1:500 for human retinas) (Santa Cruz Biotechnology), rabbit anti-LW/MW-opsins (1:200 for organoids, 1:500 for human retinas) (Millipore), and mouse anti-CRX (1:500) (Abnova), and mouse anti-Rhodopsin (1:500) (GeneTex). All secondary antibodies were Alexa Fluor-conjugated (1:400) and made in donkey (Molecular Probes).

Microscopy and image processing

Bright field images were acquired with a Nikon TE2000 or EVOS XL Core microscope. Fluorescent images were acquired with a Zeiss LSM710, LSM780, or LSM800 laser scanning confocal microscope. Confocal microscopy was performed with similar settings for laser power, photomultiplier gain and offset, and pinhole diameter. Maximum intensity projections of z-stacks

(5–80 optical sections, 1.10 μm step size) were rendered to display all cones captured in a single organoid.

Organoid age

Opsin expression time course: EP1 iPSCs-derived organoids for time course experiments were binned into 10 day increments for analysis. Organoids were binned into day 130 (actual day 129 (n=3)), day 150 (actual day 152 (n=4)), day 170 (actual day 173 (n=2)), day 200 (actual days 194-199 (n=7)), day 290 (actual day 291 (n=3)), and day 360 (actual day 361 (n=3)). Quantification of outer segment lengths and inner segment widths were measured in day 361 organoids (n=3).

Opsin expression in different conditions: iCas9 H7 ESC-derived organoids for Thr β 2 KOs and controls were analyzed at day 200. Organoids for Thr β KO, control, and wild-type + T3 were analyzed at two time points: 2 organoids were taken at day 199 for each group, and one was taken at day 277 for each group. T3-treated organoids were taken at time points between day 195 and day 200 for different differentiations. For each treatment group and genotype, organoids were compared to control organoids grown in parallel.

RNA-Seq time course: EP1 iPSC-derived organoids were analyzed at time points ranging from day 10 to day 250 of differentiation. We took samples at day 10 (n=3), day 20 (n=2), day 35 (n=3), day 69 (n=3), day 111 (n=3), day 128 (n=3), day 158 (n=2), day 173 (n=3), day 181 (n=3), day 200 (n=3), and day 250 (n=3). RNA from individual organoids was extracted using the Zymo Direct-zol RNA Microprep Kit (Zymo Research) according to manufacturer's instructions. Libraries were prepared using the Illumina TruSeq stranded mRNA kit and sequenced on an Illumina NextSeq 500 with single 200 bp reads.

WERI-Rb1 siRNA and qPCR

Varying concentrations of WERI-Rb1 cells were seeded onto 24-well plates with 500 μL of RPMI+Supplement. After \sim 24 hours, WERI-Rb1 cells were washed once with sterile DPBS (Gibco) and suspended in media with or without 100 nM T3. Negative control siRNA 1 (Thermo Fisher Scientific) or THRB ID:s14119 siRNA (Thermo Fisher Scientific) was incubated with

lipofectamine RNAiMAX (Thermo Fisher Scientific) and Opti-Mem I Reduced Serum Medium (Thermo Fisher Scientific) according to manufacturer's instructions.

After 72 hours of incubation with RNAi, RNA was extracted from WERI-Rb1 cells using the Zymo Direct-zol RNA Microprep Kit (Zymo Research) according to manufacturer's instructions. RNA concentration was determined on a Nanodrop One (Thermo Fisher Scientific) and equal concentrations of RNA for each sample were used to generate cDNA using the RETROscript Reverse Transcription Kit (Thermo Fisher Scientific) according to manufacturer's instructions.

Quantitative Real-Time PCR was performed using TaqMan Gene Expression MasterMix (Thermo Fisher Scientific) on a StepOnePlus Real-Time PCR System (Applied Biosystems). Relative gene expression levels were determined for the genes *THRβ* (Hs00230861_m1 TaqMan probe from Thermo Fisher Scientific), and *OPNILW* & *OPNIMW* (could not discriminate) (Hs01912094_s1 TaqMan probe from Thermo Fisher Scientific) and normalized to *GAPDH* (Hs02758991_g1 TaqMan probe from Thermo Fisher Scientific) using the delta-delta ct approach. For each condition, three biological replicates were performed and three technical replicates were run on the same plate for each primer set. Fold change was calculated relative to an siRNA negative control sample lacking T3.

Measurements and Quantification

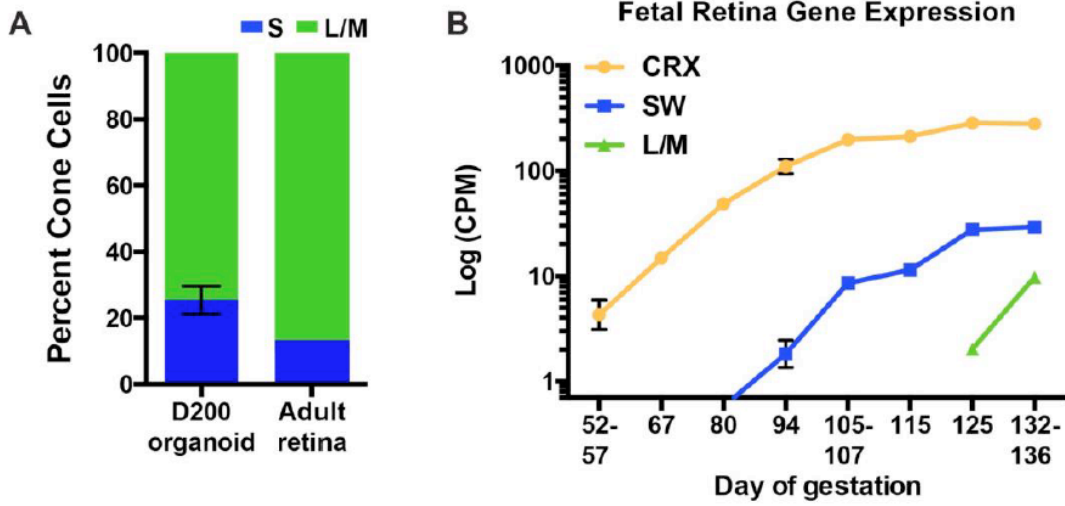
Measurements of retinal area and cell morphology were done using imageJ software. Quantifications and statistics (except for RNA-seq data) were done in GraphPad Prism, with a significance cutoff of 0.01. Statistical tests are listed in figure legends. All error bars represent the SEM.

RNA-Seq time course analysis

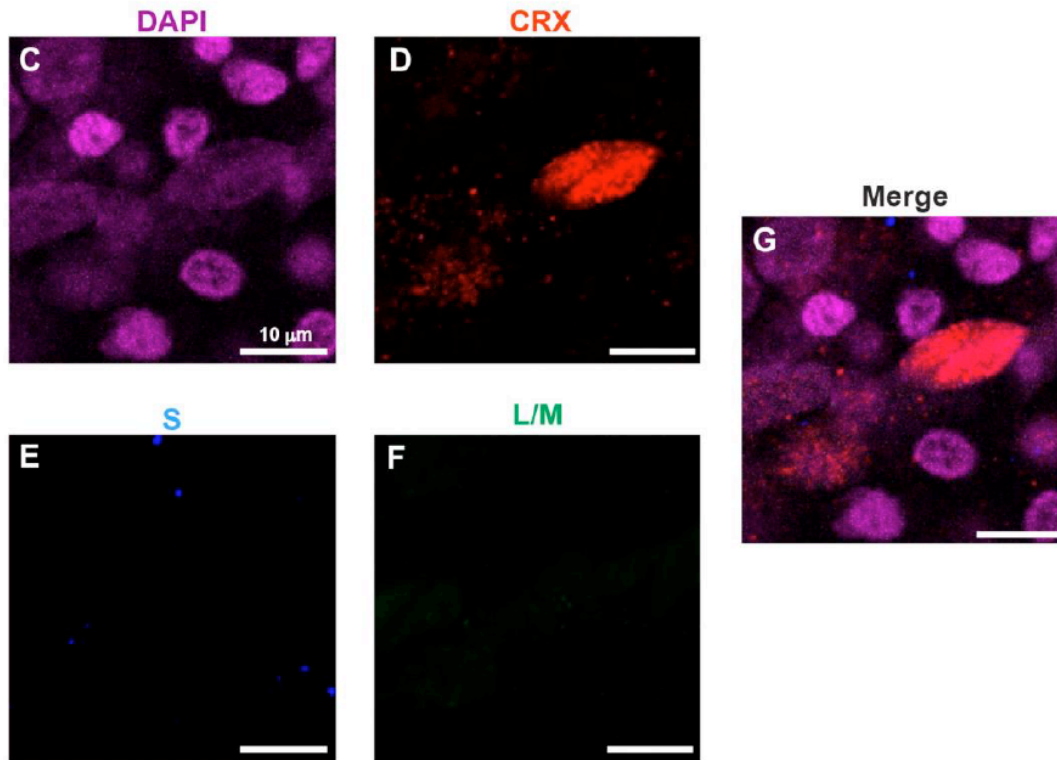
Expression levels were quantified using Kallisto (version 0.34.1) with the following parameters: "-b 100 -l 200 -s 10 -t 20 --single". The Gencode release 28 comprehensive annotation was used as the reference transcriptome (Harrow et al., 2012). Transcripts per million (TPM) values were then used to generate graphs in Prism and heatmaps in R using ggplot2. The distributions of transcripts were plotted to identify the best low TPM cutoff (**Fig. S5A**). The

threshold was determined to be $0.7 \text{ Log}(\text{TPM}+1)$, i.e. 5 TPM, and this value was used as an inflection point for heatmap. Heatmaps for **Fig. S3A-C** were made similarly, using CPM values from Hoshino, *et. al* (**Fig. S5B**) (Hoshino et al., 2017).

Supplemental Figures



Organoid Day 42

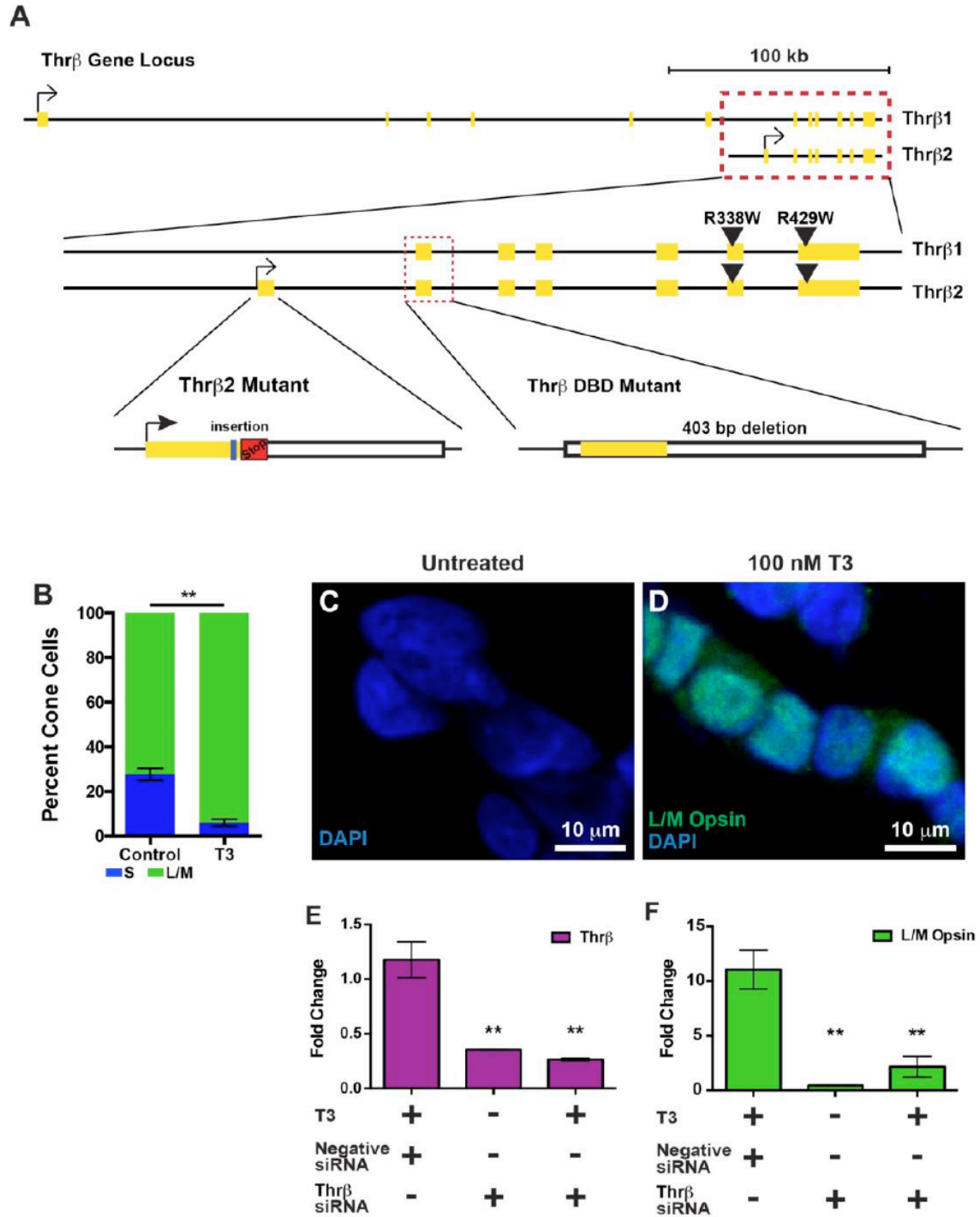


Supplemental Figure 1. *CRX* expression precedes *S-opsin* and *L/M-opsin* expression

A) Percent of S and L/M cones in day 200 organoid (n=7) and adult retina age 53 (n=1).

B) CPM values from Hoshino et. al (Hoshino et al., 2017) for *CRX*, *S*, and *L/M*.

C-G) Antibody staining for DAPI (magenta), *CRX* (red), *S-opsin* (blue), *L/M-opsin* (green).



Supplemental Figure 2. T3 signals through *Thrβ* to suppress S fate and promote L/M fate

A) Gene diagram of *Thrβ1* and *Thrβ2* locus and homozygous deletions made with CRISPR/Cas9. Arrow heads represent the point mutations described in Weiss et. al (Weiss et al., 2012). The individual was trans-heterozygous for these mutations.

B) Quantification of iPSC-derived organoids treated from day 20-200 of differentiation with 20nM T3. (Control, n=3; T3, n=3; student's t-test, P<0.001)

C-D) Fluorescence image of WERI-Rb1 cells stained with DAPI (blue) and antibody against L/M-opsin (green).

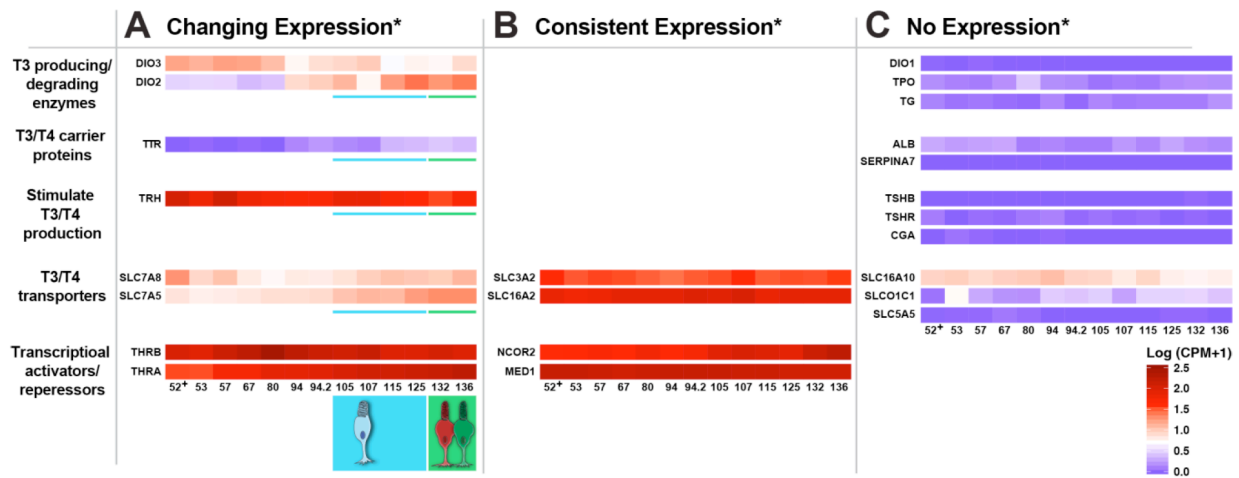
C) Untreated WERI-Rb1 cells.

D) WERI-Rb1 cells treated for 4 days with 100 nM T3.

E-F) siRNA knockdown of *Thrb* in WERI-Rb1 cells, *Thrb* and *L/M-opsin* analyzed by qPCR.

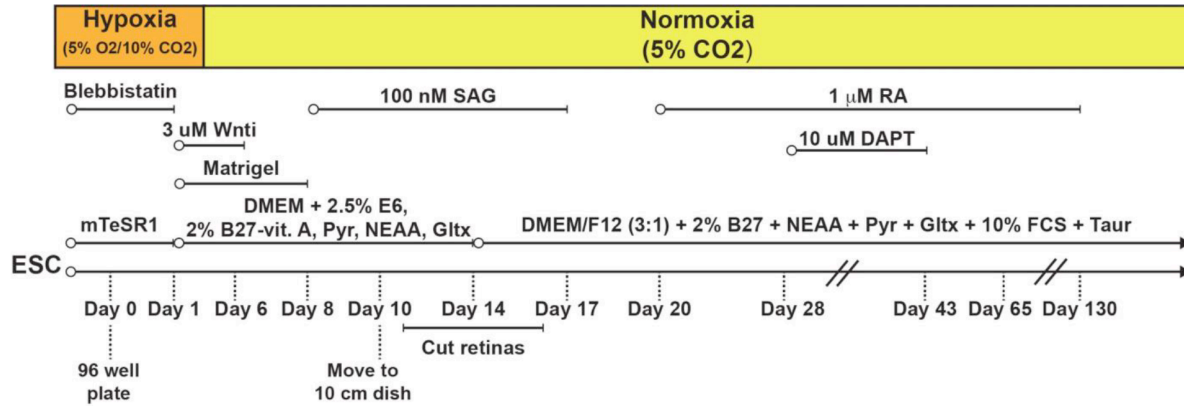
E) qPCR results of TaqMan probes for *Thrb* (n=3 biological replicates. Tukey's multiple comparisons test: Negative siRNA + T3 vs *Thrb* siRNA -T3, P<0.01; Negative siRNA+T3 vs *Thrb* siRNA + T3, P<0.01).

F) qPCR results of TaqMan probes for *L/M-opsins* (n=3 biological replicates. Tukey's multiple comparisons test: Negative siRNA + T3 vs *Thrb* siRNA -T3, P<0.01; Negative siRNA+T3 vs *Thrb* siRNA + T3, P<0.01).



Supplemental Figure 3. Expression of thyroid hormone regulators in developing human retinas

A-C) Heat maps of Log(Counts per Kilobase Million (CPM) + 1) values for genes displayed in **Fig. 4A-C**. Numbers at the bottom of heat maps indicate fetal age in days. Genes are categorized as in **Fig. 4A-C** for consistency. The gene expression patterns in developing fetal tissue are similar to the patterns observed in developing organoids.



Supplemental Figure 4. Differentiation protocol for retinal organoids

Abbreviations are as follows:

Gltx = Glutamax

Pyr = Sodium Pyruvate

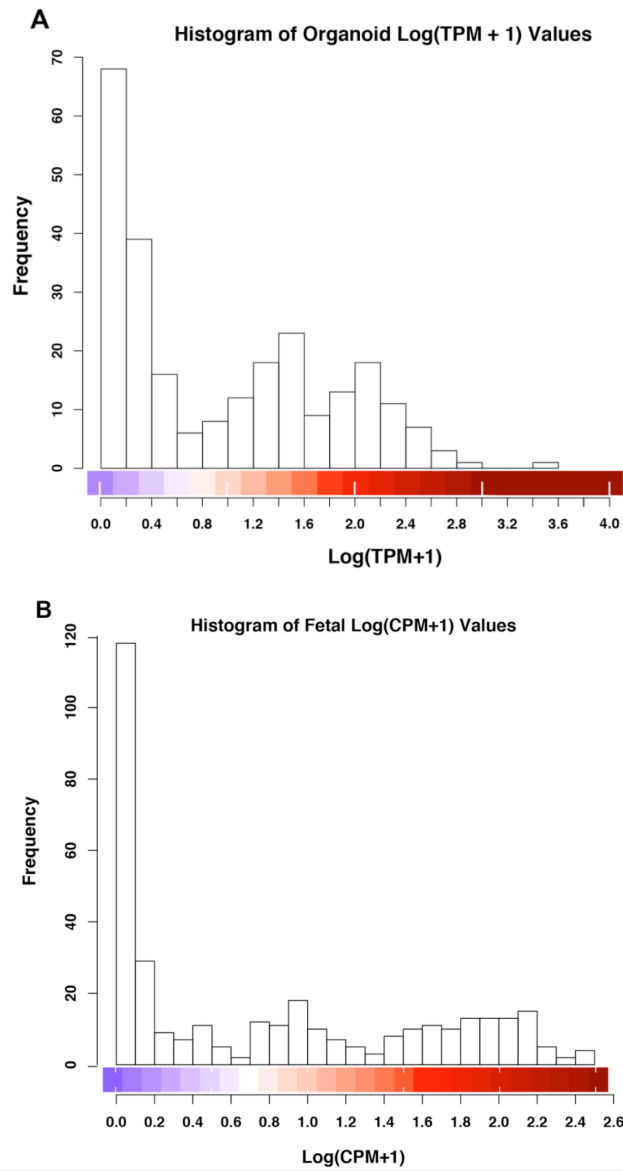
RA = Retinoic Acid

SAG = Smoothend Agonist

Taur = Taurine

Vit. A = vitamin A

Wnti = Wnt inhibitor



Supplemental Figure 5. Histogram of expression values used to identify the inflection point in the heat map of transcript expression

A) Histogram of TPM values used to identify the inflection point in the heat map included in **Fig. 4A-C**.

B) Histogram of CPM values from Hoshino et. al (Hoshino et al., 2017) to identify the inflection point in the heat map included in **Fig. S3A-C**.

Chapter III

Modeling Binary and Graded Cone Cell Fate Patterning in the Mouse Retina

This chapter describes two different types of cell fate specification, binary and graded, that give rise to a reproducible pattern of cone cells in the mouse retina. These two mechanisms of fate specification are based on different responses to the same morphogen; thyroid hormone. Cameron Avelis assisted in creating a program to identify photoreceptor cells in immunofluorescence images of the mouse retina. Elijah Roberts assisted in data analysis, computational modeling of the cell fate specification systems, and writing sections of the manuscript. This chapter is written in the form of a manuscript currently under revision at PLOS Computational Biology.

Modeling binary and graded cone cell fate patterning in the mouse retina

Kiara C. Eldred¹, Cameron Avelis², Robert J. Johnston Jr.^{1*}, and Elijah Roberts^{2*}

Abstract

Nervous systems are incredibly diverse, with myriad neuronal subtypes defined by gene expression. How binary and graded fate characteristics are patterned across tissues is poorly understood. Expression of opsin photopigments in the cone photoreceptors of the mouse retina provides an excellent model to address this question. Individual cones express S-opsin only, M-opsin, or both S-opsin and M-opsin. These cell populations are patterned along the dorsal-ventral axis, with greater M-opsin expression in the dorsal region and greater S-opsin expression in the ventral region. Thyroid hormone signaling plays a critical role in activating M-opsin and repressing S-opsin. Here, we developed an image analysis approach to identify individual cone cells and evaluate their opsin expression from immunofluorescence imaging tiles spanning roughly 6 mm along the D-V axis of the mouse retina. From analyzing the opsin expression of ~250,000 cells, we found that cones make a binary decision between S-opsin only and co-expression competent fates. Co-expression competent cells express graded levels of S- and M-opsins, depending nonlinearly on their position in the dorsal-ventral axis. M- and S-opsin expression display differential, inverse patterns. Using these single-cell data, we developed a quantitative, probabilistic model of cone cell decisions in the retinal tissue based on thyroid hormone signaling activity. The model recovers the probability distribution for cone fate patterning in the mouse retina and describes a minimal set of interactions that are necessary to reproduce the observed cell fates. Our study provides a paradigm describing how differential responses to regulatory inputs generate complex patterns of binary and graded cell fates.

Author Summary

The development of a cell in a mammalian tissue is governed by a complex regulatory network that responds to many input signals to give the cell a distinct identity, a process referred to as cell-fate specification. Some of these cell fates have binary on-or-off gene expression patterns, while others have graded gene expression that changes across the tissue. Differentiation of the photoreceptor cells that sense light in the mouse retina provides a good example of this process. Here, we explore how complex patterns of cell fates are specified in the mouse retina by building a computational model based on analysis of a large number of photoreceptor cells from microscopy images of whole retinas. We use the data and the model to study what exactly it means for a cell to have a binary or graded cell fate and how these cell fates can be distinguished from each other. Our study shows how tens-of-thousands of individual photoreceptor cells can be patterned across a complex tissue by a regulatory network, creating a different outcome depending upon the received inputs.

Introduction

How the numerous neuronal subtypes of the vertebrate nervous system are patterned is an ongoing puzzle in developmental neurobiology. Are neuronal subtypes distinct states generated by binary gene expression decisions? Or are they highly complex with ranges of graded gene expression? The answers likely lie somewhere in between, with some genes expressed in a simple switch-like fashion and other genes expressed across a range of levels to define cell fate. A challenge is to understand how cells interpret regulatory inputs to generate complex patterns of binary and graded cell fates across tissues. Here, we address this question in the context of cone photoreceptor patterning in the mouse retina.

Photoreceptors detect and translate light information into electrical signals, triggering the neuronal network yielding visual perception. There are two main classes of image-forming photoreceptors: rods and cones. Rods are mainly used in night vision, while cones are used in daytime and color vision. In most mammals, cones express S-opsin, which is sensitive to blue or UV-light, and M-opsin, which is sensitive to green light (Calderone and Jacobs, 1995; Wang et al., 2011b).

The common laboratory mouse, *Mus musculus*, displays complex patterning of cone opsin expression across its retina, providing an excellent system to study binary and graded features of cell fate specification. The dorsal third of the retina is mostly comprised of cones that express M-opsin, and a minority that exclusively express S-opsin. In the central region, most cones co-express S- and M-opsin, with small subsets that express only S- or only M-opsin. The majority of the ventral region contains cones that co-express S- and M-opsin, with significantly higher levels of S-opsin compared to M-opsin (Applebury et al., 2000; Baden et al., 2013; Calderone and Jacobs, 1995; Haverkamp et al., 2005; Rohlich et al., 1994; Szel et al., 1994). Here, we expand upon these pioneering studies to examine cone patterning along the complete dorsal to ventral (D-V) axis of the mouse retina and quantitatively model how regulatory inputs influence cone cell patterning.

Cone subtype fate is not only characterized by opsin expression, but also connectivity. Two cone subtypes have been defined primarily on connectivity to downstream bipolar neurons. 3-5% of cones are “genuine” S cones that express S-opsin only and connect to blue-cone bipolars. The remaining cones express S-opsin only, M-opsin, or both S-opsin and M-opsin and

do not connect to blue-cone bipolars (Haverkamp et al., 2005). The regulatory relationship between connectivity and opsin expression during cone subtype specification has not been established. In this work, we focus on the binary and graded nature of opsin expression, specifically examining this aspect of cone subtype fate.

Cone opsin expression is regulated by thyroid hormone (TH) signaling. TH and the nuclear thyroid hormone receptor $\text{Thr}\beta 2$ are important for activating M-opsin and repressing S-opsin expression (Roberts et al., 2006). TH exists in two main forms: T4, the circulating form, and T3, the form that binds with high affinity to nuclear receptors and acts locally to control gene expression (Samuels et al., 1974; Schroeder et al., 2014). T3 levels are highest in the dorsal part of the mouse retina and decrease ventrally (Roberts et al., 2006). Deiodinase 2 ($\text{Dio}2$), an enzyme that converts T4 to T3, is expressed at high levels in the dorsal region of the mouse retina, and is thought to maintain the gradient of T3 in the adult retina (Bedolla and Torre, 2011; Corbo et al., 2007). T3 is sufficient to induce M-opsin expression and repress S-opsin expression (Roberts et al., 2006).

$\text{Thr}\beta 2$, a receptor for TH, is expressed in all cones of the retina (Roberts et al., 2005; Sjoberg et al., 1992). $\text{Thr}\beta 2$ acts as a transcriptional repressor in the absence of T3 binding, and as a transcriptional activator when T3 is bound (Bernal, 2005). $\text{Thr}\beta 2$ activity is required for expression of M-opsin and repression of S-opsin (Applebury et al., 2007; Eldred et al., 2018; Ng et al., 2001; Pessoa et al., 2008; Roberts et al., 2006; Suzuki et al., 2013). Additionally, $\text{RXR}\gamma$, a hetero-binding partner of $\text{Thr}\beta 2$, is necessary for repressing S-opsin in dorsal cones (Roberts et al., 2005). The transcription factors $\text{Vax}2$ and Coup-TFII , which regulate and respond to retinoic acid levels, have also been implicated in photoreceptor patterning (Alfano et al., 2011; Satoh et al., 2009). For this study, we focus on modeling the contributions of TH and $\text{Thr}\beta 2$ to cell fate outcomes.

We desired to quantitatively model cone fate specification in the mouse retina. Our current theoretical understanding of cell fate determination within a tissue describes individual cell types as distinct valleys on an "epigenetic landscape" (Furusawa and Kaneko, 2012; Micheelsen et al., 2010; Wang et al., 2011a; Zhang and Wolynes, 2014; Zhou et al., 2012). Cells make fate decisions by transitioning to one of these "attractor" states on the landscape (Olsson et al., 2016). Differences in gene expression between the states give rise to phenotypic differences

between cell types. However, clustering based on single-cell transcriptomics data alone misses subpopulations unless hidden variables are accounted for (Buettner et al., 2015; Setty et al., 2019).

Recently, computational work has also focused on developing mechanistic models of cell-fate decisions (Olariu and Peterson, 2019; Rothenberg, 2019; Teles et al., 2013), especially the formation of patterns in time and space (Formosa-Jordan, 2018; Liang et al., 2015). Multiscale approaches that combine probabilistic and deterministic models of tissues at the scale of individual cells have shown promise in helping to elucidate the details of tissue patterning (Coulier and Hellander, 2018; Engblom, 2018; Engblom et al., 2018; Folguera-Blasco et al., 2019; Johnston et al., 2011). The zebrafish and goldfish retina have been studied to model cell fate decision making based on anticlustering mechanisms that give rise to a lattice structure of differentiated cell types (Cameron and Carney, 2004; Ogawa et al., 2017; Tyler et al., 2005). The highly variable arrangement of cone subtypes in the D-V axis of the mouse retina provides a paradigm to develop computational approaches that describe complex patterns of cell types across a tissue (Baden et al., 2013; Haverkamp et al., 2005; Viets et al., 2016a).

Here, we present a multiscale computational model describing the emergence of the complex arrangement of cone cells found in the adult mouse retina using both probabilistic and deterministic methods. We collect data for the model from analysis of immunofluorescence images of adult retina tissues to identify and map individual cones along the entire D-V axis of the mouse retina. Based on opsin expression in the individual cells, we find that terminally differentiated cones can be classified into two main subtypes: S-only cones and co-expression competent (CEC) cones. The S-only cones express S-opsin only, whereas the CEC cones express M- and/or S-opsins in opposing dorsal-ventral gradients, with higher levels of M-opsin in cones in the dorsal retina and higher levels of S-opsin in cones in the ventral retina. We then use the data to parameterize a mathematical model of a two-step cone patterning process. Step one is a binary choice between S-only fate and CEC fate. If CEC fate is selected, a second mechanism regulates S- and M-opsin expression in a reciprocal, graded manner, along the dorsal-ventral axis. Our quantitative modeling shows that the expression of S- and M-opsins in CEC cells are differentially activated based on dorsal-ventral patterning inputs from T3. Our model closely

recapitulates cone patterning observed in the mouse retina and provides insights into how spatial patterning inputs regulate binary and graded features of cell fate in parallel.

Results

Characterization of cone subtype patterning in the mouse retina

To globally characterize patterning of opsin expression in the adult mouse retina at 2 to 8 months old, we first examined the relative intensity of S- and M-opsin expression in the D-V and temporal-nasal (T-N) axes at low resolution for whole-mounted retinas. We immunostained and imaged S- and M-opsin proteins at 100X magnification (see Materials and Methods). Following image acquisition, we manually rotated each image so that the D-V axis was aligned vertically (**Fig. 1A, E, I**). At this resolution, individual cells cannot be identified, so we instead subdivided each image using a 25 pixel x 25 pixel grid, which is an area containing approximately one to two cells. Within each bin of the grid, we counted the number of pixels that had significant S-opsin signal alone, M-opsin signal alone, or both M- and S-opsin signals. We then normalized each bin by the total number of pixels with expression in that bin. This calculation gave us the relative density of each photoreceptor type by location in the retina (**Fig. 1B, F, J**).

Next, we quantified global differences in patterning in the D-V and temporal-to-nasal (T-N) dimensions. We averaged the binned density values to obtain the relative density as a function of either D-V (**Fig. 1C, G, K**) or T-N position (**Fig. 1D, H, L**). We observed distinct transitions in both S- and M-opsin expression along the D-V axis. High levels of M-opsin in the dorsal region exhibit a gradual transition to low levels in the ventral region (**Fig. 1C**). In contrast, S-opsin shows a rapid transition from zero to high expression in the D-V axis (**Fig. 1G**). As these opsins display an inverse yet non-complementary relationship, co-expression was most prominent in the middle third of the retina where these two transitions overlap (**Fig. 1K**). We observed minimal variation in S- and M-opsin signal in the T-N axis (**Fig. 1D, H, L**). We imaged and analyzed six wild-type retinas at this resolution and saw a similar pattern in each (**Table S1**). Together, we observed differential graded patterning for S- and M-opsin expression along the D-V axis (**Fig 1C, G, K**).

Analysis at single cell resolution reveals two distinct cone subtype populations

To further investigate photoreceptor patterning along the D-V axis, we next analyzed cone subtype specification at the single-cell level. For the same six retinas, we imaged S- and M-opsin expression at 200X magnification in a strip measuring approximately $600\ \mu\text{m} \times 6,000\ \mu\text{m}$ aligned vertically along the D-V axis (**Fig. 2A**). Previous studies analyzed $\sim 500\ \mu\text{m}$ in the dorsal-ventral axis centered on the transition region (Haverkamp et al., 2005), whereas our approach enabled evaluation of the entire $\sim 6,000\ \mu\text{m}$ length of the retina.

At 200x magnification, we were able to distinguish and identify individual cells. We developed an analysis pipeline to identify the position, size, and boundaries of the outer segment of each cone cell, a process known as segmentation (see **SI Methods, 1.1.1**). Overall, we identified $\sim 250,000$ total cells across six retinas. Using these outer segment boundaries, we calculated the expression intensity of M- and S-opsin for each cell. We classified cones into groups expressing M-opsin only (**Fig. 2E, K, Q**), S-opsin only (**Fig. 2F, L, R**), and S- and M-opsin co-expression (**Fig. 2G, M, S**). The pipeline did not identify distinct morphological or size differences among the cone outer segments (data not shown). We found that the pipeline's accuracy and false positive rate were comparable to hand-scored retinas (see **SI Methods 1.1.2**).

After obtaining the outer segment boundaries of the cone cells, we quantified the density of cone subtypes based on opsin expression relative to D-V position. Consistent with our low-resolution analysis, we observed a gradual decrease in the abundance of cones expressing M-opsin in the dorsal to ventral direction (**Fig. 3A**), contrasted by a sharp increase in S-opsin expressing cones (**Fig. 3B**). We fit these curves to Hill functions to quantify the steepness of the transition (**Fig. S1**). The transition in the S-opsin expressing cells is extremely sharp with an average Hill coefficient of ~ 30 while the M-opsin transition is much more gradual with a coefficient of $\sim 2-3$.

To compare the transition region between retinas, we established a reference point to align the images. Since the S-opsin transition is sharp and an external reference is absent, we used the midpoint of the S-opsin transition from the fit as the reference point. We aligned all of the retinas and overlaid the transition fits (**Fig. S2**). The relative position of the S-opsin and M-opsin transitions are consistent from retina to retina, suggesting that the transitions in S-opsin and M-opsin expression are driven by a common effector. M-opsin only expressing cones

decline at the transition point (**Fig. 3C**), coincident with the dramatic increase in S-opsin expression (**Fig. 3B**). At this transition point, cones begin to express both S- and M-opsins (**Fig. 3E**) and the cone populations are very diverse, comprised of those expressing M-only, S-only, and varying levels of both S- and M- opsins (**Fig. 2H-M**). The fraction of S-only cells gradually increases from ~1% of cones in the dorsal region to ~20-30% in the ventral region (**Fig. 3D, S3**). These analyses show the differential, inverse responses of S- and M-opsin expression to D-V patterning inputs on the individual cell level.

In a previous study, Haverkamp et al. measured differential opsin expression of cone cells in a window of ~500 μm near the transition point (Haverkamp et al., 2005). In agreement with our data, they observed that ~8-20% of cones expressed only S-opsin. Our results show that this measurement was part of a broader binary decision trend extending much further along the D-V axis in both directions. They also discovered that within this population, in the ventral region where S-only cones are more abundant, about 5% of S-opsin only cones contact S-cone bipolar cells and they classified these as genuine S-cones. These genuine S-cones are evenly distributed across the retina (Haverkamp et al., 2005).

To distinguish classes of cone subtypes, we performed a cluster analysis. When considering all cones in the retina, there visually appear to be three groups of cell-types corresponding to the three classifications that we defined earlier: S-only, M-only, and co-expressing. However, when we include the clustering analysis, a different pattern emerges (**Fig. 4A**). Expression levels do not cluster around single points, but rather follow along manifolds in the high dimensional space. We used HDBSCAN, a density-based clustering analysis that connects regions of high local density, to generate clusters (Campello et al., 2013). The method identified two distinct clusters of expression (**Fig. 4B**). The two clusters are separated by a region of low density in the high dimensional space.

To study the properties of these clusters, we calculated the joint probability distribution for S- and M-opsin intensity in individual cells for each retina (**Fig. 4C, S4**). First, we see an S-only cluster that has high and consistent expression of S-opsin while increasing in abundance along the D-V axis (**Fig. 4D-H, S5**). Interestingly, the other cluster changes position in a continuous way, gradually moving from low S-opsin expression and high M-opsin expression in

the dorsal region, to moderate S-opsin expression and low M-opsin expression in the ventral region (**Fig. 4D-H, S5**).

Thus, these data suggest that the mouse retina contains two main subtypes of cones: 1. S-only cones that have high S-opsin expression independent of D-V position and 2. co-expression competent (CEC) cones that express S- and/or M- opsins dependent upon D-V position. In the ventral region there is a mixture of S-only cones and CEC cones that express M-opsin at a very low level. It is difficult to distinguish these two classes using only S-opsin expression, but as can be seen in **Fig 4.**, the two populations are well separated when comparing both M- and S-opsin intensities. The S-only cones identified with our approach may, therefore, contain a subclass corresponding to the genuine S-cones identified by Haverkamp et al., but as we could not distinguish their connectivity to bipolar cells, we are only able to describe the populations of S-opsin only expressing cones.

Expression levels of S- and M-opsin in cone cell subtypes

Having classified the major subtypes of cones and related their positions and opsin expression states, we next evaluated the D-V dependence of the opsin expression intensity in individual cones. We quantified opsin expression for all M-opsin expressing cones (**Fig. 5A, F**), all S-opsin expressing cones (**Fig. 5B, G**), M- and S-opsin CEC cones (**Fig. 5C, H**), M-opsin only CEC cones (**Fig. 5D, I**), and S-opsin only cones (**Fig. 5E, J**) relative to their D-V positions within the retina.

In CEC cones, M-opsin expression levels decrease in the D-V axis, with the midpoint of expression level located at the transition point (**Fig. 5A, C, D, S6**). In contrast, S-opsin expression in CEC cells is very low in the dorsal region and increases linearly in the D-V axis starting at the transition point (**Fig. 5F, H, I, S6**). The slope of increase for S-opsin is steeper than for the M-opsin decrease (**Fig. S7**).

Compared to CEC cones, S-only cones have an overall higher expression level of S-opsin, particularly in the dorsal region (**Fig. 5J** compared to **G** and **H**). M-opsin expression in S-only cones is significantly lower than the lowest M-opsin expression seen in CEC cones (**Fig. 5E**). In **Fig. 5B**, this difference can be seen as two distinct lines of density (**Fig. 5B**, arrow

heads). Together, these analyses defined the expression of S- and M-opsin in the two cone populations in relation to their D-V positions in the retina.

Modeling cone subtype fate decisions

To interrogate how regulatory inputs could produce the complex pattern of binary and graded cell fates in the mouse retina, we developed a multiscale model describing the probability distributions of the cone subtype decisions (i.e. binary choice) and S- and M-opsin expression levels (i.e. graded) as functions of position along the D-V axis (**Fig. 6, SI Methods 1.2**). We modeled a 5 mm x 1 mm x 5 μ m section of the retina with the long dimension aligned with the D-V axis.

TH signaling activates M-opsin expression and represses S-opsin expression (Ng et al., 2001; Roberts et al., 2006). T3 is a critical regulator of cone subtype fate in the human retina (Eldred et al., 2018), and scRNA-seq data suggest that Thr β 2 is expressed in all mouse cones (Clark et al., 2019). Though other diffusible factors and transcription factors play roles (Alfano et al., 2011; Roberts et al., 2005; Satoh et al., 2009), TH signaling is the main and best-understood determinant of cone subtype fate. Thus, we built a simplified model of cone subtype specification based on the dorsal-ventral regulation of cone fates by the gradient of T3.

Within the modeled volume, T3 molecules diffuse according to the deterministic diffusion equation with constant concentration boundaries, establishing a D-V gradient. Roberts et al. (2006) reports a differential gradient in [T3] and [T4] between the dorsal and ventral regions of whole retina samples, however, it is not known what the intracellular concentrations of T3 are specifically in photoreceptor cells at a single cell level (Roberts et al., 2006). For this reason, we use relative values for [T3] to build a deterministic diffusion equation (**Eq. S1, SI Methods**). Also, within the volume, we modeled \sim 23,000 individual cones spaced on a hexagonal grid (**Fig. 7**). These cells randomly exchange T3 molecules with the surrounding deterministic microenvironment. Within each cone, T3 can bind to and activate Thr β 2 (Thr β 2*), controlling both fate specification and opsin expression (**Fig. 6B1-4**).

For the binary fate decision, we defined a fate determinant function, FD(X). Photoreceptors start in an undifferentiated fate, FD(U), and progress to either the FD(S) (S-only) fate or FD(C) (CEC) fate (**Fig. 6B2**). Selection of the FD(S) fate is negatively influenced by

Thr β 2* (**Fig. 6B2**). Once cells enter the FD(S) fate, S-opsin is constitutively expressed at a high level regardless of D-V position (**Fig. 6B2**). In FD(C) cones, M-opsin expression is induced by Thr β 2* (**Fig. 6B3**). Conversely, S-opsin in FD(C) cells is negatively regulated by Thr β 2* and positively regulated by inactive Thr β 2 receptors (**Fig. 6B4**). Full details of the model are given in the SI Methods 1.2, along with parameterization details.

Model-based simulations recapitulate experimental cone patterning

To compare the output of our probabilistic model to experimental data sets, we ran a set of 100 individual simulations and calculated the probability distributions of various observables. **Fig. 7** shows the output of one simulation. Moving from dorsal to ventral, the model reproduces the gradual increase in the fraction of S-only cones, FD(S) (**Fig. 7A1-4**), as well as the sharp transition in CEC cones, FD(C), expressing S-opsin at the transition zone (**Fig. 7B1-4**). Similarly, we observed the gradual decrease in the fraction of CEC cones expressing M-opsin (**Fig. 7C1-4**). In the overlapping region, there are a significant number of cones that co-express both S- and M-opsins (**Fig. 7D1-4**). In the dorsal region, a small number of S-only cones that highly express S-opsin are readily apparent (**Fig. 7A1-2, E1-2**).

To characterize how well our model recapitulated the observed experimental cell distributions, we calculated the mean density of cells of various phenotypes as a function of D-V position (**Fig. S8**). These average density profiles compare well to the experimental density profiles shown in **Fig. 3**. Together, cone fate patterning and expression levels are highly similar in our model and the imaged retinas: S-only cells (**Fig. 7A2-4** compared to **Fig. 2F, L, R**), S-opsin expression in CEC cones (**Fig. 7B2-4** compared to **Fig. 2E, G, K, M, Q, S**), and M-opsin expression in CEC cones (**Fig. 7C2-4** compared to **Fig. 2E, G, K, M, Q, S**).

We parameterized our model using the mean of all the retinas sampled, which exhibited retina-to-retina variability (**Fig. S1, S3, S7**). Therefore, it is not expected that our model will exactly recapitulate the patterning of any individual retina.

We next calculated the probability distributions of S- and M-opsin expression along the D-V axis for our simulation data (**Fig. S9**). The mean intensity of M-opsin in CEC cones gradually decreases as D-V position increases. The S-opsin distribution shows high expression in the ventral-most region, but has two separate populations in the dorsal region: the highly

expressing S-only cells and the lowly expressing CEC cells. The CEC cones converge to zero S-opsin expression in the dorsal region while the S-only cones maintain high expression as they decrease in abundance. Because our simulated distributions are constructed from 100 independent simulations, the probability density of the S-only cones is much smoother than in the experimental data (compare **Fig. S6 and S9**). The simulated expression features are in agreement with the experimental expression profile (**Fig. 5, S6**).

We next related the joint probability distributions for the experimental (**Fig. 8A-E**) and simulated (**Fig. 8F-J**) data along the D-V axis. The simulated and experimental data show two distinct populations: 1) S-only cones with high S-opsin expression and no M-opsin expression whose expression levels are independent of D-V position, and 2) CEC cones that gradually change from high M-opsin and low S-opsin expression to moderate M-opsin and high S-opsin expression along the D-V axis. **Fig. S10** shows the joint probability distribution between S- and M-opsin expression within 250 μm D-V bins for all 100 simulations. In the high resolution simulated data, it is evident that the position of the CEC cell cluster gradually changes with D-V position. Our model closely simulates the experimental data, and supports the hypothesis that cells respond differentially to the same morphogen gradient, producing both binary and graded cell fates.

Correlation between S-opsin and CEC fate decisions

Our quantitative simulations give us the capacity to test various hypotheses about retinal patterning. We wanted to know whether the gradual decrease in the CEC cone population and the sharp increase in S-opsin expression in these CEC cells were driven by a shared upstream signaling input. If these two processes respond to the same upstream input, we would expect that they should be coupled and be linked by D-V position. If, however, they do not respond to the same input we would expect that their transitions should be independent. In our model, they are coupled through the T3 gradient and we wanted to test if the experimental retinas were also coupled. As the experimental data show large retina-to-retina variability, we performed 100 additional simulations with parameters sampled from normal distributions parameterized using the experimental variance and checked for overlap of the corresponding probability distributions for two observables.

First, we calculated the probability of having a given CEC population fraction at the S-opsin transition point from both our simulations and experimental retinas (**Fig. 9A**). Second, we calculated the rate at which the CEC population decreases at the transition point (**Fig. 9B**). As can be seen from both plots, the experimental and simulated probability distributions are in good agreement. In particular, the widths of the experimental probability distributions are similar to the widths from the probabilistic simulations. With the small number of experimental data points, we do not assign a level of statistical significance to the overlaps, but they provide qualitative evidence that the two transitions are in fact coupled through a shared upstream input.

Comparison of Thr β 2 mutant retinas to wild-type retinas

Finally, to elucidate the effect of the T3 gradient on cone cell patterning in the mouse retina, we dissected and imaged Thr β 2 knockout mutant retinas (Δ Thr β 2). In the absence of functional Thr β 2, no M-opsin is expressed (Applebury et al., 2000; Ng et al., 2001; Roberts et al., 2006). Consistent with previous work, we observed no M-opsin expression in these mutant retinas. Fluorescence from anti-M-opsin antibodies was nonspecific and stained cell and background with equal intensity (**Fig. S11**).

The expression of S-opsin in cones was also markedly different between Δ Thr β 2 and WT retinas. Both the density of S-opsin-expressing cones and the expression distribution are flat with respect to the D-V axis (**Fig. 10B, S12**). Also, the relative intensity of the S-opsin signal across the retina was much lower in Δ Thr β 2 retinas than the maximum value seen in WT retinas (e.g., from cones in the ventral region). Δ Thr β 2 retinas and wildtype retinas were taken at the same time and stained with the same batch of antibody, then imaged with the same laser intensity for comparison of opsin levels. We found that the relative intensity of opsin staining in cones was most similar to the middle region of WT retinas. This effect is consistent with our model in which S-opsin expression is controlled through a combination of negative regulation by active Thr β 2* and positive regulation by inactive Thr β 2 (**Fig. 6B4**).

Discussion

In these studies, we described the distribution of cone photoreceptors in the mouse retina and developed a quantitative model for the specification of binary and graded cell fates in

response to D-V regulatory inputs. By using high-resolution microscopy combined with automated image analysis, we expanded on previous studies and mapped the cell fate decisions of cone cells across an entire dorsal to ventral region of the mouse retina. By analyzing cell fates in the context of their position in the tissue, we found that cones could be classified into two subclasses with a graded gene expression profile changing nonlinearly. This study exemplifies the benefits of quantitatively analyzing populations of cells in a tissue when classifying fate decisions.

In the mouse retina, we defined two cone subtypes, S-only cones and CEC cones, based strictly on opsin expression profiles. Interestingly, the population of S-only cones in the dorsal region have higher S-opsin expression than most S-only cones in the ventral region (**Fig. 5J**). These highly expressing S-only cones are found at a steady density across the D-V axis of the retina. It is possible that this subset of evenly distributed, high S-opsin expressing cells could comprise the “genuine” S-cones that connect to blue-cone bipolar neurons (Haverkamp et al., 2005). We were not able to mathematically distinguish genuine S-cones from the total population of S-only cones. Together, opsin expression and connectivity suggest three possible distinct cone subtypes: 1. CEC cones that do not connect to blue-cone bipolars, 2. “genuine” S-only cones that connect to blue-cone bipolars, and 3. S-only cones that do not connect to blue-cone bipolars. Examination of connectivity in conditions that perturb thyroid hormone signaling may inform the relationship between opsin expression and connectivity and their relationship to cone subtype.

Our study models how the terminal pattern of opsin expression and cone subtypes can be regulated by thyroid hormone signaling. A next step is to address the temporal dynamics of this process during development. Thyroid hormone signaling through $\text{Thr}\beta 2$ is necessary and sufficient to induce M-opsin and inhibit S-opsin (Ng et al., 2001; Roberts et al., 2006). S-opsin mRNA is expressed highly in the ventral region and M-opsin mRNA is expressed highly in the dorsal region at P0 (Aavani et al., 2017). Interestingly, distinct differences in T3 levels conducted on dorsal and ventral halves are only observed by P10 (Roberts et al., 2006). These observations suggest two main possibilities. First, earlier differences in T3 levels may be cell-type-specific and/or below the threshold for detectability and these subtle differences in TH establish the cone subtype pattern. Second, a two-step mechanism controls patterning whereby opsin expression is (1) initially patterned by a TH signaling independent pathway and then (2)

maintained and/or reinforced by TH signaling to determine the terminal pattern. As TH signaling is necessary and sufficient to determine the terminal pattern, our model is consistent with either of these possibilities.

Additional developmental studies support our model for cone fate specification. Daniele et al. 2011 studied the effects when S-opsin was knocked out. Mice lacking S-opsin have a significant number of cone cells in the ventral region that do not express any opsin and have disrupted cone morphology. We hypothesize that this degrading cone cell population is the S-only cones. In the cells of the mid and dorsal retinal regions, the M-opsin protein levels are higher than in wild type mice, presumably due to less competition for translation machinery, and therefore higher translation of M-opsin mRNA transcripts. In addition, other factors that modulate opsin levels in could be added to the model, such as RNA transcript availability (Daniele et al., 2011).

We developed a mathematical model that described both the binary fate specification process of cones and the graded expression of opsins, all driven by an external gradient. Probabilistic modeling of this complex process generated probability distributions that we used to compare with experimentally observed cell distributions to test hypotheses about the connections between cell fates. Probabilistic modeling is now sufficiently mature to perform detailed simulations of tissue-level cell-fate decisions. Combining probabilistic models with high-throughput microscopy is a powerful tool for helping to understand complex relationships in tissues.

These methods advance our understanding of how regulatory inputs influence complex cellular decisions to specify binary and graded cell fates within the same cell type in the same tissue. A next step will be to integrate more signaling inputs into our model for retinal development. Numerous signaling molecules are expressed in D-V gradients and are involved in retinal and cone cell development. Specifically, retinoic acid (RA) is an important morphogen that is expressed at high levels ventrally during development, and then at moderate levels in the dorsal region in the adult mouse (McCaffery et al., 1992; McCaffery et al., 1993). Moreover, further studies would include integrating transcription factor binding partners of Thr β 2 into the model, as Thr β 2 acts as a homodimer and as a heterodimer with RXR γ (Roberts et al., 2006).

This work represents an important first step towards modeling the complex network of interactions that guide binary and graded cell fate specification.

The retina provides an excellent paradigm to study how signaling inputs generate patterns in two dimensions. The next challenge will be developing models for patterning in more complex 3-dimensional neural tissue found in brain structures. Quantitative modeling has enormous potential to integrate multiple signals across a tissue and build networks to better understand and predict the outcomes of development when variables are changed, for instance in disease states.

Chapter III Figures:

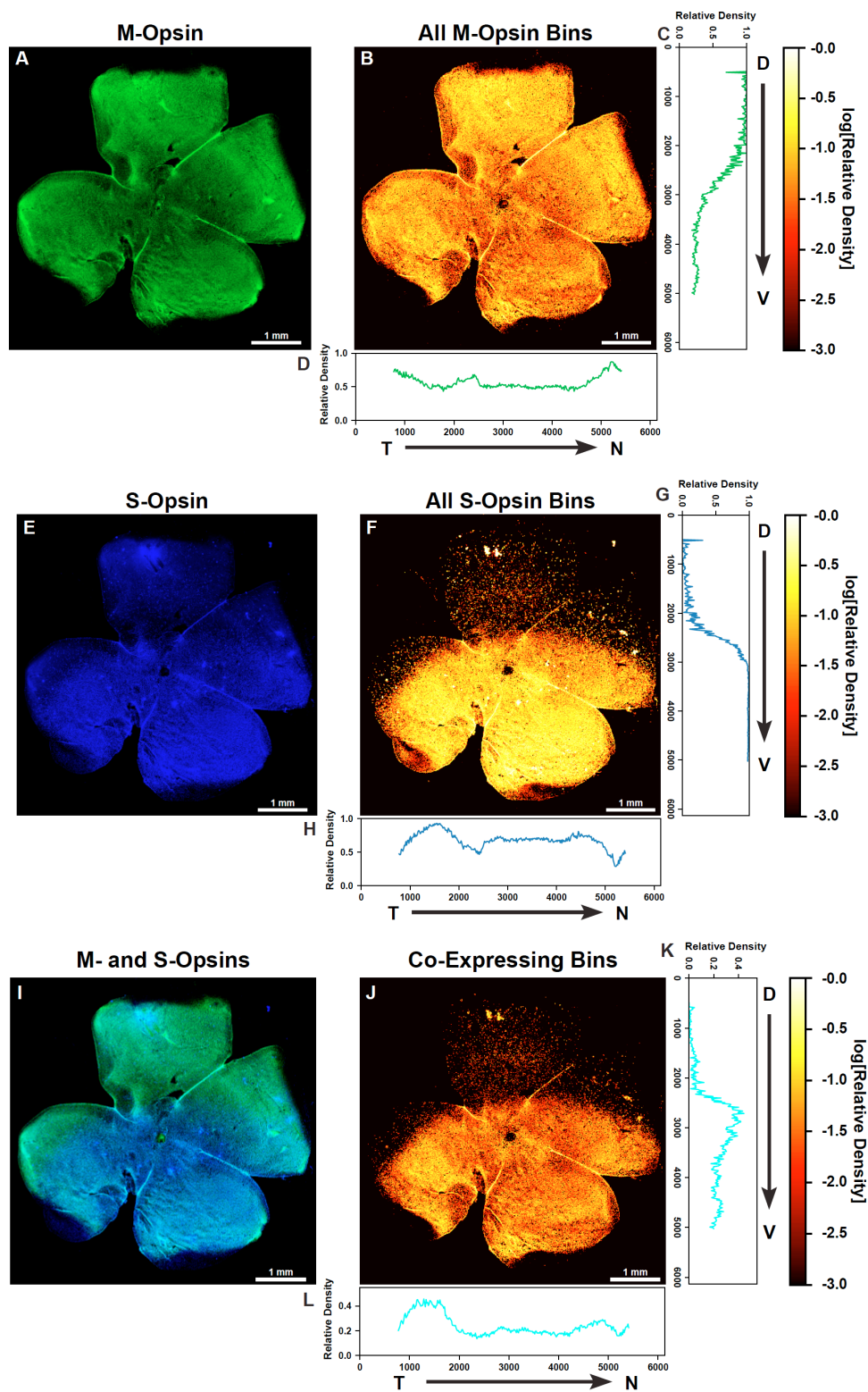


Figure 1. Analysis of opsin expression intensity across the mouse retina.

A, E, I) Whole mounted C57BL/6 mouse retina stained for M-opsin (green) and S-opsin (blue).

B, F, J) Heatmap displaying the log relative density of pixels that have opsin signal identified in a 25 mm² region.

A) M-opsin signal.

B) Heatmap of total M-opsin density bins.

C) Graph of the relative density of pixels that are expressing M-opsin summed horizontally (D - V).

D) Graph of the relative density of pixels that are expressing M-opsin summed vertically (T - N).

E) S-opsin signal.

F) Heatmap of total S-opsin density bins.

G) Graph of the relative density of pixels that are expressing S-opsin summed horizontally (D - V).

H) Graph of the relative density of pixels that are expressing S-opsin summed vertically (T - N).

I) M-opsin and S-opsin (co-expression) signal.

J) Heatmap of co-expressing opsin density bins.

K) Graph of the relative density of pixels that are co-expressing S- and M-opsin summed horizontally (D - V).

L) Graph of the relative density of pixels that are co-expressing S- and M-opsin summed vertically (T - N).

T = Temporal, N = Nasal, D = Dorsal, V = Ventral.

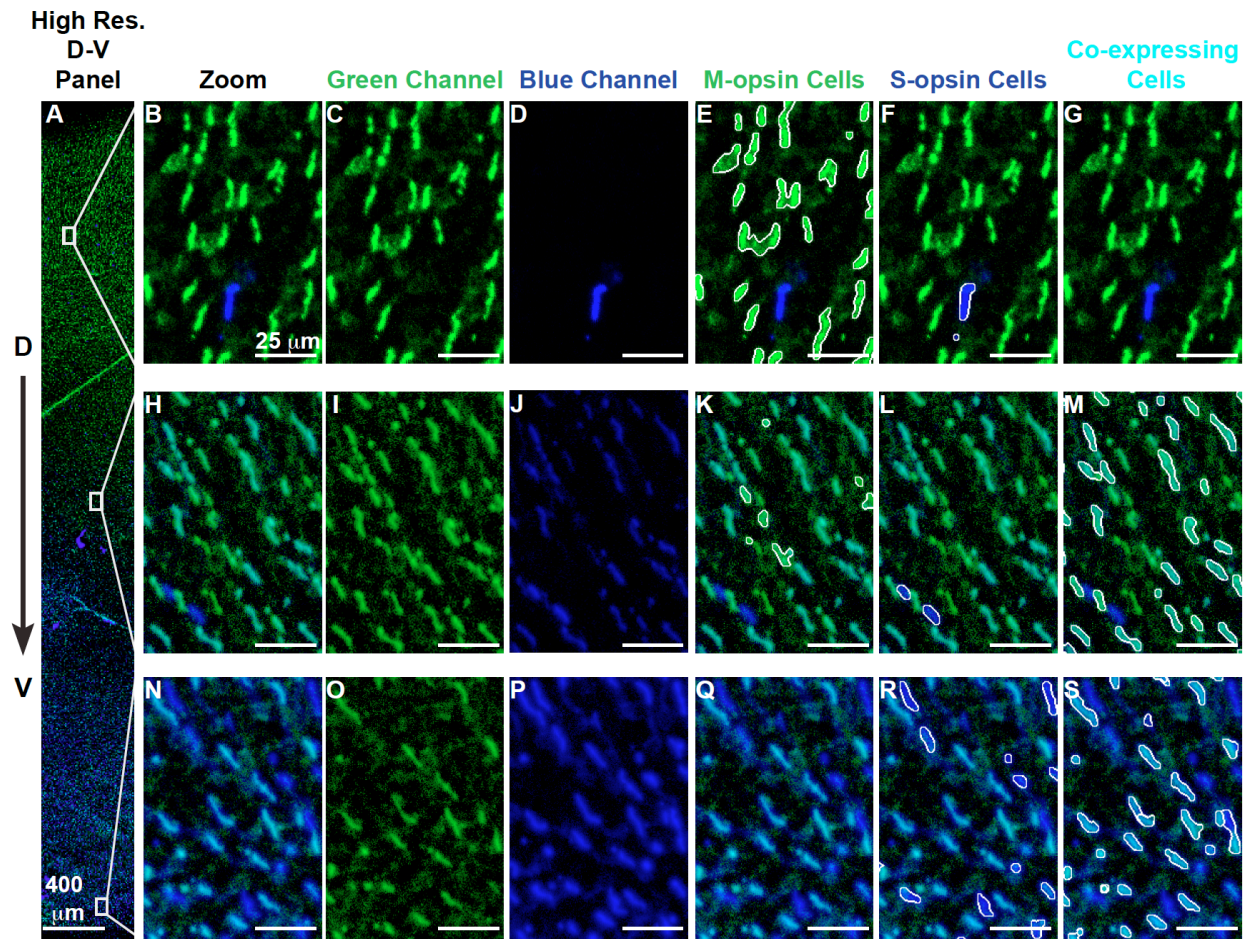


Figure 2. Identification of cone subtypes.

A-S) Retina stained with antibodies against M-opsin (green) and S-opsin (blue)

A) High-resolution region spanning the dorsal to ventral retina.

B-G) A region of the dorsal retina.

F-M) A region of the central retina.

N-S) A region of the ventral retina.

B, H, N) Blue and green channels.

C, I, O) Green channel only.

D, J, P) Blue channel only.

E, K, Q) White outline indicates identified M-opsin expressing cells.

F, L, R) White outline indicates identified S-opsin expressing cells.

G, M, S) White outline indicates identified co-expressing cells.

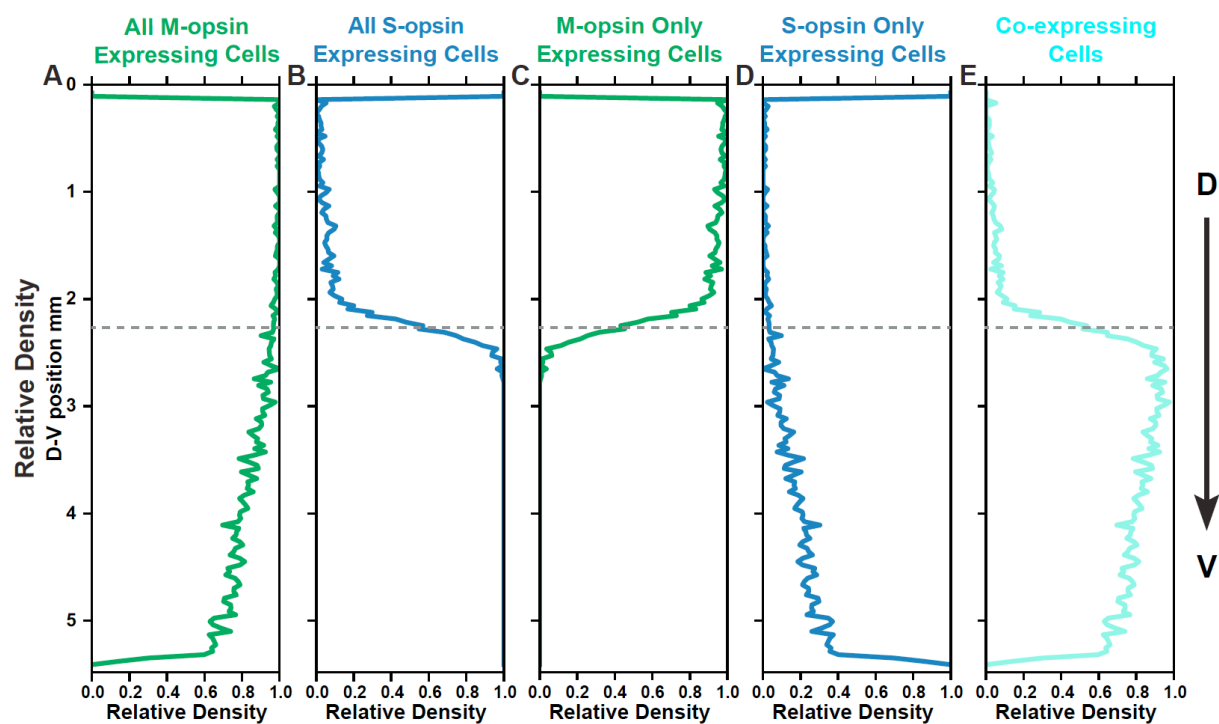


Figure 3. Spatial distribution of M- and S-opsins in cone cells.

Relative density of a cone population summed horizontally across the image and displayed in the dorsal to ventral position. Dotted line represents midpoint of transition zone.

- A) All M-opsin expressing cells.
- B) All S-opsin expressing cells.
- C) M-opsin only expressing cells.
- D) S-opsin only expressing cells.
- E) Co-expressing cells.

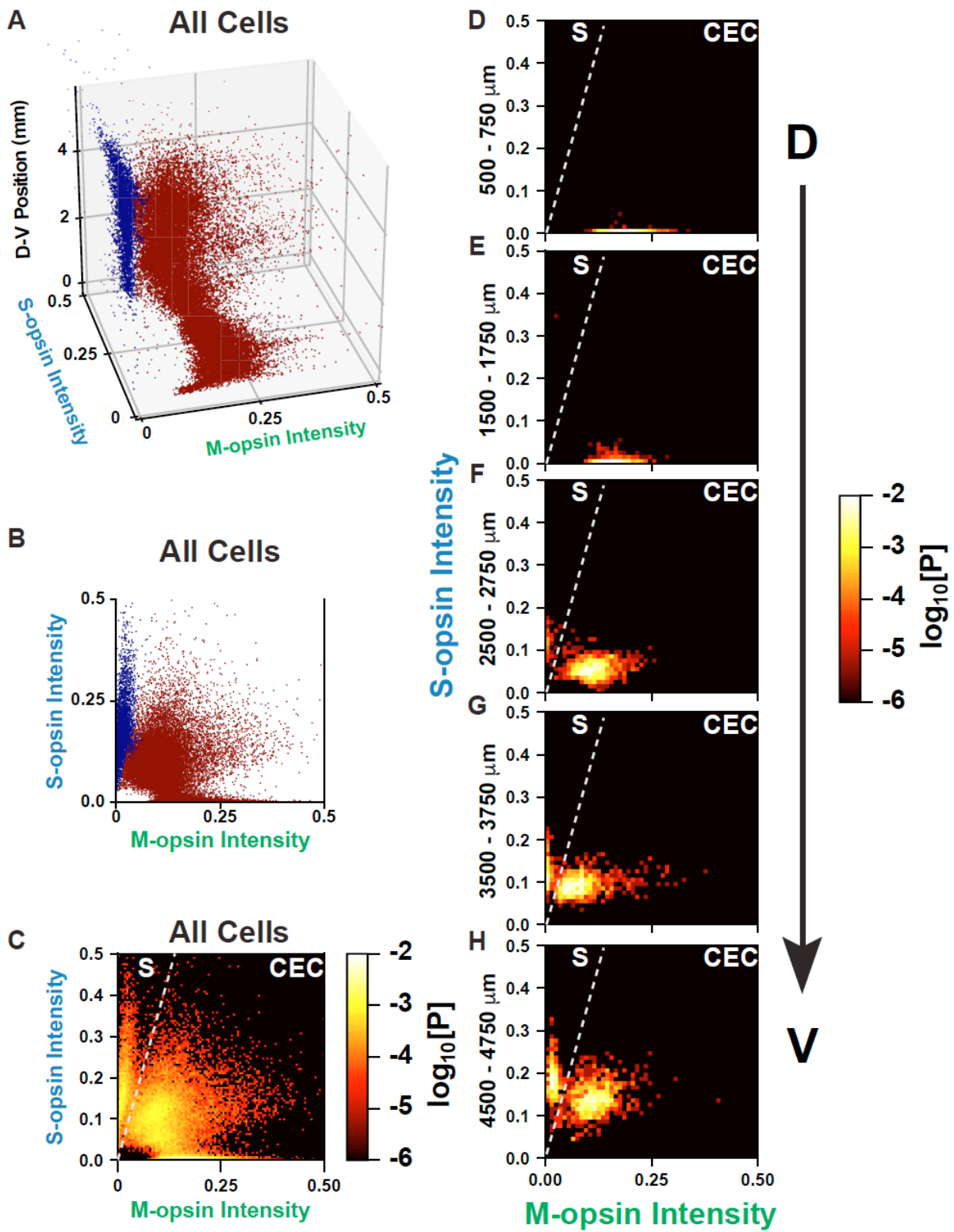


Figure 4. S- and M-opsin intensities in cones.

A - B) Clustering analysis of cone populations. Cluster one = dark blue; cluster two = maroon.

C-H) Cones are ranked according to the intensity of S- and M-opsin expression levels. Intensity values are represented in arbitrary units. Each point is colored according to the \log_{10} [Probability] of expression levels. A line is drawn on the graph to show the separation between the two discrete populations of S-opsin only and CEC cone populations.

C) All cones in the regions imaged.

D) Cones in the dorsal 500-750 mm.

E) Cones in the dorsal 1500-1750 mm.

F) Cones in the central 2500-2750 mm.

G) Cones in the ventral 3500-3750 mm.

H) Cones in the ventral 4500-4750 mm.

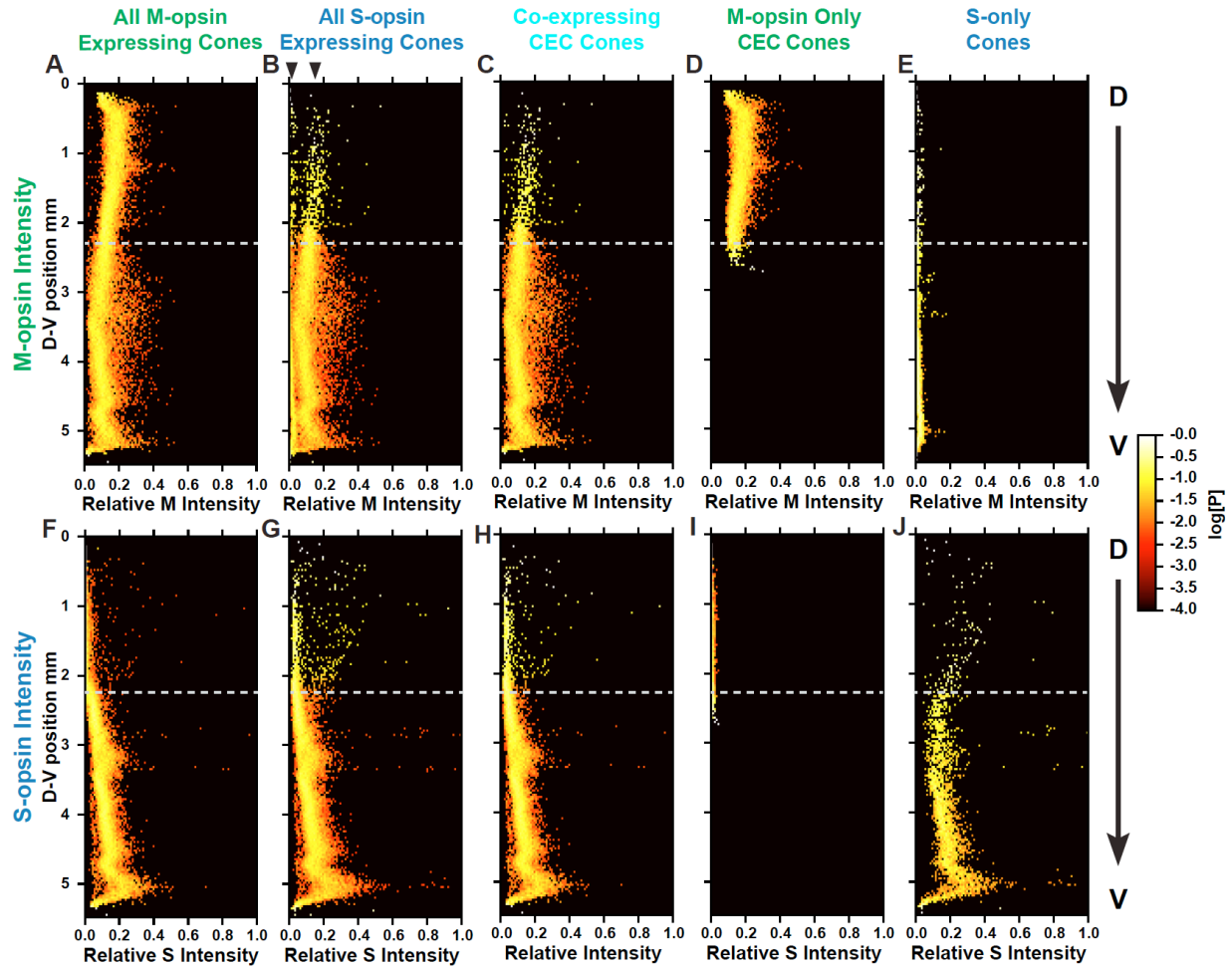


Figure 5. Intensity of M- and S-opsins in cones.

Relative intensity of M- or S-opsin in a cone population (X-axis) is displayed as a function of dorsal to ventral position. Each point is colored according to the $\log_{10}[\text{Probability}]$ of expression levels.

A-E) Relative intensity of M-opsin expression

F-J) Relative intensity of S-opsin expression

A, F) All M-opsin expressing cells.

B, G) All S-opsin expressing cells. For **B)**, arrow heads mark two distinct groups of cells in the dorsal region.

C, H) CEC cones co-expressing both S- and M-opsins.

D, I) M-opsin only expressing CEC cones.

E, J) S-opsin only expressing CEC cones.

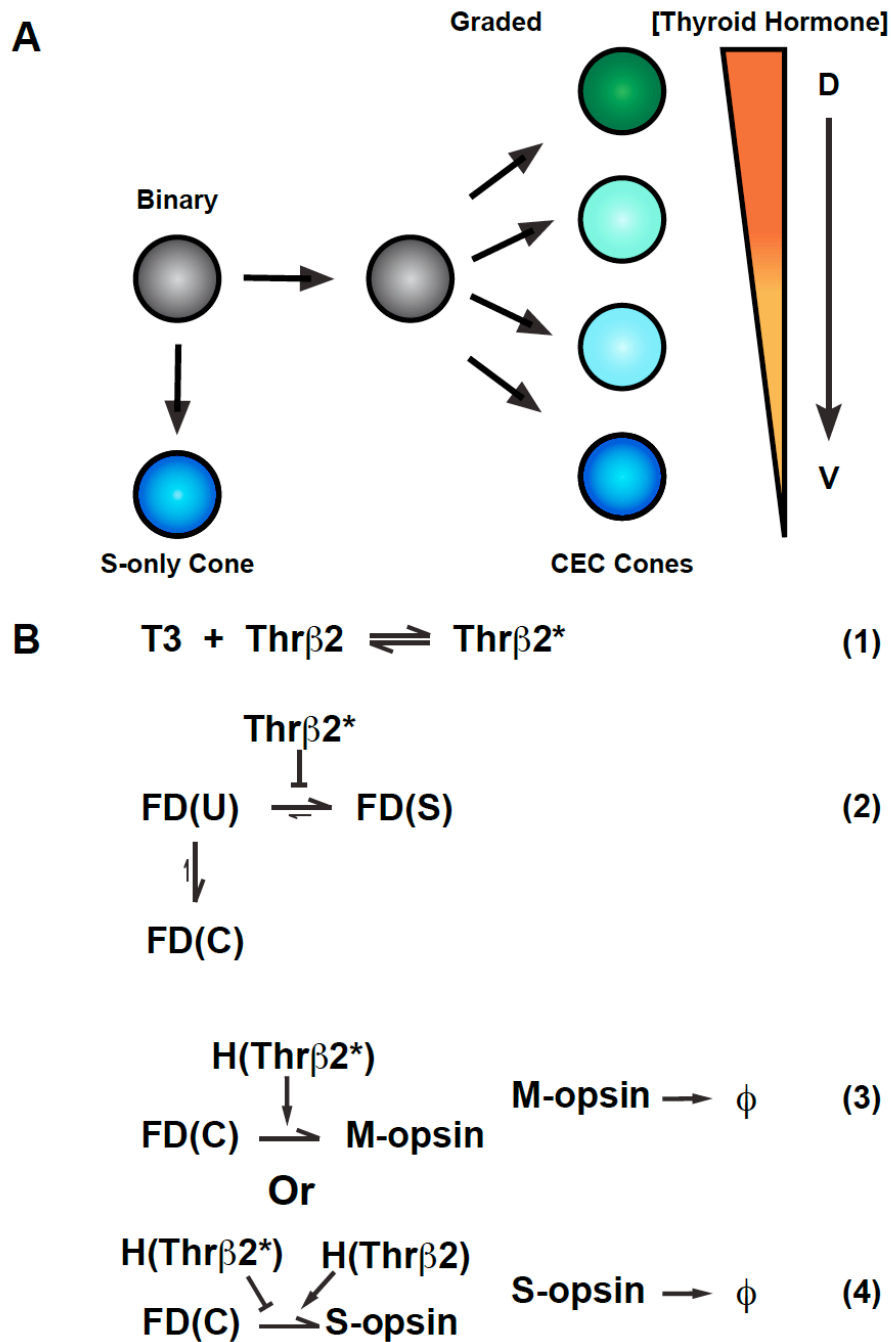


Figure 6. Model for cone cell fate specification

A) A naïve cell (grey) makes a binary decision between S-opsin only (blue) or co-expressing competent (CEC) cone fate (green, cyan or blue). The CEC cone expresses graded levels of M- and S-opsin dependent on the D-V concentration of thyroid hormone.

B1-4) T3 (Thyroid hormone), Thr β 2* (active Thr β 2 binding T3), FD (fate determinate function), U (undifferentiated cell), S (S-only cone), C (Co-expressing cone), H (Hill function), ϕ (degradation constant of opsin proteins).

B1) Binding of T3 to Thr β 2 activates Thr β 2 (Thr β 2*)

B2) Thr β 2 controls the binary decision between S-opsin only/FD(S) or CEC/FD(C) cone fate

B3) Thr β 2* promotes M-opsin expression

B4) Thr β 2* inhibits S-opsin expression, whereas inactive Thr β 2 promotes S-opsin expression

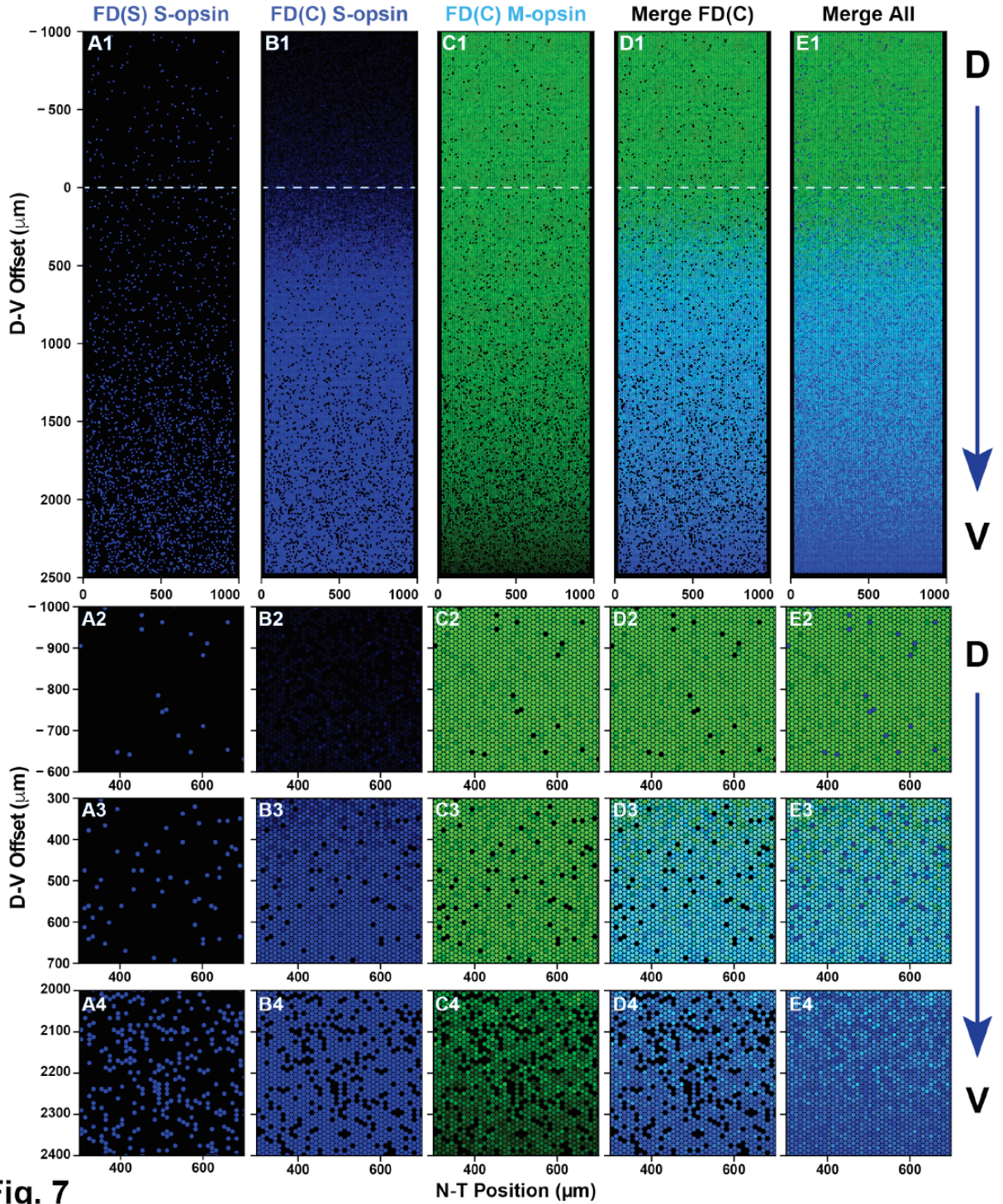


Fig. 7

Figure 7. Simulated cone mosaic produced by the quantitative model.

Simulated cone photoreceptor mosaic generated by the quantitative model displaying expression of S-opsin (blue), and M-opsin (green). A dorsal to ventral region is shown.

- A1, B1, C1, D1)** Complete simulated D-V strip.
- A2, B2, C2, D2)** Zoom in the dorsal region.
- A3, B3, C3, D3)** Zoom in the central region.
- A3, B3, C3, D3)** Zoom in the ventral region.
- A1-4)** S-opsin only cones.
- B1-4)** S-opsin expression in CEC cones.
- C1-4)** M-opsin expression in CEC cones.
- D1-4)** S- and M-opsin expression in CEC cones
- E1-4)** All cones including S-opsin only and CEC cones.

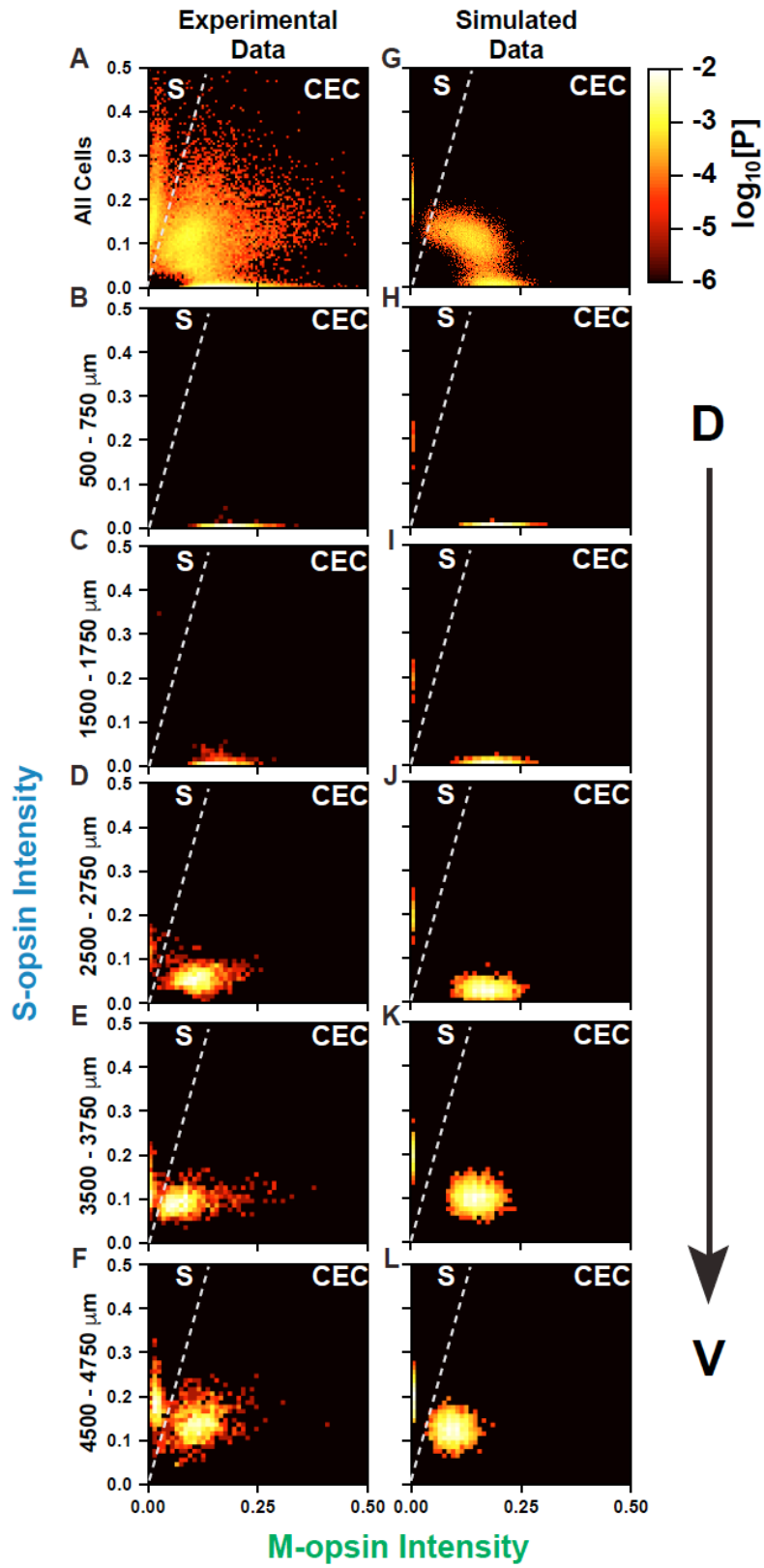


Figure 8. D-V cone pattering in simulated and experimental data.

Cones are ranked according to the intensity of S- and M-opsin expression levels. Intensity values are represented in arbitrary units. Each point is colored according to the \log_{10} [Probability] of expression levels.

A-F) Experimental data, as seen in **Fig. 4C-H**.

G-L) Simulated data.

A, G) All cone cells

B, H) Cones in the dorsal 500-750 mm.

C, I) Cones in the dorsal 1500-1750 mm.

D, J) Cones in the central 2500-2750 mm.

E, K) Cones in the ventral 3500-3750 mm.

F, L) Cones in the ventral 4500-4750 mm.

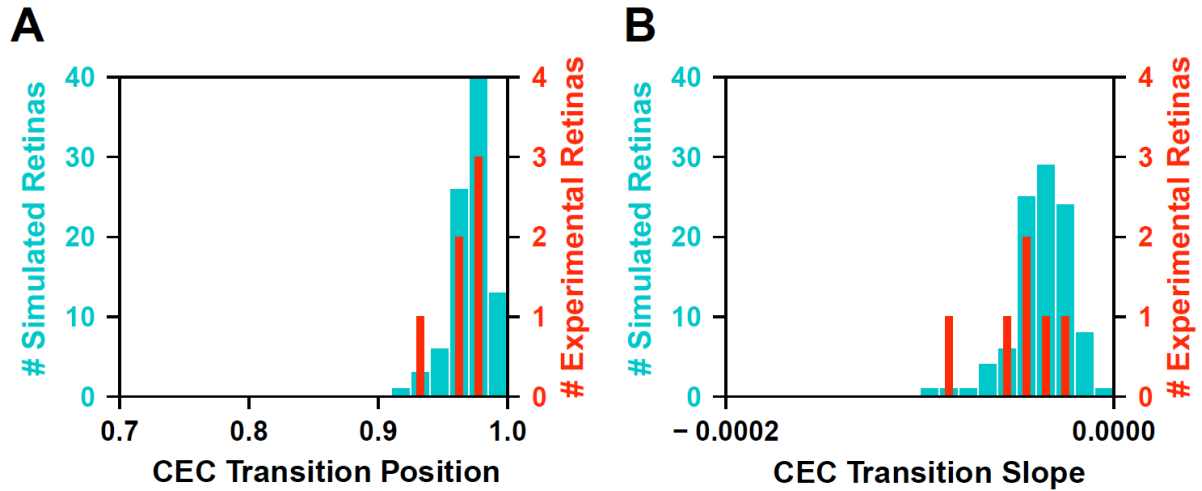


Figure 9. Correlation between CEC fate and S-opsin transitions.

A) The fraction of CEC cells at the point where the S-opsin transition is at its midpoint. Data are shown for both experimental (red) and modeled (cyan) retinas.

B) The slope of the CEC transition at the S-opsin midpoint, for both experimental (red) and modeled (cyan) retinas. Note: the distributions of only 5 of the 6 retinas are included here, as one of the images had major disruptions at the transition zone due to dissecting and mounting.

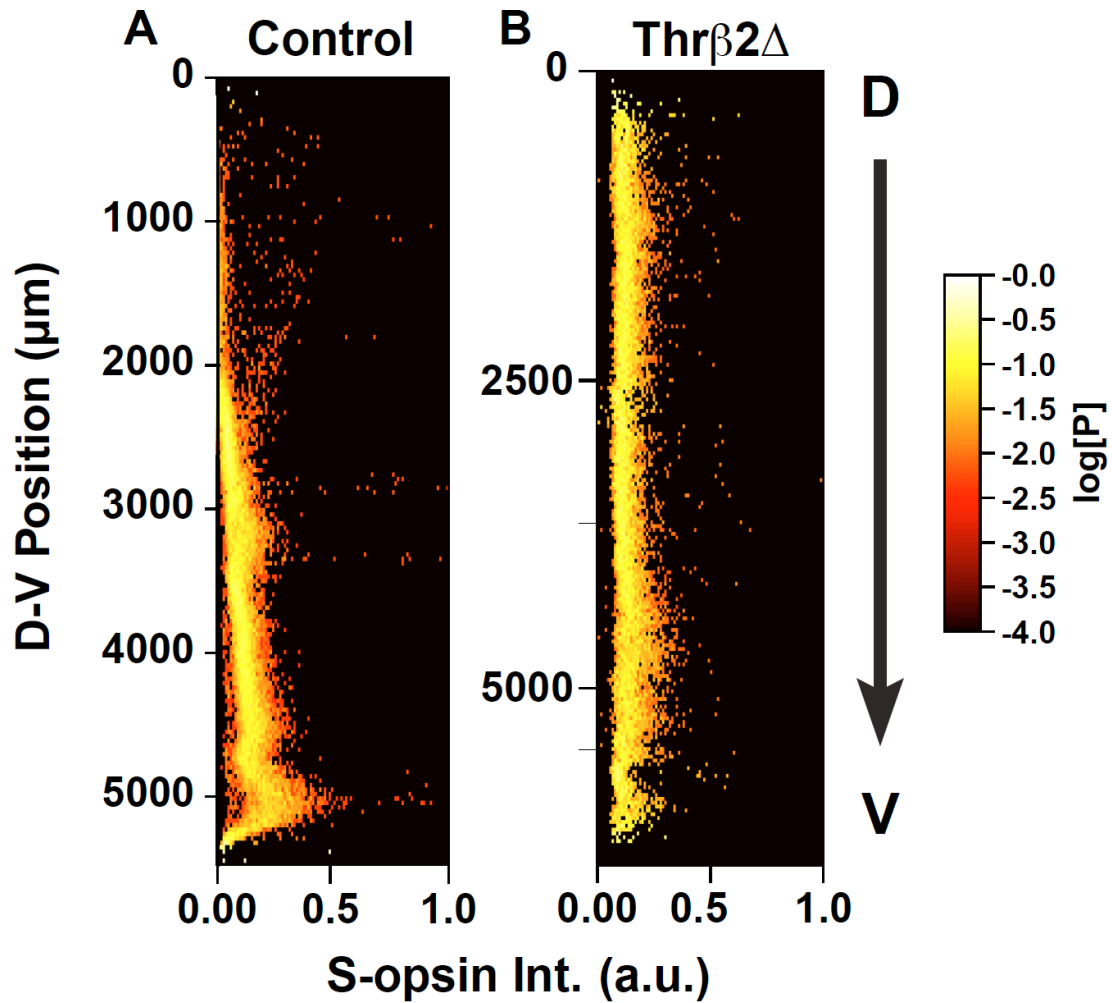


Figure 10. ThrB2Δ mouse Intensity Plots

Relative intensity of S-opsin cone cells (X-axis) displayed as a function of dorsal to ventral position. Each point is colored according to the \log_{10} [Probability] of expression levels.

A) Control Retina, as seen in **Fig. 5F**.

B) ThrB2Δ retina.

Materials and Methods:

Animals

Mice (strain C57BL/6) were housed under a 12 h light:12 h dark (T24) cycle at a temperature of 22°C with food and water *ad libitum*. Male and female mice were housed in plastic translucent cages with steel-lined lids in an open room. Ambient room temperature and humidity were monitored daily and tightly controlled. Wild-type mice (C57BL/6; Jackson Laboratory), and *Thrb^{m2Df}* mutant mice (gift from the Forrest Lab) were used in this study. *Thrb^{m2Df}* mutant mice specifically knock out expression of Thrβ2, and leave Thrβ1 intact as previously described (Ng et al., 2001). Retinal dissections were performed on mice at 2–8 months old. All animals were handled in accordance with guidelines of the Animal Care and Use Committees of Johns Hopkins University. All efforts were made to minimize the pain and the number of animals used.

Immunohistochemistry

Retinas were dissected in PBS, then fixed in fresh 4% formaldehyde and 5% sucrose in PBS for 1 hour. The dorsal portion of the retina was marked with a cut. Tissue was rinsed 3X for 15 min in PBS. Retinas were incubated for 2 hours in blocking solution (0.2-0.3% Triton X-100, 2-4% donkey serum in PBS). Retinas were incubated with primary antibodies in blocking solution overnight at 4°C. Retinas were washed 3X for 30 min in PBS, and then incubated with secondary antibodies in blocking solution for 2 hours at room temperature. At the end of staining, retinas were cut to lay flat on a slide, and were mounted for imaging in slow fade (S36940, Thermo Fisher Scientific).

Antibodies

Primary antibodies were used at the following dilutions: polyclonal goat anti-SW-opsin (1:200) (Santa Cruz Biotechnology), polyclonal rabbit anti-LW/MW-opsins (1:200) (Millipore). All secondary antibodies were Alexa Fluor-conjugated (1:400) and made in donkey (Molecular Probes).

Microscopy and image processing

Fluorescent images were acquired with a Zeiss LSM780 or LSM800 laser scanning confocal microscope. Confocal microscopy was performed with similar settings for laser power, photomultiplier gain and offset, and pinhole diameter. Whole retinas were imaged with a 10X objective, and maximum intensity projections of z-stacks (5–80 optical sections, 4.9 μm step size) were rendered to display all cones imaged in a single retina. Retinal strips were imaged with a 20X objective, and maximum intensity projections of z-stacks (5–80 optical sections, 1.10 μm step size) were rendered to display all cones imaged in a single retina. $\Delta\text{Thr}\beta\text{2}$ retinas and wildtype retinas were taken at the same time and stained with the same batch of antibody, then imaged with the same laser intensity for comparison of opsin levels.

Segmentation of cone cells from microscopy images

Microscopy images were analyzed using a custom parallel image processing pipeline in Biospark (Klein et al., 2017). Briefly, each fluorescence channel was first normalized and filtered to remove small bright features. Then, each remaining peak in fluorescence intensity was identified and an independent active contour segmentation (Marquez-Neila et al., 2014) was performed starting from the peak. If the resulting contour passed validation checks it was included in the list of segmented cone cells for the channel. Finally, the outer segment boundaries of cone cells were reconciled across both channels to obtain a complete list of identified cells. Full details are given in the SI Methods.

Modeling cone cells fate decisions and opsin expression

Multiscale modeling of the retina strip was performed using a hybrid deterministic-probabilistic method. Diffusion of T3 in the microenvironment of the retinal strip was modeled using the diffusion partial differential equation (PDE). The PDE was solved using an explicit finite difference method. The cone cells were modeled using the chemical master equation (CME) to describe the probabilistic reaction scheme implementing the cell fate decision-making. The CME for each of the 23,760 cone cells was independently sampled using Gillespie's probabilistic simulation algorithm (Gillespie, 1977). Reconciliation between the CME trajectories and the PDE microenvironment was done using a time-stepping approach. Complete

mathematical details of the model and simulation methods are available in the SI Methods. All simulations were performed using a custom solver added to the LMES software (Roberts et al., 2013), which is available on our website: <https://www.robertslabjhu.info/home/software/lmes/>.

Data Availability

Immunofluorescence images (<https://osf.io/e5ckg/>) and analysis code (<https://osf.io/b438a>) are available in the Open Science Framework database.

Supporting Information

The supporting information file contains the text of the Supplementary Methods as well as Supplementary Tables S1-S3 and Supplementary Figures S1-S14. References sighted in supplementary materials are as follows: (Anderson et al., 2017; Gillespie, 1977; Klein et al., 2017; Marquez-Neila et al., 2014; Roberts et al., 2013)

Supplementary Material for
“Modeling binary and graded cell fate patterning in the mouse
retina”

Kiara C. Eldred¹, Cameron Avelis², Robert J. Johnston Jr.^{1†}, and Elijah Roberts^{2†}

May 14, 2019

¹ Department of Biology, Johns Hopkins University, Baltimore, MD 21218, USA

² Department of Biophysics, Johns Hopkins University, Baltimore, MD 21218, USA

† Correspondence to:

Robert Johnston

Department of Biology, Johns Hopkins University

Mudd Hall 309, 3400 N Charles St, Baltimore, MD 21218

Ph: 410-516-2384

Email: robertjohnston@jhu.edu

or

Elijah Roberts

Department of Biophysics, Johns Hopkins University

Jenkins Hall 110, 3400 N Charles St, Baltimore, MD 21218

Ph: 410-516-2384

Email: eroberts@jhu.edu

Supplementary Text

1 Methods

1.1 Analysis of retina microscopy images

1.1.1 Segmentation of individual photoreceptor cells in 20X images

To identify and segment individual cone cells in the immunostained fluorescence images, we developed an image processing pipeline similar to that used previously [1]. The analysis begins by finding potential cone cells by looking for connected regions in our 20X fluorescence images. Because some cells are present in only the blue (S-opsin) or green (M-opsin) channels and some cells are present in both, we combine all potential cells into a joint list for additional analysis. Algorithm 1 outlines this first step of our processing pipeline.

Algorithm 1: Extract the subimage surrounding each potential cone cell.

```
1 lg,lb = load green and blue fluorescence channels;
2 Ng,Nb = subtract background and normalize (lg,lb);
3 Mg,Mb = threshold images (Ng,Nb);
4 Og,Ob = find connected regions (Mg,Mb);
5 Lg,Lb = remove small regions (Og,Ob);
6 Fg,Fb = apply Gaussian smoothing (Lg,Lb);
7 Cg,Cb = find connected regions (Fg,Fb);
8 subimages = [];
9 for C in {Cg,Cb} do
10 |   l = extract local subimage (C);
11 |   append to subimages (l);
12 end
13 return subimages;
```

Next, we find the outline of each potential cell using an active contouring method known as

morphological snakes [2]. Because we are segmenting tens-of-thousands of individual potential cells from each image, we perform this step of the pipeline in parallel using the Biospark framework [3], which is a data intensive parallel analysis package for Python. We perform validation of the segmented boundaries before classifying the object as a cone cell.

Algorithm 2: Identify and segment any cone cells in each subimage.

```
1 cells = [];  
2 parallel for I in subimages do  
3   P = find peak (I);  
4   C = active contour (I,P);  
5   if validate (C) then  
6     append to cells (C);  
7   end  
8 end
```

Finally, we perform a reconciliation step in which overlapping cells are merged and/or split to obtain an estimated final segmentation for the image. The pixel indices associated with each cell are stored so that the properties of each cone cell can be later calculated.

All of the scripts and Jupyter notebooks implementing our analysis pipeline are available for download from our website https://www.robertslabjhu.info/home/software/mouse_eye.

1.1.2 Validation of segmentation results

We validated that our segmentation algorithm produced results similar to human annotators by comparing manually and automatically generated statistics from representative samples of our data set. We picked seven different regions and manually counted the number of S-opsin only, M-opsin only, and coexpressing cells. We then analyzed the same regions using our segmentation algorithm and obtained the automatically generated classifications.

Table S2 shows the counts of cell types from these regions from both human and computer

annotations. Overall, there is excellent agreement in the relative abundance of the different cell types. The absolute counts have some systematic difference, with the automatic segmentation typically identifying more cells than human annotators. This is mostly due to what appear to be single long cells that are split into multiple bright pieces separated by low fluorescence breaks. Human annotators tend to regard the trace as a single long cell, while the automatic segmentation tends to identify multiple smaller cells. Importantly, we do not know the true underlying cell morphology, so we cannot generally say whether the human or automatic annotators are more accurate. In any case, since the cell parts are identified correctly and the segmentation is consistent across retinas, we expect these minor difference to have no impact on our results.

1.2 Modeling of photoreceptor cells

1.2.1 Modeling cone cell fate determination and opsin expression in a retinal strip

To model the cone fate decisions in a large retinal strip we use a combination of stochastic and deterministic modeling. We start with a three-dimensional volume 5 mm long in the X dimension, 1 mm wide in the Y dimension, and $5 \mu\text{m}$ in the Z dimension representing the microenvironment of the dorsal-ventral (DV) strip. The small z dimension make this an effectively two-dimensional system and we include z below only for completeness. Within this volume we model diffusion of thyroid hormone (T3) using the deterministic diffusion equation:

$$\frac{\partial C(\mathbf{r}, t)}{\partial t} = D\nabla^2 C(\mathbf{r}, t), \quad (\text{S1})$$

where $C(\mathbf{r}, t)$ is the concentration of T3 at position \mathbf{r} and time t , D is the diffusion coefficient used for T3, and ∇^2 is the Laplace operator ($\frac{\partial^2 C}{\partial x^2} + \frac{\partial^2 C}{\partial y^2} + \frac{\partial^2 C}{\partial z^2}$). See Table [S3](#) for all parameter values used.

We numerically solve the diffusion partial differential equation (PDE) using a explicit finite difference method with grid spacing dx and a time step $dt = (dx^2)/(2 \cdot 6D)$, where the extra factor of 2 in the denominator ensures numerical stability. We fix the concentration at the $X = 0$ boundary to C_{hi} and at the opposite boundary to C_{lo} to establish a stationary concentration gradient in the X dimension. The Y and Z boundaries are taken to be reflective. We initialize the concentrations

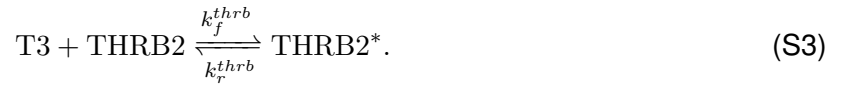
$C(\mathbf{r}, 0)$ according to a linear decrease in r to follow to the boundary conditions.

Within the microenvironment, we place 23,760 individual photoreceptor cells spaced on a hexagonal grid spanning the X-Y plane, with center-to-center distance $d_{cell-cell}$ and with a radius r_{cell} . Each cell is modeled independently using the chemical master equation (CME) describing the probability to have a particular count of each species:

$$\frac{dP_t(\mathbf{x})}{dt} = \mathbf{A}P_t(\mathbf{x}), \quad (\text{S2})$$

where $P_t(\mathbf{x})$ is the probability for a cell to have a particular state vector \mathbf{x} giving the count for each chemical species and \mathbf{A} is a transition matrix describing all of the reactions between the chemical species.

Within each photoreceptor cell a series of reactions describing the fate of the cell and also its opsin expression levels take place. First, cells contain thyroid hormone receptors THRB2. T3 can bind reversibly to THRB2 to switch it to an activated state THRB2*:



Note that T3 is also diffusing across the PDE microenvironment and the value of T3 is synchronized between the PDE and CME models. The synchronization procedure is discussed below.

Next, the cells switch between three cell fates. FD(U) cells are undifferentiated and do not express opsins, FD(S) cells occupy an S-only cone cell fate with high expression of only S-opsin, and FD(C) cells are typical cone cells that express some combination of S- and M-opsin depending on various factors. The transition between cone cell fates in real cells depends on a number of unknown fate determining steps. Little is known about these steps, but the fate decisions appear to be stable. Therefore, we model photoreceptor fate decision-making as barrier crossing process with a variable number of cooperative steps n .

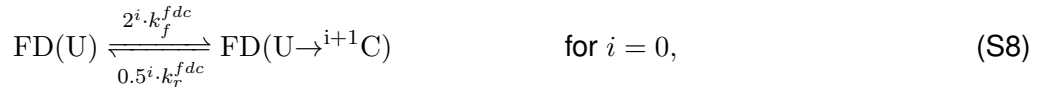
The FD(U) \leftrightarrow FD(S) transition is described by



Here, the syntax FD(U \rightarrow^i S) denotes a cell that has progressed i steps along the path from the FD(U) to FD(S) fate. Also, H' is an inhibiting Hill-like kinetic function defined by

$$H'(X) = k_{lo} + \frac{(k_{hi} - k_{lo})k_m^h}{k_m^h + x^h}, \quad (\text{S7})$$

with k_{lo} and k_{hi} the lower and upper limits of the kinetic process, respectively, k_m the midpoint of the transition, and h the Hill exponent giving the cooperativity of the transition. Likewise, the FD(U) \leftrightarrow FD(C) transition is described by



Then, both S-opsin and M-opsin proteins can be expressed by photoreceptor cells, depending on the cell type and the local concentration of T3. We model opsin expression using the following kinetic equations



H is an activating Hill-like kinetic function

$$H(X) = k_{lo} + \frac{(k_{hi} - k_{lo})x^h}{x_m^h + x^h}. \quad (\text{S14})$$

Finally, both opsins can be degraded according to



We initialize each cell at $t = 0$ to the FD(U) state with a copy number of THRB2 proteins independently sampled from a Gaussian distribution with a mean concentration of μ_{thrb} and a variance of σ_{thrb}^2 . The number of T3 molecules available to the cell is initialized according to the T3 concentration at the cell's D-V position. Likewise, the fraction of activated THRB2 is initialized to its equilibrium value according to the cell's D-V position. All opsin counts are initialized to zero. We then model the stochastic time evolution of each cell using the standard Gillespie stochastic simulation algorithm (SSA) [4, 5].

1.2.2 Microenvironment modeling of combined PDE and CME dynamics

Since we are performing two parallel simulations, PDE and CME, we need to partition the molecules between them. Each cell has a volume smaller than a PDE subvolume and each cell is assumed to be completely contained within a single subvolume. We initialize the T3 molecule count in each cell to be the rounded number of molecules corresponding to the subvolume's concentration time the cell volume. In this way T3 molecules are represented in each simulation

During each timestep these molecules

We initialize

To integrate the PDE and CME dynamics, we implement a parallel time-stepping approach. We divide time into discrete synchronization intervals Δt and evolve overall time according to

$$t_{i+1} = t_i + \Delta t. \quad (\text{S17})$$

During each Δt we update the state each cell through using the SSA and each external subvolume using a finite difference algorithm. At the end of each time step, the total number

Our code is implemented as the new Microenvironment solver in our LMES software and is freely available on our website:

<https://www.robertslabjhu.info/home/software/lmes>.

1.2.3 Parameterization of retinal strip microenvironment model

We parameterized our model by globally fitting the model parameters to five different dorsal-ventral (D-V) data sets: (1) the fraction of all cells expressing M-opsin, (2) the fraction of all cells expressing S-opsin, (3) the fraction of FD(S) cells expressing only S-opsin, (4) the per cell M-opsin expression level, and (5) the per cell S-opsin expression level. Because our data were collected from multiple retinas, we first fit the raw data to functions that we could use to describe a hypothetical mean retina.

We describe the fraction of cells in the various subfates as (modified) Hill-like functions. The fraction of cells expressing S-opsin as a function of D-V position x is described by:

$$F_S(x) = m \cdot x + b + [1 - (m \cdot x + b)] \cdot \frac{x^h}{x_{mid}^h + x^h}, \quad (\text{S18})$$

where m and b are the slope and x-intercept of a baseline fraction, respectively, x_{mid} is the midpoint of the transition, and h is the Hill coefficient. Likewise, the fraction of M-opsin expressing cells is given by:

$$F_M(x) = \frac{x_{mid}^h}{x_{mid}^h + x^h}, \quad (\text{S19})$$

and the fraction of FD(S) cells is given by:

$$F_{FDS}(x) = F_{min} + (F_{max} - F_{min}) \cdot \frac{x^h}{x_{mid}^h + x^h}. \quad (\text{S20})$$

Figures [S1](#), [S2](#), and [S3](#) show the fits of these functions to the raw data for the various retinas. We then took the mean of the various parameters to construct a hypothetical mean retina. Figure [S13](#) shows the fraction of cells in these states as a function of D-V position in our mean retina.

We describe the mean per cell expression level of M- and S-opsin as piecewise linear functions with a low and a high limit separated by a biphasic region with two different slopes:

$$I(x) = y_0 \quad \text{if } x < x_0, \quad (\text{S21})$$

$$= y_0 + m_1 \cdot (x - x_0) \quad \text{if } x_0 < x < x_1, \quad (\text{S22})$$

$$= y_0 + m_1 \cdot (x_1 - x_0) + m_2 \cdot (x - x_1) \quad \text{if } x_1 < x < x_2, \quad (\text{S23})$$

$$= y_0 + m_1 \cdot (x_1 - x_0) + m_2 \cdot (x_2 - x_1) + y_1 \quad \text{if } x > x_2. \quad (\text{S24})$$

Here, y_0 and y_1 are the left and right baselines, x_0 , x_1 , and x_2 are the D-V points where the slope changes, and m_1 and m_2 are the two slopes. Figure S7 shows the fit to the M- and S-opsin expression for the various experimental retinas. Figure S13 shows the values of these functions for our hypothetical mean retina.

Once we had a hypothetical mean retina, we used it to parameterize our model. We derived expressions for the mean value of the various observables as a function of D-V position by solving the deterministic system of equations described by Equations S3-S16. We then used non-linear least squares with Nelder-Mead minimization to globally optimize the parameters using all five data sets. Table S3 gives the best fits values for the free parameters and Figure S14 shows a comparison of the deterministic model calculated using the best-fit parameters against our hypothetical mean retina.

Supplementary Tables

Table S1: Retina image names and genotypes.

Retina	Filename	Genotype	Num. Cells
R07	170505_2M_WT_F1_Left_20x_Stitch_MIP	WT	65467
R08	170505_2M_WT_F1_Right_20x-Stitch-MIP	WT	50437
R09	170505_2M_WT_F2_Left_20x-Stitch-MIP	WT	34381
R22	170817_pregnantMALE_CONTROL_BL6_1_20x-Stitch-MIP_c1+2	WT	40660
R25	171026_WT_F1_Left_20x-Stitch-MIP	WT	29831
R26	171026_WT_F1_Right_20x-Stitch-MIP	WT	29962
R31	180123_ThrB2_KO_4M_DV_Right_slide1_20x_Stitch-MIP	Δ THRB2	10781
R32	180123_ThrB2_KO_4M_DV_Right_slide2_20x-Stitch-MIP	Δ THRB2	10508
R33	180123_ThrB2_KO_4M_whole_Right_slide1_20X-Stitch-MIP	Δ THRB2	15570

Table S2: Comparison of hand (H) and computer (C) segmented retinal sections.

Retina Section Filename	S- & M-opsin (H/C)	S-only (H/C)	M-only (H/C)
171026_WT_F1_Left_20x-Stitch-MIP-DORSAL	13/23	4/6	584/753
171026_WT_F2p_Left_780_20x-Stitch-MIP-VENTRAL	267/313	82/70	2/1
171026_WT_F2p_Left_780_20x-Stitch-MIP-CENTER	186/277	20/26	0/1
171026_WT_F2p_Left_780_20x-Stitch-MIP-DORSAL	4/5	10/13	427/377
171026_WT_F2p_Right_800_20x-Stitch-MIP-VENTRAL	380/783	198/303	0/0
171026_WT_F2p_Right_800_20x-Stitch-MIP-CENTER	515/1060	64/81	8/1
171026_WT_F2p_Right_800_20x-Stitch-MIP-DORSAL	17/29	3/4	259/264

Table S3: Parameters used in the microenvironment model.

Name	Value	Fit	Description
<i>Simulation Setup</i>			
<i>strip_width</i>	1000×10^{-6} m		Retinal strip width
<i>strip_height</i>	5000×10^{-6} m		Retinal strip height
<i>dx</i>	5×10^{-6} m		PDE lattice spacing
<i>dt</i>	8.33×10^{-2} s		PDE time step
<i>d_{cell-cell}</i>	15×10^{-6} m		Center-to-center spacing between cells
<i>r_{cell}</i>	5×10^{-6} m		Cell radius
<i>t_{sync}</i>	1.0×10^0 s		Synchronization time between PDE and CME simulations
<i>PDE Model</i>			
<i>D</i>	1×10^{-10} m ² s ⁻¹		T3 diffusion coefficient
<i>C_{hi}</i>	1×10^{-7} M		T3 dorsal concentration
<i>C_{lo}</i>	1×10^{-9} M		T3 ventral concentration
<i>CME Model - THRβ2 activity</i>			
<i>μ_{thrb}</i>	1×10^{-8} M		Mean of the cellular THRβ2 concentration
<i>σ_{thrb}²</i>	$1.0 \cdot \mu_{thrb}$ M ²		Variance of the cellular THRβ2 concentration
<i>k_D^{thrb}</i>	1.51×10^{-7} M	Y	THRβ2-T3 equilibrium dissociation constant
<i>k_f^{thrb}</i>	1×10^6 M ⁻¹ s ⁻¹		THRβ2-T3 kinetic on rate
<i>k_r^{thrb}</i>	$k_D^{thrb} \cdot k_f^{thrb}$ s ⁻¹		THRβ2-T3 kinetic off rate
<i>CME Model - fate determination</i>			
<i>k_f^{fds}</i>	10 s ⁻¹		Forward rate for FD(S) regulation
<i>k_{lo}^{fds}</i>	9.72×10^{-4}	Y	Lower limit for FD(S) regulation
<i>k_{hi}^{fds}</i>	2.41×10^{-1}	Y	Upper limit for FD(S) regulation
<i>k_m^{fds}</i>	4.37×10^2 molecules	Y	Midpoint of THRβ2* for FD(S) regulation
<i>h₁^{fds}</i>	3.61×10^0	Y	Hill exponent for FD(S) regulation
<i>k_r^{fds}</i>	100 s ⁻¹		Reverse rate for FD(S) regulation
<i>k_f^{fdc}</i>	10 s ⁻¹		Forward rate for FD(C) regulation
<i>k_r^{fdc}</i>	100 s ⁻¹		Reverse rate for FD(C) regulation
<i>CME Model - opsin expression</i>			
<i>k_{deg}^s</i>	0.01 s ⁻¹		S-opsin degradation rate
<i>k_{deg}^m</i>	0.01 s ⁻¹		M-opsin degradation rate
<i>k_{eq}^{ss}</i>	2×10^{-10} M		FD(S) S-opsin equilibrium concentration
<i>k_f^{ss}</i>	$k_{eq}^{ss} \cdot k_{deg}^s$ M s ⁻¹		FD(S) S-opsin expression rate
<i>k_{eq}^{cs}</i>	2×10^{-10} M		FD(C) S-opsin equilibrium concentration
<i>k_f^{cs}</i>	$k_{eq}^{cs} \cdot k_{deg}^s$ M s ⁻¹		Forward rate for FD(C) S-opsin expression
<i>k_{lo1}^{cs}</i>	3.05×10^{-4}	Y	Lower limit for FD(C) S-opsin expression
<i>k_{hi1}^{cs}</i>	6.44×10^{-1}	Y	Upper limit for FD(C) S-opsin expression
<i>k_{m1}^{cs}</i>	6.87×10^2 molecules	Y	Midpoint of THRβ2* for S-opsin expression
<i>h₁^{cs}</i>	1.40×10^1	Y	Hill exponent for FD(C) S-opsin expression
<i>k_{lo2}^{cs}</i>	1.09×10^{-3}	Y	Lower limit for FD(C) S-opsin expression
<i>k_{hi2}^{cs}</i>	7.45×10^{-1}	Y	Upper limit for FD(C) S-opsin expression
<i>k_{m2}^{cs}</i>	2.66×10^3 molecules	Y	Midpoint of THRβ2 for FD(C) S-opsin expression
<i>h₂^{cs}</i>	1.39×10^1	Y	Hill exponent for FD(C) S-opsin expression
<i>k_{eq}^{cm}</i>	2×10^{-10} M		FD(C) M-opsin equilibrium concentration
<i>k_f^{cm}</i>	$k_{eq}^{cm} \cdot k_{deg}^m$ M s ⁻¹		Forward rate for FD(C) M-opsin expression
<i>k_{lo}^{cm}</i>	2.34×10^{-14}	Y	Lower limit for FD(C) M-opsin expression
<i>k_{hi}^{cm}</i>	1.26×10^0	Y	Upper limit for FD(C) M-opsin expression
<i>k_m^{cm}</i>	6.17×10^2 molecules	Y	Midpoint of THRβ2* for FD(C) M-opsin expression
<i>h_{cm}</i>	6.60×10^{-1}	Y	Hill exponent for FD(C) M-opsin expression

Supplementary Figures

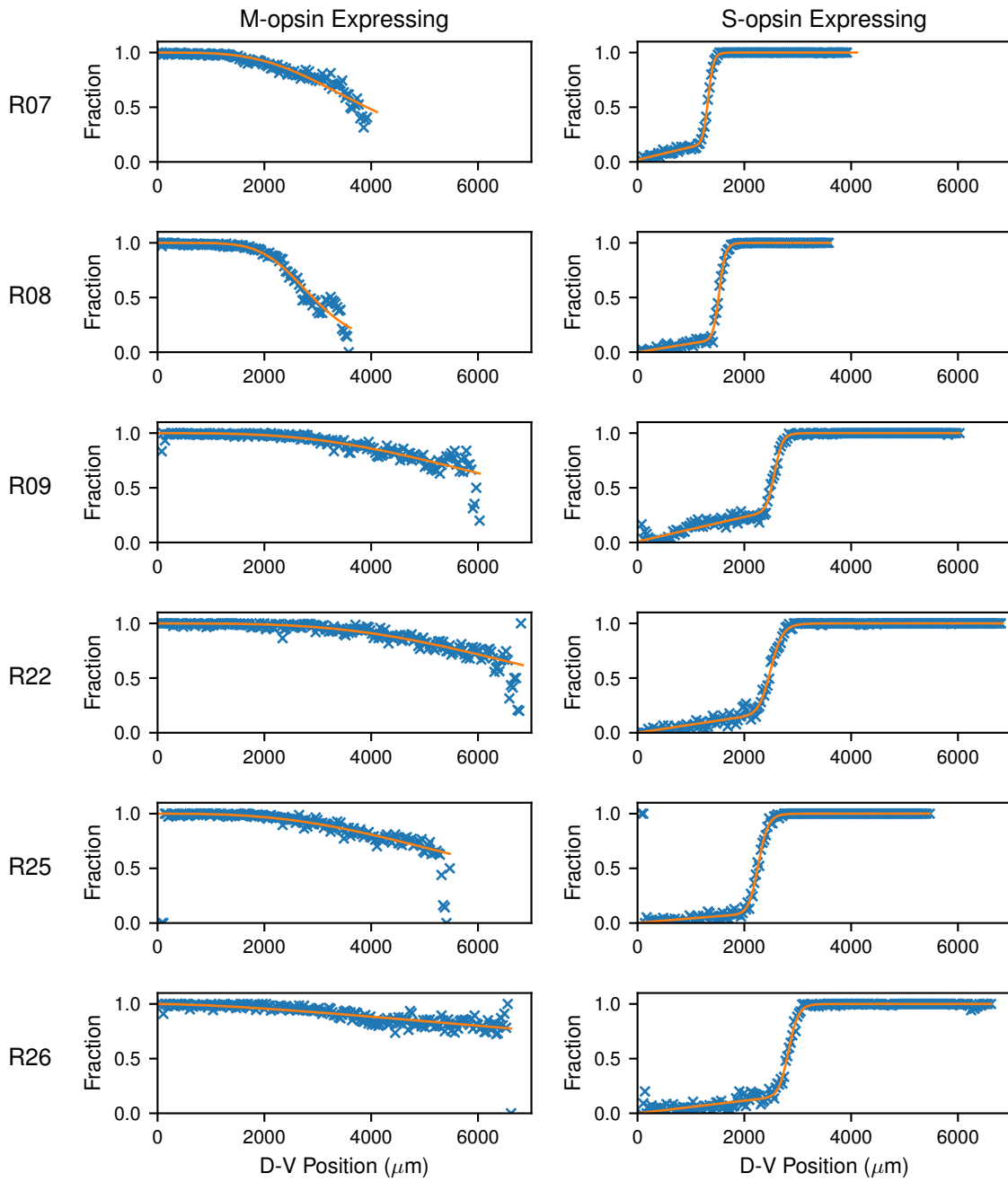


Figure S1: Fitting of cell expression data. Fraction of cells expressing (left) M-opsin and (right) S-opsin by position along the D-V axis. The data from the microscopy analysis (x) are overlaid with the best fit (line) to a fitting function (see text). Rows show different retinas (RXX).

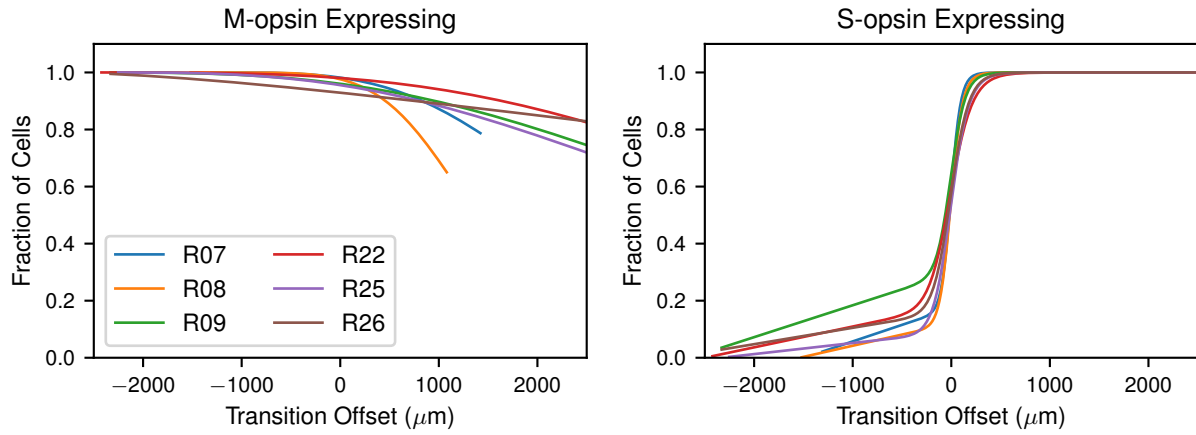


Figure S2: Comparison of D-V profiles between retinas. Overlap of the fraction of cells expressing (left) M-opsin and (right) S-opsin aligned to the transition midpoint as determined from the S-opsin expression profile.

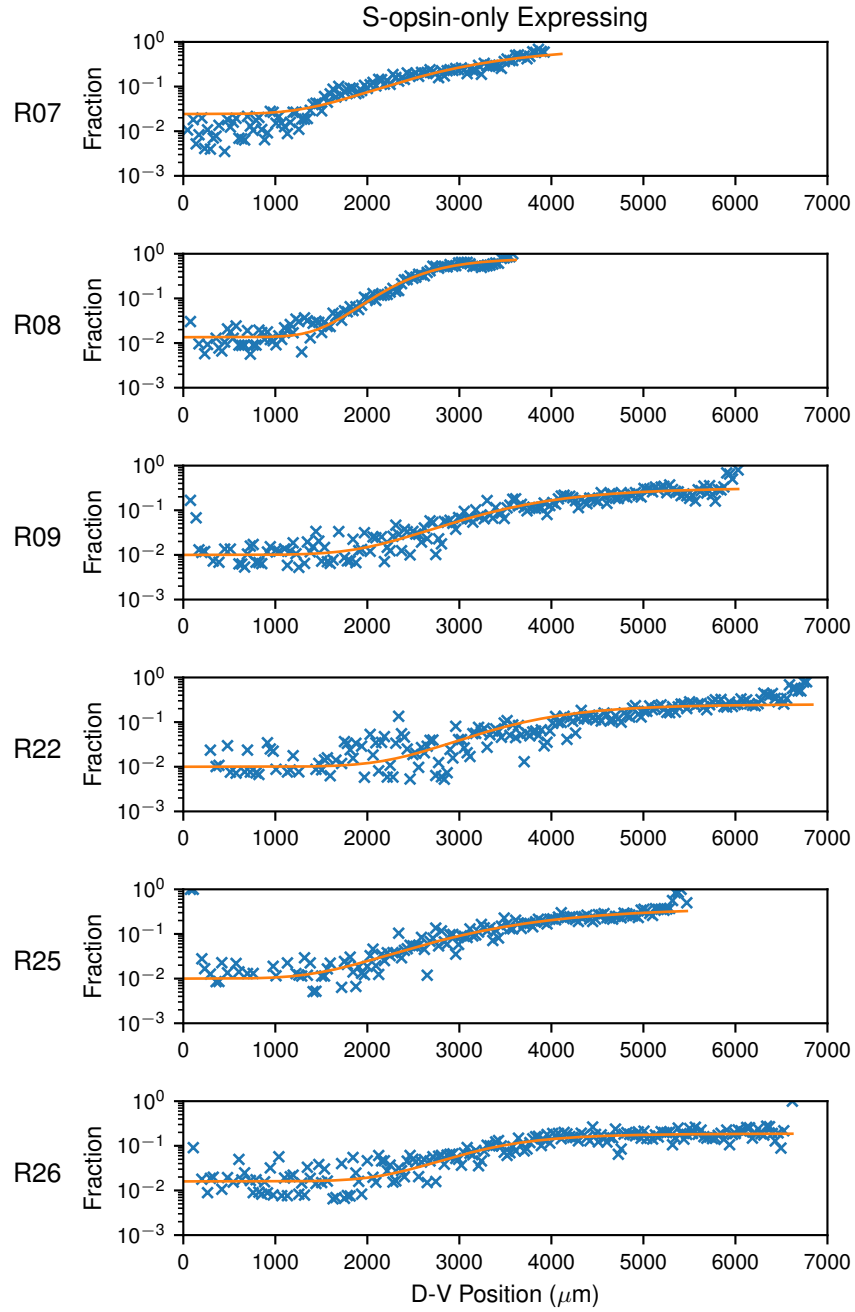


Figure S3: S-only cell fraction. Fraction of cells expressing only S-opsin by position along the D-V axis. The data from the microscopy analysis (x) are overlaid with the best fit (line) to a fitting function (see text). Rows show different retinas (RXX).

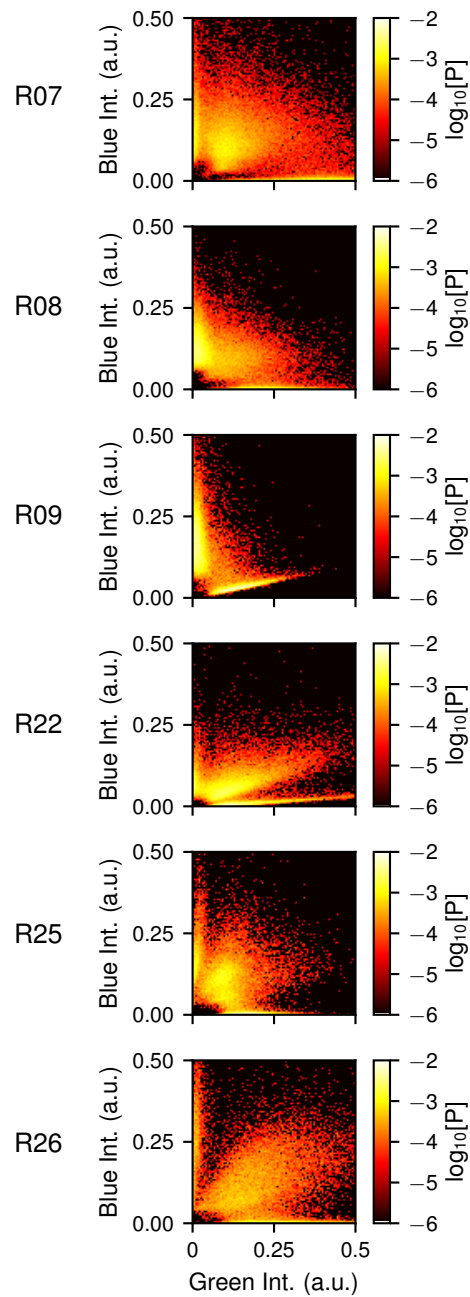


Figure S4: Correlation between S- and M-opsin in retinal cells. Joint probability distributions for the abundance of S-opsin (blue intensity) and M-opsin (green intensity) in cells. Rows show different retinas (RXX). Colors range from $\log_{10}[P] = -2$ (white/yellow) to $\log_{10}[P] = -6$ (red/black).

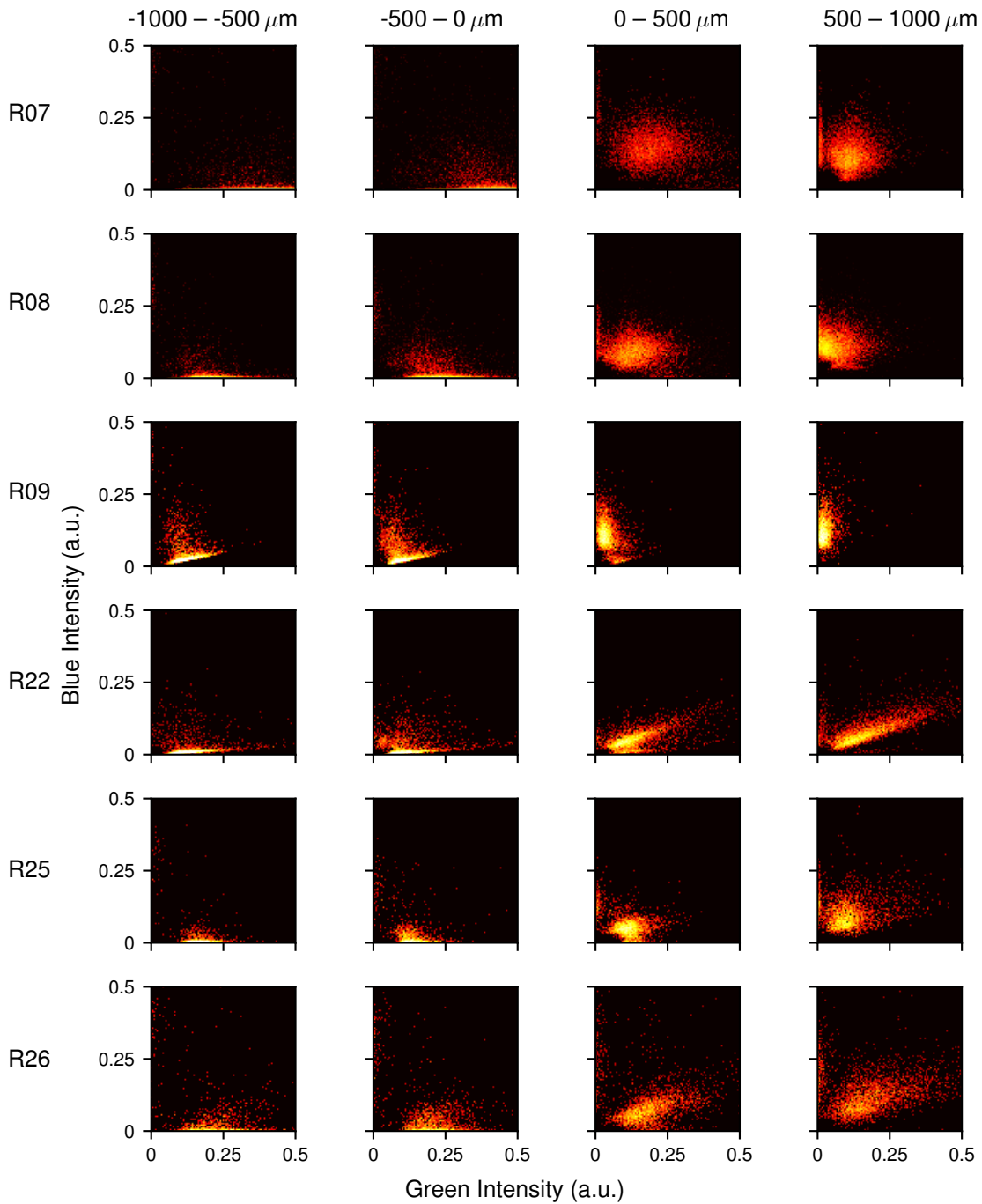


Figure S5: Correlation between S- and M-opsin in retinal cells. Joint probability distributions for the abundance of S-opsin (blue intensity) and M-opsin (green intensity) in cells. Columns show cells binned from four different regions according to distance from the transition midpoint. Rows show different retinas (RXX). Colors range from $\log_{10}[P] = -2$ (white/yellow) to $\log_{10}[P] = -4$ (red/black).

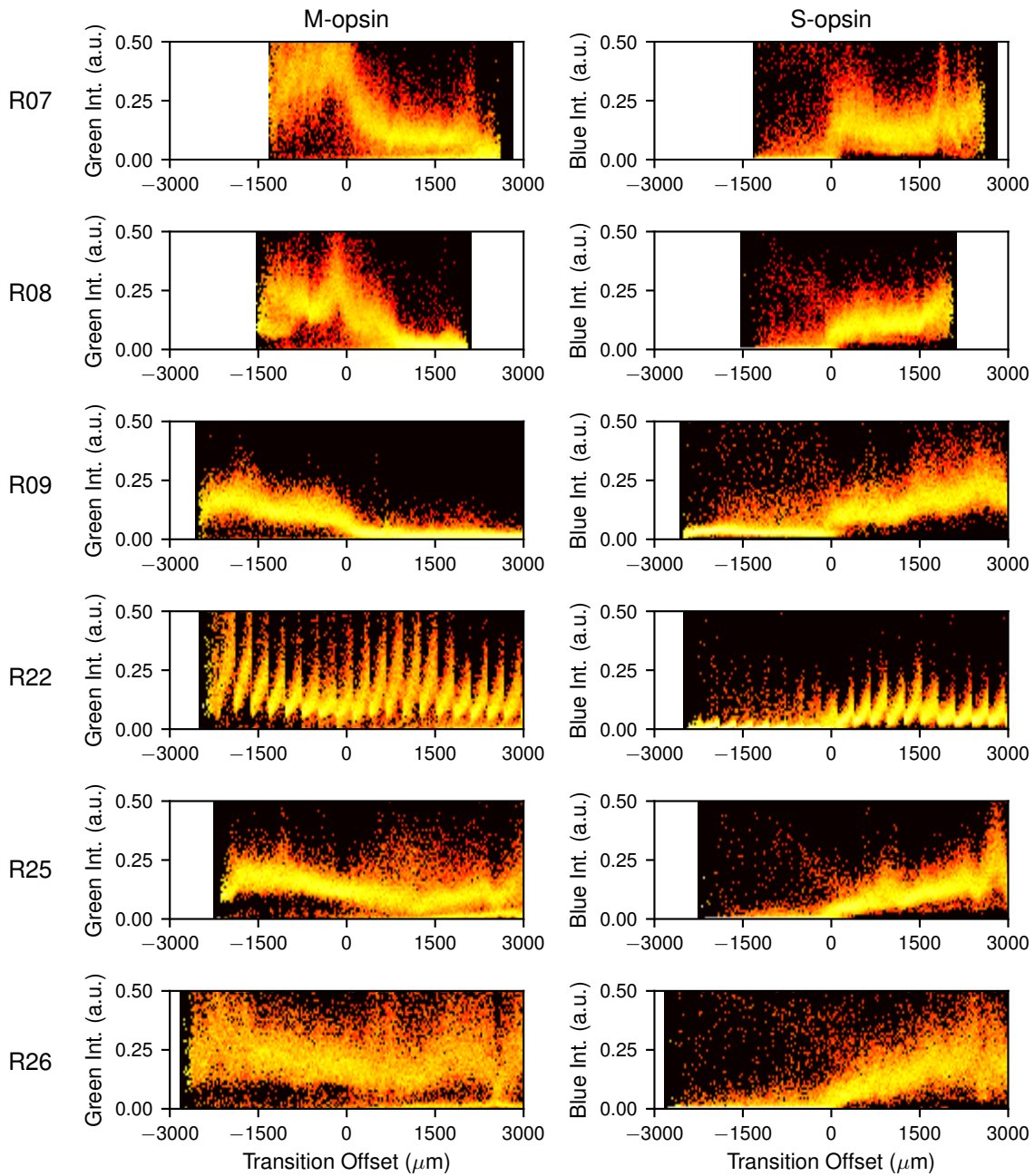


Figure S6: Expression of S- and M-opsin in retinal cells. Probability distribution for the abundance of (left) M-opsin and (right) S-opsin in cells by distance from the transition midpoint. Rows show different retinas (RXX). Colors range from $\log_{10}[P] = 0$ (white/yellow) to $\log_{10}[P] = -4$ (red/black).

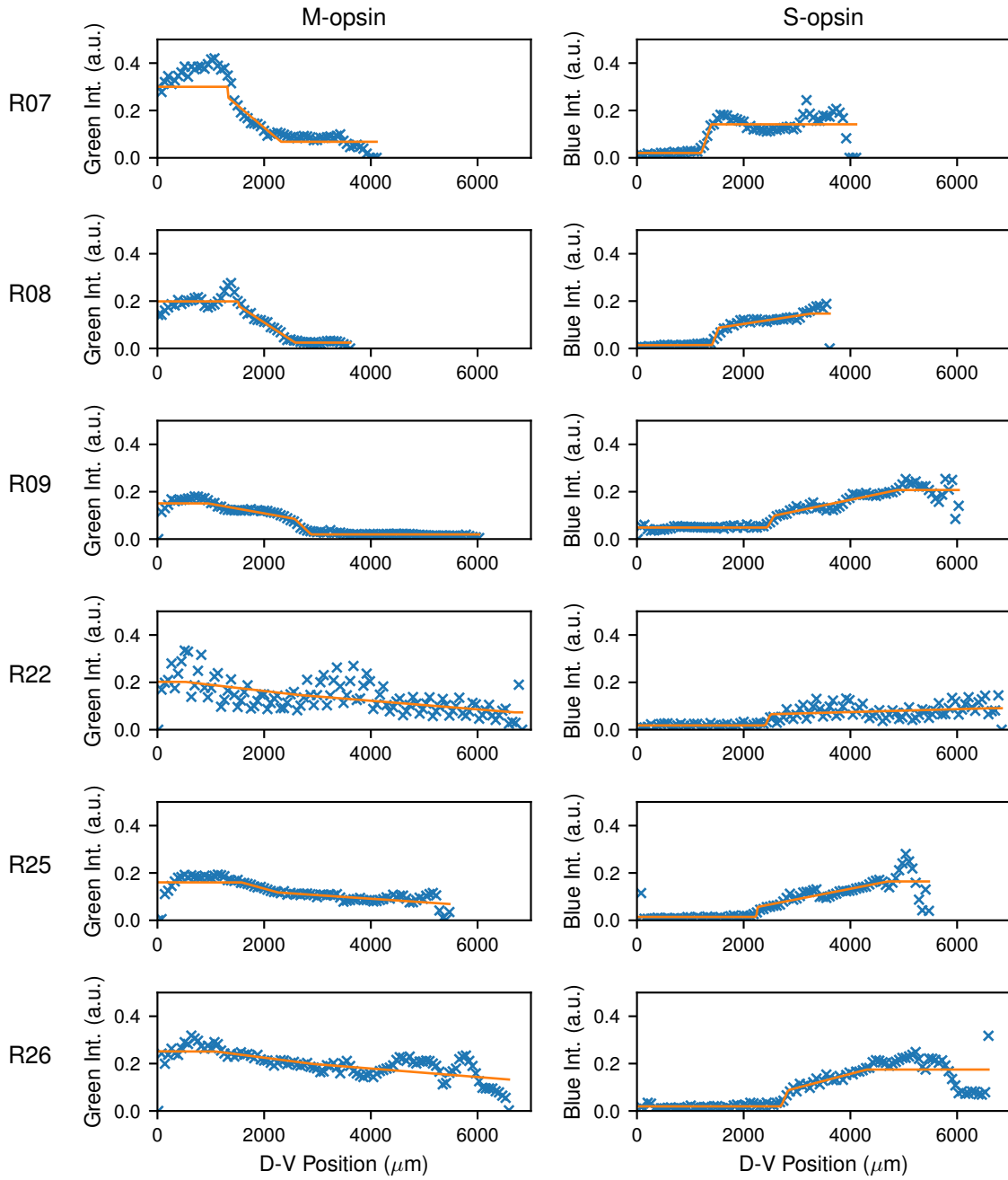


Figure S7: Fitting of cell expression intensity data. Mean intensity in all cells of (left) M-opsin and (right) S-opsin by position along the D-V axis. The data from the microscopy analysis (x) are overlaid with the best fit (line) to a fitting function (see text). Rows show different retinas (RXX).

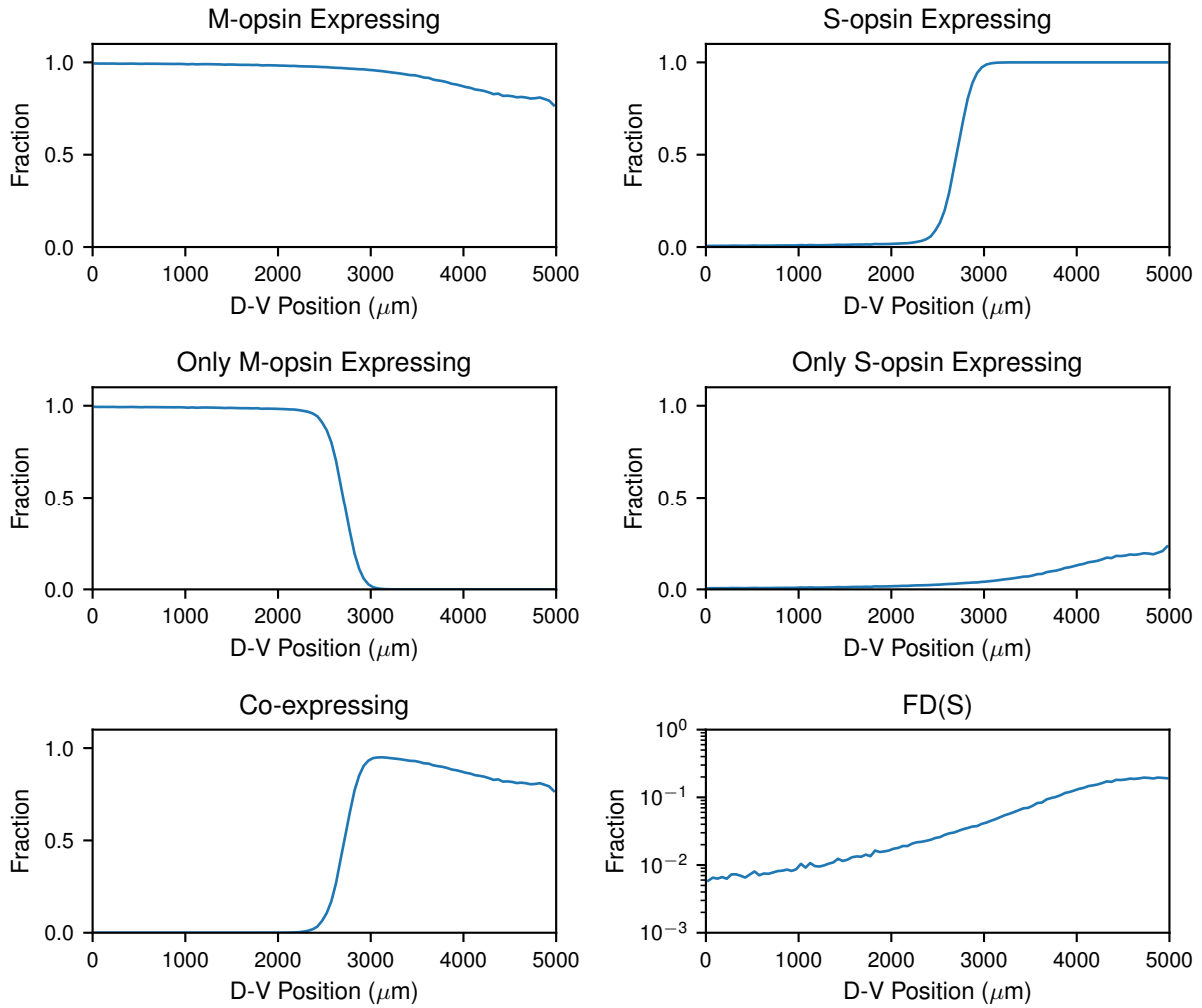


Figure S8: Expression in modeled cell populations. Mean fraction of cells in various cell populations along the D-V axis from numerical simulations of the model. Plots show the mean value computed from 100 independent simulations.

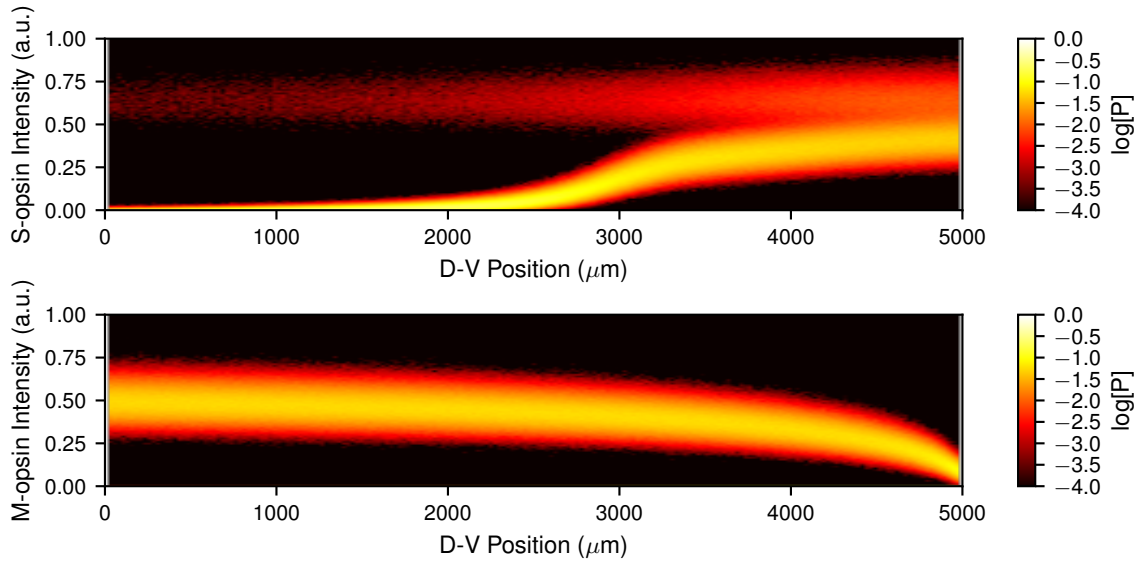


Figure S9: Opsin concentrations in modeled cells. Probability distribution of the abundance of S-opsin (blue intensity) and M-opsin (green intensity) in cells along the D-V axis from numerical simulations of the model. Distributions were computed from 100 independent simulations.

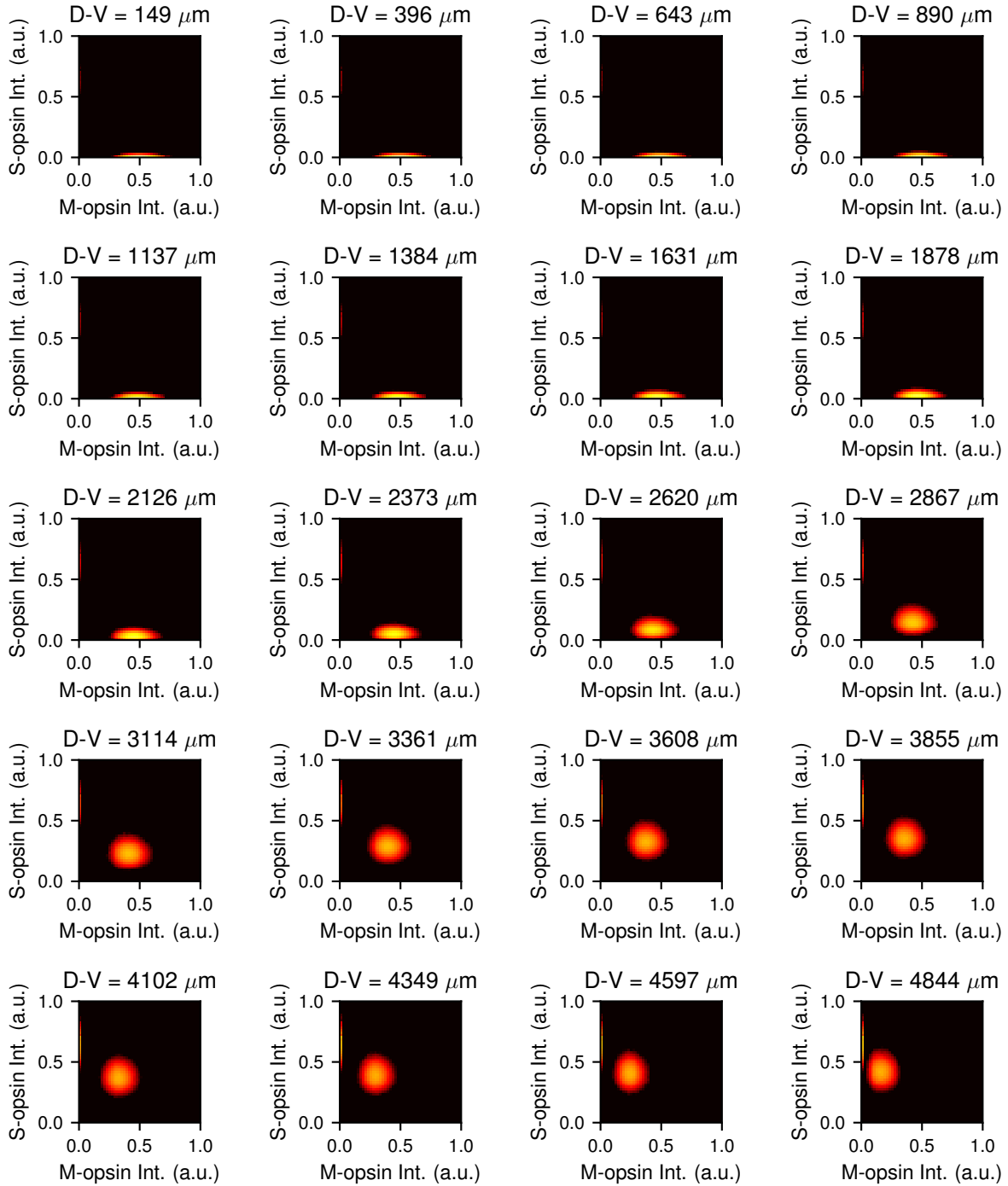


Figure S10: Correlation between S- and M-opsin in modeled cells. Joint probability distributions for the abundance of S-opsin (blue intensity) and M-opsin (green intensity) in cells located in $\sim 250\mu\text{m}$ wide bins along the D-V axis. Colors range from $\log_{10}[P] = -2$ (white/yellow) to $\log_{10}[P] = -5$ (red/black). Distributions were computed from 100 independent simulations. The low density tails leading to 0,0 are from cells that were sampled during the process of switching phenotypes.

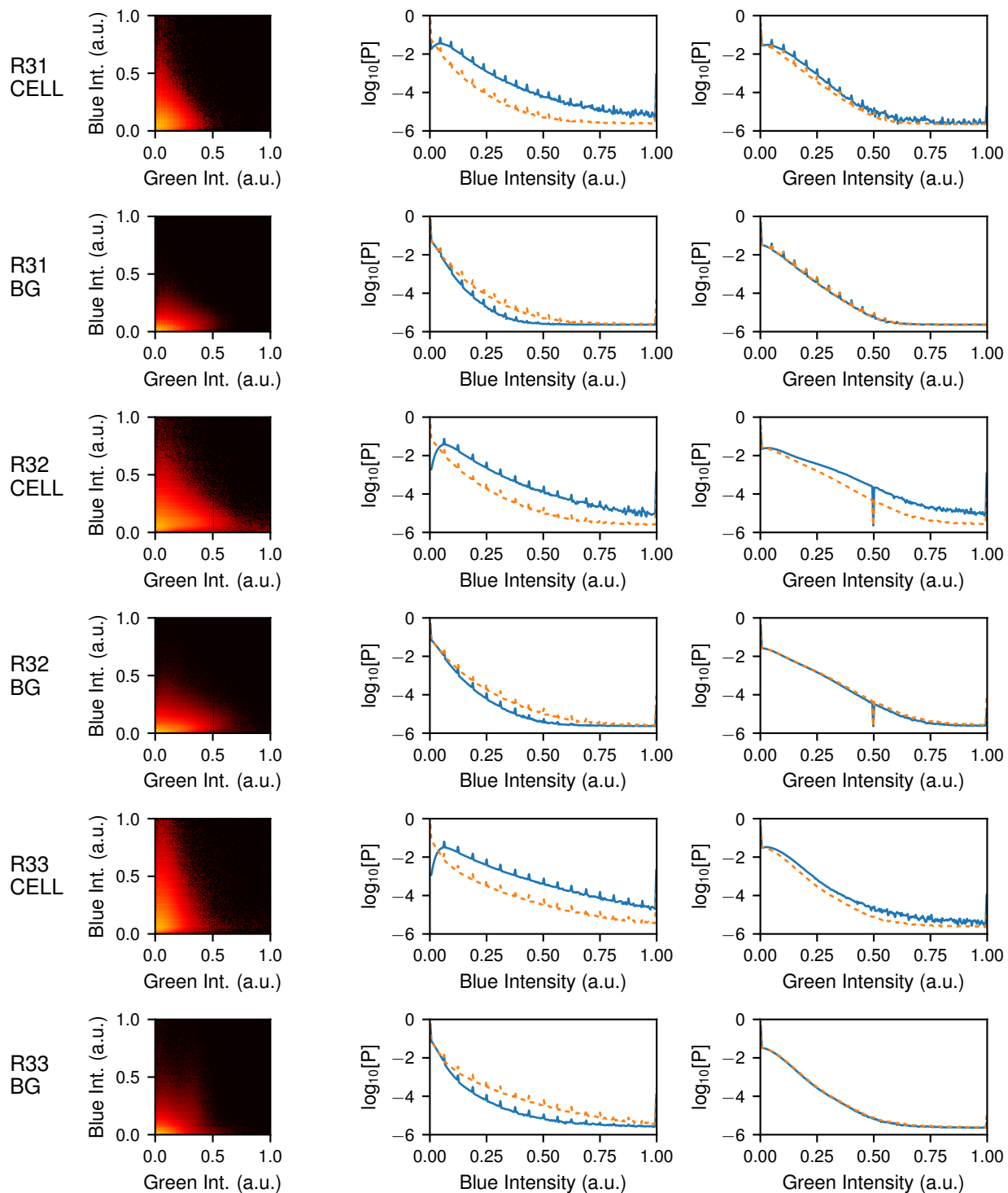


Figure S11: Analysis of pixel intensities in images of Δ THR2 cells. (left) Joint probability distribution of the blue and green intensity of pixels located either inside of cell boundaries (RXX CELL) or the background outside of cells (RXX BG) as indicated. Colors range from $\log_{10}[P] = 0$ (white/yellow) to $\log_{10}[P] = -8$ (red/black). (center) Probability for a pixel of the indicated type to have a particular blue intensity (solid line) compared with the distribution for all pixels (dashed line). (right) The same for green intensity. Δ THR2 cells do not exhibit green expression above background.

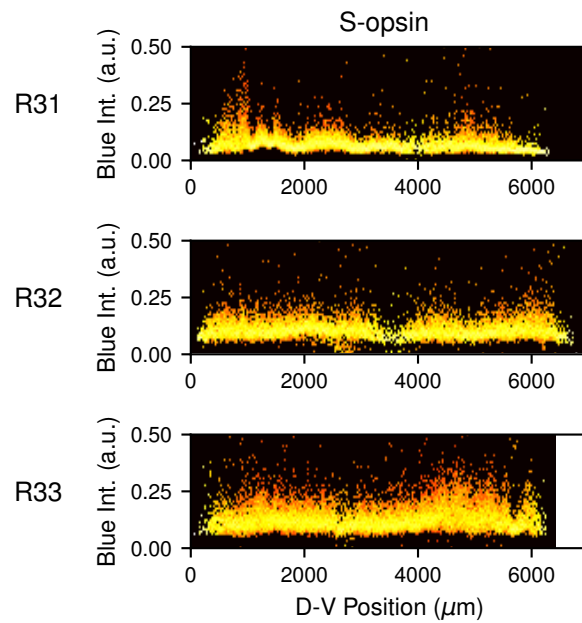


Figure S12: Expression of S-opsin in Δ THR_{B2} retinal cells. Probability distribution for the abundance of S-opsin in cells by distance along the D-V axis. Rows show different Δ THR_{B2} retinas (RXX). Colors range from $\log_{10}[P] = 0$ (white/yellow) to $\log_{10}[P] = -4$ (red/black).

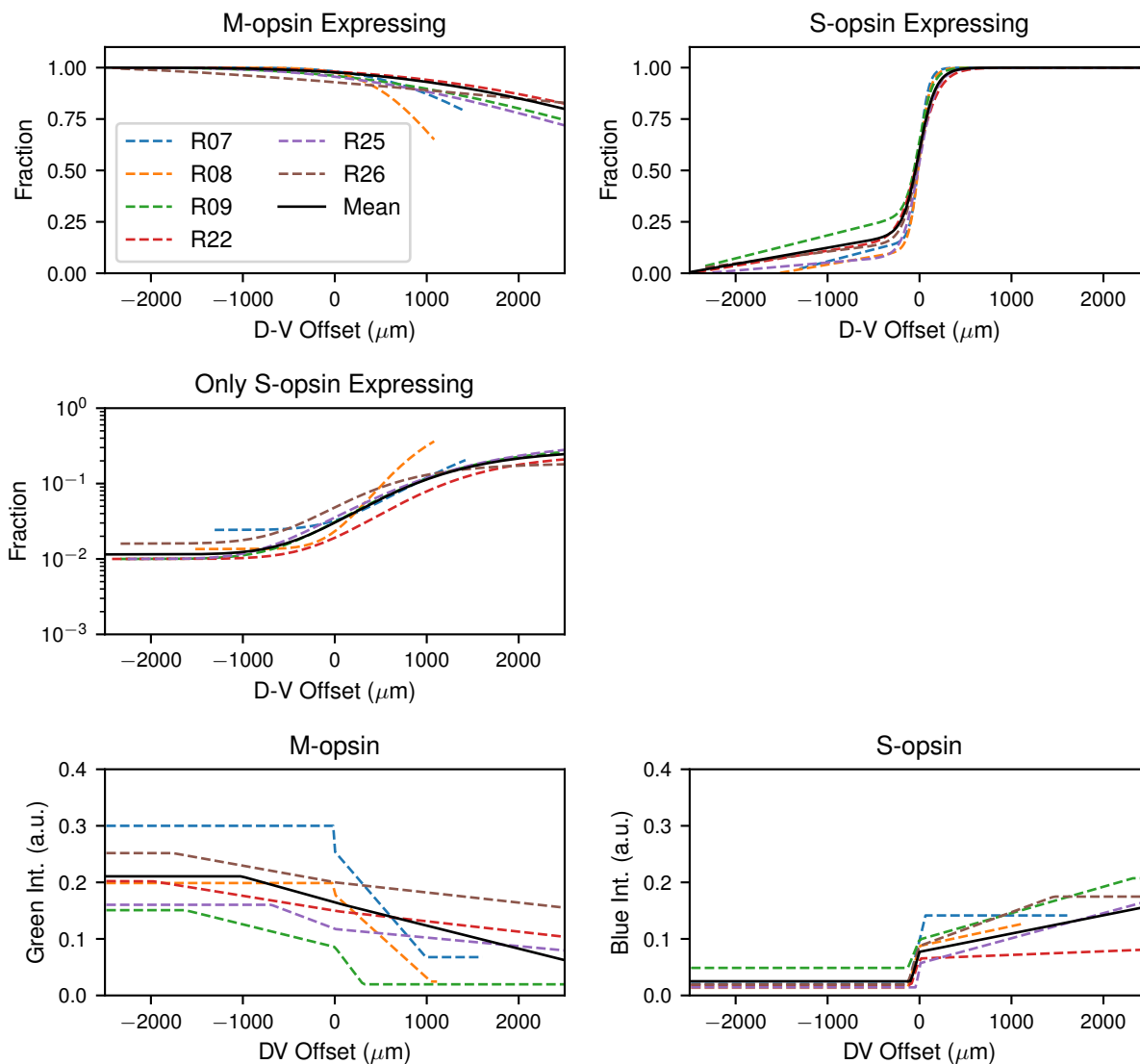


Figure S13: Mean retina description. Comparison of the fits for individual retinas (dashed lines) with our hypothetical mean retina used for model parameterization (solid line) along the D-V axis. The top row shows a comparison of the fraction of cells expressing M- and S- opsin, respectively. The middle row shows the fraction of FD(S) cells. The bottom row shows the mean M- and S-opsin expression intensity, respectively.

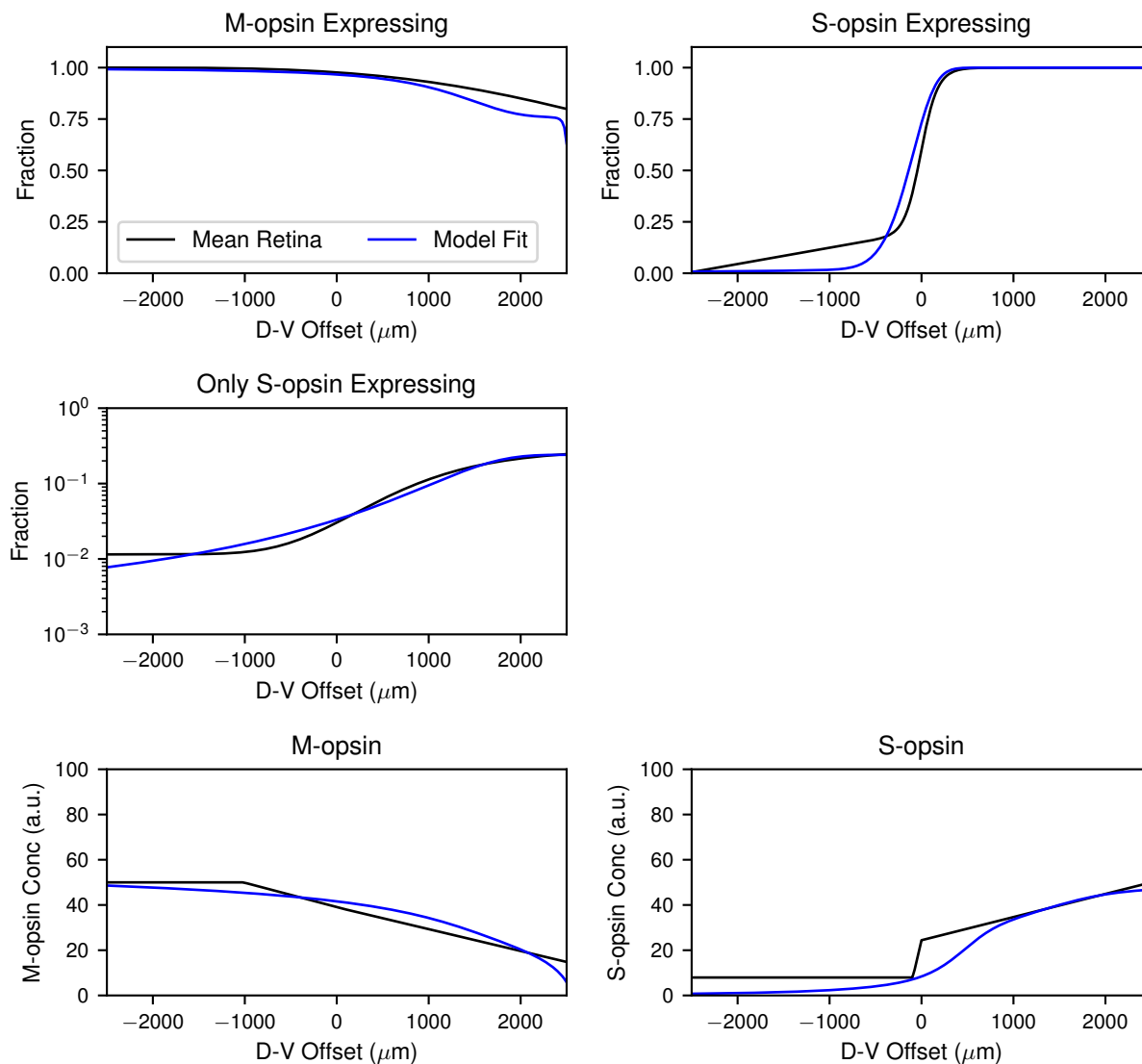


Figure S14: Best fit parameterization. Comparison of the best fit model parameterization (blue) with the hypothetical mean retina (black). The top row shows a comparison of the fraction of cells expressing M- and S- opsin, respectively. The middle row shows the fraction of FD(S) cells. The bottom row shows the mean M- and S-opsin concentration per cell, respectively.

References:

- Aavani, T., Tachibana, N., Wallace, V., Biernaskie, J., and Schuurmans, C. (2017). Temporal profiling of photoreceptor lineage gene expression during murine retinal development. *Gene expression patterns : GEP* 23-24, 32-44.
- Ahnelt, P.K. (1998). The photoreceptor mosaic. *Eye (London, England)* 12 (Pt 3b), 531-540.
- Ahnelt, P.K., Kolb, H., and Pflug, R. (1987). Identification of a subtype of cone photoreceptor, likely to be blue sensitive, in the human retina. *J Comp Neurol* 255, 18-34.
- Akagi, T., Akita, J., Haruta, M., Suzuki, T., Honda, Y., Inoue, T., Yoshiura, S., Kageyama, R., Yatsu, T., Yamada, M., *et al.* (2005). Iris-derived cells from adult rodents and primates adopt photoreceptor-specific phenotypes. *Investigative ophthalmology & visual science* 46, 3411-3419.
- Alfano, G., Conte, I., Caramico, T., Avellino, R., Arno, B., Pizzo, M.T., Tanimoto, N., Beck, S.C., Huber, G., Dolle, P., *et al.* (2011). Vax2 regulates retinoic acid distribution and cone opsin expression in the vertebrate eye. *Development* 138, 261-271.
- Ali, M.A. (1975). Retinomotor responses. In *Vision in Fishes*, M.A. Ali, ed. (New York: Plenum), pp. 313-355.
- Allison, W.T., Barthel, L.K., Skebo, K.M., Takechi, M., Kawamura, S., and Raymond, P.A. (2010). Ontogeny of cone photoreceptor mosaics in zebrafish. *The Journal of comparative neurology* 518, 4182-4195.
- Alvarez-Delfin, K., Morris, A.C., Snelson, C.D., Gamse, J.T., Gupta, T., Marlow, F.L., Mullins, M.C., Burgess, H.A., Granato, M., and Fadool, J.M. (2009). Tbx2b is required for ultraviolet photoreceptor cell specification during zebrafish retinal development. *Proceedings of the National Academy of Sciences of the United States of America* 106, 2023-2028.
- Anderson, C., Reiss, I., Zhou, C., Cho, A., Siddiqi, H., Mormann, B., Avelis, C.M., Deford, P., Bergland, A., Roberts, E., *et al.* (2017). Natural variation in stochastic photoreceptor specification and color preference in *Drosophila*. *eLife* 6.
- Applebury, M.L., Antoch, M.P., Baxter, L.C., Chun, L.L., Falk, J.D., Farhangfar, F., Kage, K., Krzystolik, M.G., Lyass, L.A., and Robbins, J.T. (2000). The murine cone photoreceptor: a single cone type expresses both S and M opsins with retinal spatial patterning. *Neuron* 27, 513-523.

- Applebury, M.L., Farhangfar, F., Glosmann, M., Hashimoto, K., Kage, K., Robbins, J.T., Shibusawa, N., Wondisford, F.E., and Zhang, H. (2007). Transient expression of thyroid hormone nuclear receptor TRbeta2 sets S opsin patterning during cone photoreceptor genesis. *Developmental dynamics : an official publication of the American Association of Anatomists* 236, 1203-1212.
- Araki, M., Fukada, Y., Shichida, Y., and Yoshizawa, T. (1990). Localization of iodopsin in the chick retina during in vivo and in vitro cone differentiation. *Investigative ophthalmology & visual science* 31, 1466-1473.
- Artero Castro, A., Lukovic, D., Jendelova, P., and Erceg, S. (2018). Concise Review: Human Induced Pluripotent Stem Cell Models of Retinitis Pigmentosa. *Stem cells (Dayton, Ohio)* 36, 474-481.
- Asaoka, Y., Hata, S., Namae, M., Furutani-Seiki, M., and Nishina, H. (2014). The Hippo pathway controls a switch between retinal progenitor cell proliferation and photoreceptor cell differentiation in zebrafish. *PloS one* 9, e97365.
- Baden, T., Schubert, T., Chang, L., Wei, T., Zaichuk, M., Wissinger, B., and Euler, T. (2013). A tale of two retinal domains: near-optimal sampling of achromatic contrasts in natural scenes through asymmetric photoreceptor distribution. *Neuron* 80, 1206-1217.
- Bagci, E., Heijlen, M., Vergauwen, L., Hagenaaars, A., Houbrechts, A.M., Esguerra, C.V., Blust, R., Darras, V.M., and Knapen, D. (2015). Deiodinase knockdown during early zebrafish development affects growth, development, energy metabolism, motility and phototransduction. *PloS one* 10, e0123285.
- Baonza, A., Casci, T., and Freeman, M. (2001). A primary role for the epidermal growth factor receptor in ommatidial spacing in the Drosophila eye. *Current biology : CB* 11, 396-404.
- Barnea-Cramer, A.O., Wang, W., Lu, S.J., Singh, M.S., Luo, C., Huo, H., McClements, M.E., Barnard, A.R., MacLaren, R.E., and Lanza, R. (2016). Function of human pluripotent stem cell-derived photoreceptor progenitors in blind mice. *Sci Rep* 6, 29784.
- Barrett, E.J. (2012). *Medical Physiology*. In *Medical Physiology, 2e Updated Edition*, W.B.E. Boulpaep, ed. (Philadelphia, PA: Elsevier, Inc.).
- Bedolla, D.E., and Torre, V. (2011). A component of retinal light adaptation mediated by the thyroid hormone cascade. *PloS one* 6, e26334.

Bell, M.L., Earl, J.B., and Britt, S.G. (2007). Two types of *Drosophila* R7 photoreceptor cells are arranged randomly: a model for stochastic cell-fate determination. *The Journal of comparative neurology* 502, 75-85.

Bernal, J. (2005). Thyroid hormones and brain development. *Vitam Horm* 71, 95-122.

Bessant, D.A., Payne, A.M., Mitton, K.P., Wang, Q.L., Swain, P.K., Plant, C., Bird, A.C., Zack, D.J., Swaroop, A., and Bhattacharya, S.S. (1999). A mutation in *NRL* is associated with autosomal dominant retinitis pigmentosa. *Nature genetics* 21, 355-356.

Bhise, N.S., Wahlin, K.J., Zack, D.J., and Green, J.J. (2013). Evaluating the potential of poly(beta-amino ester) nanoparticles for reprogramming human fibroblasts to become induced pluripotent stem cells. *Int J Nanomedicine* 8, 4641-4658.

Bianco, A.C., Salvatore, D., Gereben, B., Berry, M.J., and Larsen, P.R. (2002). Biochemistry, cellular and molecular biology, and physiological roles of the iodothyronine selenodeiodinases. *Endocr Rev* 23, 38-89.

Bonezzi, P.J., Stabio, M.E., and Renna, J.M. (2018). The Development of Mid-Wavelength Photoresponsivity in the Mouse Retina. *Current eye research*, 1-8.

Bovolenta, P., Mallamaci, A., Briata, P., Corte, G., and Boncinelli, E. (1997). Implication of *OTX2* in pigment epithelium determination and neural retina differentiation. *The Journal of neuroscience : the official journal of the Society for Neuroscience* 17, 4243-4252.

Bowmaker, J.K. (2008). Evolution of vertebrate visual pigments. *Vision research* 48, 2022-2041.

Brainard, D.R., Austin; Yamauchi, Yasuki; Calderone, Jack; Metha, Andrew; Neitz, Maureen; Neitz, Jay; Williams, David; Jacobs, Gerald (2000). Functional consequences of the relative numbers of L and M cones. *Optical Society of America* 17, 607-614.

Branchek, T., and Bremiller, R. (1984). The development of photoreceptors in the zebrafish, *Brachydanio rerio*. I. Structure. *The Journal of comparative neurology* 224, 107-115.

Bruhn, S.L., and Cepko, C.L. (1996). Development of the pattern of photoreceptors in the chick retina. *The Journal of neuroscience : the official journal of the Society for Neuroscience* 16, 1430-1439.

Bueno, J.M., Giakoumaki, A., Gualda, E.J., Schaeffel, F., and Artal, P. (2011). Analysis of the chicken retina with an adaptive optics multiphoton microscope. *Biomedical optics express* 2, 1637-1648.

Buettner, F., Natarajan, K.N., Casale, F.P., Proserpio, V., Scialdone, A., Theis, F.J., Teichmann, S.A., Marioni, J.C., and Stegle, O. (2015). Computational analysis of cell-to-cell heterogeneity in single-cell RNA-sequencing data reveals hidden subpopulations of cells. *Nat Biotechnol* 33, 155-160.

Cakir, M., Turgut Ozturk, B., Turan, E., Gonulalan, G., Polat, I., and Gunduz, K. (2015). The effect of hypothyroidism on color contrast sensitivity: a prospective study. *European thyroid journal* 4, 43-47.

Calderone, J.B., and Jacobs, G.H. (1995). Regional variations in the relative sensitivity to UV light in the mouse retina. *Visual neuroscience* 12, 463-468.

Calkins, D.J., Schein, S.J., Tsukamoto, Y., and Sterling, P. (1994). M and L cones in macaque fovea connect to midget ganglion cells by different numbers of excitatory synapses. *Nature* 371, 70-72.

Cameron, D.A., and Carney, L.H. (2004). Cellular patterns in the inner retina of adult zebrafish: quantitative analyses and a computational model of their formation. *J Comp Neurol* 471, 11-25.

Campello, R.J.G.B., Moulavi, D., and Sander, J. (2013). *Density-Based Clustering Based on Hierarchical Density Estimates* (Berlin, Heidelberg: Springer Berlin Heidelberg).

Campenhausen, M., and Kirschfeld, K. (1998). Spectral sensitivity of the accessory optic system of the pigeon. *Journal of Comparative Physiology A* 183, 1-6.

Carter-Dawson, L.D., and LaVail, M.M. (1979). Rods and cones in the mouse retina. II. Autoradiographic analysis of cell generation using tritiated thymidine. *J Comp Neurol* 188, 263-272.

Chang, L., Breuninger, T., and Euler, T. (2013). Chromatic coding from cone-type unselective circuits in the mouse retina. *Neuron* 77, 559-571.

Chen, C.M., and Cepko, C.L. (2002). The chicken RaxL gene plays a role in the initiation of photoreceptor differentiation. *Development* 129, 5363-5375.

Chen, J., Rattner, A., and Nathans, J. (2005). The rod photoreceptor-specific nuclear receptor Nr2e3 represses transcription of multiple cone-specific genes. *The Journal of neuroscience : the official journal of the Society for Neuroscience* 25, 118-129.

Chen, S., Wang, Q.L., Nie, Z., Sun, H., Lennon, G., Copeland, N.G., Gilbert, D.J., Jenkins, N.A., and Zack, D.J. (1997). Crx, a novel Otx-like paired-homeodomain protein, binds to and transactivates photoreceptor cell-specific genes. *Neuron* 19, 1017-1030.

Chinen, A., Hamaoka, T., Yamada, Y., and Kawamura, S. (2003). Gene duplication and spectral diversification of cone visual pigments of zebrafish. *Genetics* 163, 663-675.

Chou, W.H., Hall, K.J., Wilson, D.B., Wideman, C.L., Townson, S.M., Chadwell, L.V., and Britt, S.G. (1996). Identification of a novel *Drosophila* opsin reveals specific patterning of the R7 and R8 photoreceptor cells. *Neuron* 17, 1101-1115.

Chou, W.H., Huber, A., Bentrop, J., Schulz, S., Schwab, K., Chadwell, L.V., Paulsen, R., and Britt, S.G. (1999). Patterning of the R7 and R8 photoreceptor cells of *Drosophila*: evidence for induced and default cell-fate specification. *Development* 126, 607-616.

Chuang, J.C., Mathers, P.H., and Raymond, P.A. (1999). Expression of three Rx homeobox genes in embryonic and adult zebrafish. *Mechanisms of development* 84, 195-198.

Clark, B.S., Stein-O'Brien, G.L., Shiao, F., Cannon, G.H., Davis-Marcisak, E., Sherman, T., Santiago, C.P., Hoang, T.V., Rajaii, F., James-Esposito, R.E., *et al.* (2019). Single-Cell RNA-Seq Analysis of Retinal Development Identifies NFI Factors as Regulating Mitotic Exit and Late-Born Cell Specification. *Neuron* 102, 1111-1126 e1115.

Cook, T., Pichaud, F., Sonnevile, R., Papatsenko, D., and Desplan, C. (2003). Distinction between color photoreceptor cell fates is controlled by Prospero in *Drosophila*. *Developmental cell* 4, 853-864.

Corbo, J.C., Myers, C.A., Lawrence, K.A., Jadhav, A.P., and Cepko, C.L. (2007). A typology of photoreceptor gene expression patterns in the mouse. *Proceedings of the National Academy of Sciences of the United States of America* 104, 12069-12074.

Cornish, E.E., Hendrickson, A.E., and Provis, J.M. (2004). Distribution of short-wavelength-sensitive cones in human fetal and postnatal retina: early development of spatial order and density profiles. *Vision research* 44, 2019-2026.

Cornish, E.E., Madigan, M.C., Natoli, R., Hales, A., Hendrickson, A.E., and Provis, J.M. (2005). Gradients of cone differentiation and FGF expression during development of the foveal depression in macaque retina. *Visual neuroscience* 22, 447-459.

Coulier, A., and Hellander, A. (2018). Orchestral: A Lightweight Framework for Parallel Simulations of Cell-Cell Communication. 2018 IEEE 14th International Conference on e-Science (e-Science), 168-176.

Curcio, C.A., Allen, K.A., Sloan, K.R., Lerea, C.L., Hurley, J.B., Klock, I.B., and Milam, A.H. (1991). Distribution and morphology of human cone photoreceptors stained with anti-blue opsin. *The Journal of Comparative Neurology* 312, 610-624.

Curcio, C.A., Sloan, K.R., Kalina, R.E., and Hendrickson, A.E. (1990). Human photoreceptor topography. *J Comp Neurol* 292, 497-523.

Daniele, L.L., Insinna, C., Chance, R., Wang, J., Nikonov, S.S., and Pugh, E.N., Jr. (2011). A mouse M-opsin monochromat: retinal cone photoreceptors have increased M-opsin expression when S-opsin is knocked out. *Vision research* 51, 447-458.

Darras, V.M., Houbrechts, A.M., and Van Herck, S.L. (2015). Intracellular thyroid hormone metabolism as a local regulator of nuclear thyroid hormone receptor-mediated impact on vertebrate development. *Biochimica et biophysica acta* 1849, 130-141.

de Melo, J., Peng, G.H., Chen, S., and Blackshaw, S. (2011). The Spalt family transcription factor Sall3 regulates the development of cone photoreceptors and retinal horizontal interneurons. *Development* 138, 2325-2336.

DeAngelis, M.M., Grimsby, J.L., Sandberg, M.A., Berson, E.L., and Dryja, T.P. (2002). Novel mutations in the NRL gene and associated clinical findings in patients with dominant retinitis pigmentosa. *Arch Ophthalmol* 120, 369-375.

Deeb, S.S. (2005). The molecular basis of variation in human color vision. *Clinical genetics* 67, 369-377.

Dentice, M., Marsili, A., Zavacki, A., Larsen, P.R., and Salvatore, D. (2013). The deiodinases and the control of intracellular thyroid hormone signaling during cellular differentiation. *Biochimica et biophysica acta* 1830, 3937-3945.

Diaz-Araya, C., and Provis, J.M. (1992). Evidence of photoreceptor migration during early foveal development: a quantitative analysis of human fetal retinae. *Visual neuroscience* 8, 505-514.

Dinet, V., An, N., Ciccotosto, G.D., Bruban, J., Maoui, A., Bellingham, S.A., Hill, A.F., Andersen, O.M., Nykjaer, A., Jonet, L., *et al.* (2011). APP involvement in retinogenesis of mice. *Acta Neuropathol* 121, 351-363.

Dowdeswell, H.J., Slater, A.M., Broomhall, J., and Tripp, J. (1995). Visual deficits in children born at less than 32 weeks' gestation with and without major ocular pathology and cerebral damage. *Br J Ophthalmol* 79, 447-452.

Dubovy, S.R., Fernandez, M.P., Echegaray, J.J., Block, N.L., Unoki, N., Perez, R., Vidaurre, I., Lee, R.K., Nadji, M., and Schally, A.V. (2017). Expression of hypothalamic neurohormones and their receptors in the human eye. *Oncotarget* 8, 66796-66814.

Duval, M.G., Oel, A.P., and Allison, W.T. (2014). *gdf6a* is required for cone photoreceptor subtype differentiation and for the actions of *tbx2b* in determining rod versus cone photoreceptor fate. *PLoS one* 9, e92991.

Ehrlich, D. (1981). Regional specialization of the chick retina as revealed by the size and density of neurons in the ganglion cell layer. *J Comp Neurol* 195, 643-657.

Eldred, K.C., Hadyniak, S.E., Hussey, K.A., Brennerman, B., Zhang, P.W., Chamling, X., Sluch, V.M., Welsbie, D.S., Hattar, S., Taylor, J., *et al.* (2018). Thyroid hormone signaling specifies cone subtypes in human retinal organoids. *Science* 362.

Emerson, M.M., and Cepko, C.L. (2011). Identification of a retina-specific *Otx2* enhancer element active in immature developing photoreceptors. *Developmental biology* 360, 241-255.

Emerson, M.M., Surzenko, N., Goetz, J.J., Trimarchi, J., and Cepko, C.L. (2013). *Otx2* and *Onecut1* promote the fates of cone photoreceptors and horizontal cells and repress rod photoreceptors. *Developmental cell* 26, 59-72.

Engblom, S. (2018). Stochastic Simulation of Pattern Formation in Growing Tissue: A Multilevel Approach. *Bull Math Biol*.

Engblom, S., Wilson, D.B., and Baker, R.E. (2018). Scalable population-level modelling of biological cells incorporating mechanics and kinetics in continuous time. *R Soc Open Sci* 5, 180379.

Engstrom, K. (1963). Cone Types and Cone Arrangements in Teleost Retinae. *Acta Zoologica* 44, 179-243.

Fadool, J.M. (2003). Development of a rod photoreceptor mosaic revealed in transgenic zebrafish. *Developmental biology* 258, 277-290.

Folguera-Blasco, N., Perez-Carrasco, R., Cuyas, E., Menendez, J.A., and Alarcon, T. (2019). A multiscale model of epigenetic heterogeneity-driven cell fate decision-making. *PLoS Comput Biol* 15, e1006592.

Formosa-Jordan, P., Teles, J, Jönsson, H (2018). *Mathematical Modelling in Plant Biology* (Springer, Cham).

Fortini, M.E., and Rubin, G.M. (1990). Analysis of cis-acting requirements of the Rh3 and Rh4 genes reveals a bipartite organization to rhodopsin promoters in *Drosophila melanogaster*. *Genes & development* 4, 444-463.

Frasson, M., Picaud, S., Leveillard, T., Simonutti, M., Mohand-Said, S., Dreyfus, H., Hicks, D., and Sabel, J. (1999). Glial cell line-derived neurotrophic factor induces histologic and functional protection of rod photoreceptors in the rd/rd mouse. *Investigative ophthalmology & visual science* 40, 2724-2734.

Freeman, M. (1994). The spitz gene is required for photoreceptor determination in the *Drosophila* eye where it interacts with the EGF receptor. *Mechanisms of development* 48, 25-33.

Freeman, M. (1996). Reiterative use of the EGF receptor triggers differentiation of all cell types in the *Drosophila* eye. *Cell* 87, 651-660.

Freund, C.L., Gregory-Evans, C.Y., Furukawa, T., Papaioannou, M., Looser, J., Ploder, L., Bellingham, J., Ng, D., Herbrick, J.A., Duncan, A., *et al.* (1997). Cone-rod dystrophy due to mutations in a novel photoreceptor-specific homeobox gene (CRX) essential for maintenance of the photoreceptor. *Cell* 91, 543-553.

Furukawa, T., Kozak, C.A., and Cepko, C.L. (1997a). rax, a novel paired-type homeobox gene, shows expression in the anterior neural fold and developing retina. *Proceedings of the National Academy of Sciences of the United States of America* 94, 3088-3093.

Furukawa, T., Morrow, E.M., and Cepko, C.L. (1997b). Crx, a novel otx-like homeobox gene, shows photoreceptor-specific expression and regulates photoreceptor differentiation. *Cell* 91, 531-541.

Furukawa, T., Morrow, E.M., Li, T., Davis, F.C., and Cepko, C.L. (1999). Retinopathy and attenuated circadian entrainment in Crx-deficient mice. *Nature genetics* 23, 466-470.

Furukawa, T., Mukherjee, S., Bao, Z.Z., Morrow, E.M., and Cepko, C.L. (2000). rax, Hes1, and notch1 promote the formation of Muller glia by postnatal retinal progenitor cells. *Neuron* 26, 383-394.

Furusawa, C., and Kaneko, K. (2012). A dynamical-systems view of stem cell biology. *Science* 338, 215-217.

Gamse, J.T., Shen, Y.C., Thisse, C., Thisse, B., Raymond, P.A., Halpern, M.E., and Liang, J.O. (2002). Otx5 regulates genes that show circadian expression in the zebrafish pineal complex. *Nature genetics* 30, 117-121.

Gibson-Brown, J.J., S, I.A., Silver, L.M., and Papaioannou, V.E. (1998). Expression of T-box genes Tbx2-Tbx5 during chick organogenesis. *Mechanisms of development* 74, 165-169.

Gillespie, D.T. (1977). Exact stochastic simulation of coupled chemical reactions. *The Journal of Physical Chemistry* 81, 2340-2361.

Glaschke, A., Glosmann, M., and Peichl, L. (2010). Developmental changes of cone opsin expression but not retinal morphology in the hypothyroid Pax8 knockout mouse. *Investigative ophthalmology & visual science* 51, 1719-1727.

Glaschke, A., Weiland, J., Del Turco, D., Steiner, M., Peichl, L., and Glosmann, M. (2011). Thyroid hormone controls cone opsin expression in the retina of adult rodents. *The Journal of neuroscience : the official journal of the Society for Neuroscience* 31, 4844-4851.

Govardovskii, V.I., and Zueva, L.V. (1977). Visual pigments of chicken and pigeon. *Vision research* 17, 537-543.

Gowdy, P.D., and Cicerone, C.M. (1998). The spatial arrangement of the L and M cones in the central fovea of the living human eye. *Vision research* 38, 2575-2589.

Guo, C., Chen, X., Song, H., Maynard, M.A., Zhou, Y., Lobanov, A.V., Gladyshev, V.N., Ganis, J.J., Wiley, D., Jugo, R.H., *et al.* (2014). Intrinsic expression of a multiexon type 3 deiodinase gene controls zebrafish embryo size. *Endocrinology* 155, 4069-4080.

Haider, N.B., Demarco, P., Nystuen, A.M., Huang, X., Smith, R.S., McCall, M.A., Naggert, J.K., and Nishina, P.M. (2006). The transcription factor Nr2e3 functions in retinal progenitors to suppress cone cell generation. *Visual neuroscience* 23, 917-929.

Haider, N.B., Jacobson, S.G., Cideciyan, A.V., Swiderski, R., Streb, L.M., Searby, C., Beck, G., Hockey, R., Hanna, D.B., Gorman, S., *et al.* (2000). Mutation of a nuclear receptor gene, NR2E3, causes enhanced S cone syndrome, a disorder of retinal cell fate. *Nature genetics* 24, 127-131.

Haider, N.B., Naggert, J.K., and Nishina, P.M. (2001). Excess cone cell proliferation due to lack of a functional NR2E3 causes retinal dysplasia and degeneration in rd7/rd7 mice. *Human molecular genetics* 10, 1619-1626.

Hao, H., Kim, D.S., Klocke, B., Johnson, K.R., Cui, K., Gotoh, N., Zang, C., Gregorski, J., Gieser, L., Peng, W., *et al.* (2012). Transcriptional regulation of rod photoreceptor homeostasis revealed by in vivo NRL targetome analysis. *PLoS genetics* 8, e1002649.

Harrow, J., Frankish, A., Gonzalez, J.M., Tapanari, E., Diekhans, M., Kokocinski, F., Aken, B.L., Barrell, D., Zadissa, A., Searle, S., *et al.* (2012). GENCODE: the reference human genome annotation for The ENCODE Project. *Genome research* 22, 1760-1774.

Hart, N.S. (2001). Variations in cone photoreceptor abundance and the visual ecology of birds. *Journal of comparative physiology A, Sensory, neural, and behavioral physiology* 187, 685-697.

Haverkamp, S., Wassle, H., Duebel, J., Kuner, T., Augustine, G.J., Feng, G., and Euler, T. (2005). The primordial, blue-cone color system of the mouse retina. *The Journal of neuroscience : the official journal of the Society for Neuroscience* 25, 5438-5445.

Headington, K., Choi, S.S., Nickla, D., and Doble, N. (2011). Single cell imaging of the chick retina with adaptive optics. *Current eye research* 36, 947-957.

Heberlein, U., Wolff, T., and Rubin, G.M. (1993). The TGF beta homolog dpp and the segment polarity gene hedgehog are required for propagation of a morphogenetic wave in the *Drosophila* retina. *Cell* 75, 913-926.

Hendrickson, A. (1992). A morphological comparison of foveal development in man and monkey. *Eye (London, England)* 6 (Pt 2), 136-144.

Hendrickson, A., Bumsted-O'Brien, K., Natoli, R., Ramamurthy, V., Possin, D., and Provis, J. (2008). Rod photoreceptor differentiation in fetal and infant human retina. *Experimental eye research* 87, 415-426.

Hendrickson, A., and Drucker, D. (1992). The development of parafoveal and mid-peripheral human retina. *Behav Brain Res* 49, 21-31.

Hennig, A.K., Peng, G.H., and Chen, S. (2008). Regulation of photoreceptor gene expression by Crx-associated transcription factor network. *Brain research* 1192, 114-133.

Hernandez, R.E., Putzke, A.P., Myers, J.P., Margaretha, L., and Moens, C.B. (2007). Cyp26 enzymes generate the retinoic acid response pattern necessary for hindbrain development. *Development* 134, 177-187.

Hoang, Q.V., Linsenmeier, R.A., Chung, C.K., and Curcio, C.A. (2002). Photoreceptor inner segments in monkey and human retina: mitochondrial density, optics, and regional variation. *Visual neuroscience* 19, 395-407.

Hofer, H., Carroll, J., Neitz, J., Neitz, M., and Williams, D.R. (2005). Organization of the human trichromatic cone mosaic. *The Journal of neuroscience : the official journal of the Society for Neuroscience* 25, 9669-9679.

Hofmann, C.M., and Carleton, K.L. (2009). Gene duplication and differential gene expression play an important role in the diversification of visual pigments in fish. *Integrative and comparative biology* 49, 630-643.

Hoover, F., Seleiro, E.A., Kielland, A., Brickell, P.M., and Glover, J.C. (1998). Retinoid X receptor gamma gene transcripts are expressed by a subset of early generated retinal cells and eventually restricted to photoreceptors. *J Comp Neurol* 391, 204-213.

Hoshino, A., Ratnapriya, R., Brooks, M.J., Chaitankar, V., Wilken, M.S., Zhang, C., Starostik, M.R., Gieser, L., La Torre, A., Nishio, M., *et al.* (2017). Molecular Anatomy of the Developing Human Retina. *Developmental cell* 43, 763-779 e764.

Hu, M., and Easter, S.S. (1999). Retinal neurogenesis: the formation of the initial central patch of postmitotic cells. *Developmental biology* 207, 309-321.

Hunt, D.M. (2001). Seeing rainbows. *Biologist (London)* 48, 67-71.

Hyatt, G.A., Schmitt, E.A., Fadool, J.M., and Dowling, J.E. (1996). Retinoic acid alters photoreceptor development in vivo. *Proceedings of the National Academy of Sciences of the United States of America* 93, 13298-13303.

Inoue, M., Iida, A., Satoh, S., Kodama, T., and Watanabe, S. (2010). COUP-TFI and -TFII nuclear receptors are expressed in amacrine cells and play roles in regulating the differentiation of retinal progenitor cells. *Experimental eye research* 90, 49-56.

Jacobson, S.G., Cideciyan, A.V., Huang, Y., Hanna, D.B., Freund, C.L., Affatigato, L.M., Carr, R.E., Zack, D.J., Stone, E.M., and McInnes, R.R. (1998). Retinal degenerations with truncation mutations in the cone-rod homeobox (CRX) gene. *Investigative ophthalmology & visual science* 39, 2417-2426.

Jacobson, S.G., Sumaroka, A., Aleman, T.S., Cideciyan, A.V., Schwartz, S.B., Roman, A.J., McInnes, R.R., Sheffield, V.C., Stone, E.M., Swaroop, A., *et al.* (2004). Nuclear receptor NR2E3 gene mutations distort human retinal laminar architecture and cause an unusual degeneration. *Human molecular genetics* 13, 1893-1902.

Jadhav, A.P., Mason, H.A., and Cepko, C.L. (2006). Notch 1 inhibits photoreceptor production in the developing mammalian retina. *Development* 133, 913-923.

Jarman, A.P., Grell, E.H., Ackerman, L., Jan, L.Y., and Jan, Y.N. (1994). Atonal is the proneural gene for *Drosophila* photoreceptors. *Nature* 369, 398-400.

Jarman, A.P., Sun, Y., Jan, L.Y., and Jan, Y.N. (1995). Role of the proneural gene, atonal, in formation of *Drosophila* chordotonal organs and photoreceptors. *Development* 121, 2019-2030.

Jeon, C.J., Strettoi, E., and Masland, R.H. (1998). The major cell populations of the mouse retina. *The Journal of neuroscience : the official journal of the Society for Neuroscience* 18, 8936-8946.

Johns, P.R., and Fernald, R.D. (1981). Genesis of rods in teleost fish retina. *Nature* 293, 141-142.

Johnston, R.J., Jr. (2013). Lessons about terminal differentiation from the specification of color-detecting photoreceptors in the *Drosophila* retina. *Annals of the New York Academy of Sciences* 1293, 33-44.

Johnston, R.J., Jr., and Desplan, C. (2014). Interchromosomal communication coordinates intrinsically stochastic expression between alleles. *Science (New York, NY)* 343, 661-665.

Johnston, R.J., Jr., Otake, Y., Sood, P., Vogt, N., Behnia, R., Vasiliauskas, D., McDonald, E., Xie, B., Koenig, S., Wolf, R., *et al.* (2011). Interlocked feedforward loops control cell-type-specific Rhodopsin expression in the *Drosophila* eye. *Cell* 145, 956-968.

Jukam, D., and Desplan, C. (2011). Binary regulation of Hippo pathway by Merlin/NF2, Kibra, Lgl, and Melted specifies and maintains postmitotic neuronal fate. *Developmental cell* 21, 874-887.

Julius, D., and Nathans, J. (2012). Signaling by sensory receptors. *Cold Spring Harbor perspectives in biology* 4, a005991.

Kaewkhaw, R., Kaya, K.D., Brooks, M., Homma, K., Zou, J., Chaitankar, V., Rao, M., and Swaroop, A. (2015). Transcriptome Dynamics of Developing Photoreceptors in Three-Dimensional Retina Cultures Recapitulates Temporal Sequence of Human Cone and Rod Differentiation Revealing Cell Surface Markers and Gene Networks. *Stem cells (Dayton, Ohio)* 33, 3504-3518.

Kainz, P.M.N., Jay; Neitz, Maureen (1998). Recent evolution of uniform trichromacy in a New World monkey. *Vision research* 38, 3315-3320.

Kautzmann, M.A., Kim, D.S., Felder-Schmittbuhl, M.P., and Swaroop, A. (2011). Combinatorial regulation of photoreceptor differentiation factor, neural retina leucine zipper gene NRL, revealed by in vivo promoter analysis. *The Journal of biological chemistry* 286, 28247-28255.

Kawakami, Y., Uchiyama, Y., Rodriguez Esteban, C., Inenaga, T., Koyano-Nakagawa, N., Kawakami, H., Marti, M., Kmita, M., Monaghan-Nichols, P., Nishinakamura, R., *et al.* (2009). Sall genes regulate region-specific morphogenesis in the mouse limb by modulating Hox activities. *Development* 136, 585-594.

Kelley, M.W., Turner, J.K., and Reh, T.A. (1995). Ligands of steroid/thyroid receptors induce cone photoreceptors in vertebrate retina. *Development* 121, 3777-3785.

Kim, J.W., Yang, H.J., Oel, A.P., Brooks, M.J., Jia, L., Plachetzki, D.C., Li, W., Allison, W.T., and Swaroop, A. (2016). Recruitment of Rod Photoreceptors from Short-Wavelength-Sensitive Cones during the Evolution of Nocturnal Vision in Mammals. *Developmental cell* 37, 520-532.

Kitambi, S.S., and Hauptmann, G. (2007). The zebrafish orphan nuclear receptor genes nr2e1 and nr2e3 are expressed in developing eye and forebrain. *Gene expression patterns : GEP* 7, 521-528.

Klein, M., Sharma, R., Bohrer, C.H., Avelis, C.M., and Roberts, E. (2017). Biospark: scalable analysis of large numerical datasets from biological simulations and experiments using Hadoop and Spark. *Bioinformatics* 33, 303-305.

Kram, Y.A., Mantey, S., and Corbo, J.C. (2010). Avian cone photoreceptors tile the retina as five independent, self-organizing mosaics. *PloS one* 5, e8992.

La Vail, M.M., Rapaport, D.H., and Rakic, P. (1991). Cytogenesis in the monkey retina. *J Comp Neurol* 309, 86-114.

- Ladekjaer-Mikkelsen, A.S., Rosenberg, T., and Jorgensen, A.L. (1996). A new mechanism in blue cone monochromatism. *Hum Genet* 98, 403-408.
- Lamba, D.A., Gust, J., and Reh, T.A. (2009). Transplantation of human embryonic stem cell-derived photoreceptors restores some visual function in Crx-deficient mice. *Cell stem cell* 4, 73-79.
- Larison, K.D., and Bremiller, R. (1990). Early onset of phenotype and cell patterning in the embryonic zebrafish retina. *Development* 109, 567-576.
- Lee, T.C., Almeida, D., Claros, N., Abramson, D.H., and Cobrinik, D. (2006). Cell cycle-specific and cell type-specific expression of Rb in the developing human retina. *Investigative ophthalmology & visual science* 47, 5590-5598.
- Legent, K., and Treisman, J.E. (2008). Wingless signaling in Drosophila eye development. *Methods in molecular biology* 469, 141-161.
- Li, K.Y., and Roorda, A. (2007). Automated identification of cone photoreceptors in adaptive optics retinal images. *Journal of the Optical Society of America A, Optics, image science, and vision* 24, 1358-1363.
- Li, W.H., Zhou, L., Li, Z., Wang, Y., Shi, J.T., Yang, Y.J., and Gui, J.F. (2015). Zebrafish Lbh-like Is Required for Otx2-mediated Photoreceptor Differentiation. *International journal of biological sciences* 11, 688-700.
- Liang, J., Cao, Y., Gursoy, G., Naveed, H., Terebus, A., and Zhao, J. (2015). Multiscale Modeling of Cellular Epigenetic States: Stochasticity in Molecular Networks, Chromatin Folding in Cell Nuclei, and Tissue Pattern Formation of Cells. *Crit Rev Biomed Eng* 43, 323-346.
- Liu, Y., Fu, L., Chen, D.G., and Deeb, S.S. (2007). Identification of novel retinal target genes of thyroid hormone in the human WERI cells by expression microarray analysis. *Vision research* 47, 2314-2326.
- Liu, Y., Shen, Y., Rest, J.S., Raymond, P.A., and Zack, D.J. (2001). Isolation and characterization of a zebrafish homologue of the cone rod homeobox gene. *Investigative ophthalmology & visual science* 42, 481-487.
- Lucini, C., Maruccio, L., Patruno, M., Martinello, T., Mascarello, F., and Castaldo, L. (2007). Glial cell line-derived neurotrophic factor expression in the retina of adult zebrafish (*Danio rerio*). *Neuroscience letters* 429, 156-160.

Lukats, A., Szabo, A., Rohlich, P., Vigh, B., and Szel, A. (2005). Photopigment coexpression in mammals: comparative and developmental aspects. *Histology and histopathology* *20*, 551-574.

Lythgoe, J. (1979). *The Ecology of Vision* (Claredon Press).

Ma, C., Zhou, Y., Beachy, P.A., and Moses, K. (1993). The segment polarity gene hedgehog is required for progression of the morphogenetic furrow in the developing *Drosophila* eye. *Cell* *75*, 927-938.

MacNichol, E.F., Jr., Kunz, Y.W., Levine, J.S., Harosi, F.I., and Collins, B.A. (1978). Ellipsosomes: organelles containing a cytochrome-like pigment in the retinal cones of certain fishes. *Science (New York, NY)* *200*, 549-552.

Marquez-Neila, P., Baumela, L., and Alvarez, L. (2014). A morphological approach to curvature-based evolution of curves and surfaces. *IEEE Trans Pattern Anal Mach Intell* *36*, 2-17.

Martino, E., Nardi, M., Vaudagna, G., Simonetti, S., Cilotti, A., Pinchera, A., Venturi, G., Seo, H., and Baschieri, L. (1980). Thyrotropin-releasing hormone-like material in human retina. *Journal of endocrinological investigation* *3*, 267-271.

Masai, I., Stemple, D.L., Okamoto, H., and Wilson, S.W. (2000). Midline signals regulate retinal neurogenesis in zebrafish. *Neuron* *27*, 251-263.

Mazzoni, E.O., Celik, A., Wernet, M.F., Vasiliauskas, D., Johnston, R.J., Cook, T.A., Pichaud, F., and Desplan, C. (2008). Iroquois complex genes induce co-expression of rhodopsins in *Drosophila*. *PLoS biology* *6*, e97.

McCaffery, P., Lee, M.O., Wagner, M.A., Sladek, N.E., and Drager, U.C. (1992). Asymmetrical retinoic acid synthesis in the dorsoventral axis of the retina. *Development* *115*, 371-382.

McCaffery, P., Wagner, E., O'Neil, J., Petkovich, M., and Drager, U.C. (1999a). Dorsal and ventral retinoic territories defined by retinoic acid synthesis, break-down and nuclear receptor expression. *Mechanisms of development* *85*, 203-214.

McCaffery, P., Wagner, E., O'Neil, J., Petkovich, M., and Drager, U.C. (1999b). Dorsal and ventral retinal territories defined by retinoic acid synthesis, break-down and nuclear receptor expression. *Mechanisms of development* *82*, 119-130.

McCaffrery, P., Posch, K.C., Napoli, J.L., Gudas, L., and Drager, U.C. (1993). Changing patterns of the retinoic acid system in the developing retina. *Developmental biology* 158, 390-399.

Mears, A.J., Kondo, M., Swain, P.K., Takada, Y., Bush, R.A., Saunders, T.L., Sieving, P.A., and Swaroop, A. (2001). Nrl is required for rod photoreceptor development. *Nature genetics* 29, 447-452.

Mey, J., McCaffery, P., and Drager, U.C. (1997). Retinoic acid synthesis in the developing chick retina. *The Journal of neuroscience : the official journal of the Society for Neuroscience* 17, 7441-7449.

Meyer, D.B., and May, H.C., Jr. (1973). The topographical distribution of rods and cones in the adult chicken retina. *Experimental eye research* 17, 347-355.

Micheelsen, M.A., Mitarai, N., Sneppen, K., and Dodd, I.B. (2010). Theory for the stability and regulation of epigenetic landscapes. *Phys Biol* 7, 026010.

Mikeladze-Dvali, T., Wernet, M.F., Pistillo, D., Mazzoni, E.O., Teleman, A.A., Chen, Y.W., Cohen, S., and Desplan, C. (2005). The growth regulators warts/lats and melted interact in a bistable loop to specify opposite fates in *Drosophila* R8 photoreceptors. *Cell* 122, 775-787.

Milam, A.H., Rose, L., Cideciyan, A.V., Barakat, M.R., Tang, W.X., Gupta, N., Aleman, T.S., Wright, A.F., Stone, E.M., Sheffield, V.C., *et al.* (2002). The nuclear receptor NR2E3 plays a role in human retinal photoreceptor differentiation and degeneration. *Proceedings of the National Academy of Sciences of the United States of America* 99, 473-478.

Mitchell, D.M., Stevens, C.B., Frey, R.A., Hunter, S.S., Ashino, R., Kawamura, S., and Stenkamp, D.L. (2015). Retinoic Acid Signaling Regulates Differential Expression of the Tandemly-Duplicated Long Wavelength-Sensitive Cone Opsin Genes in Zebrafish. *PLoS genetics* 11, e1005483.

Mitton, K.P., Swain, P.K., Chen, S., Xu, S., Zack, D.J., and Swaroop, A. (2000). The leucine zipper of NRL interacts with the CRX homeodomain. A possible mechanism of transcriptional synergy in rhodopsin regulation. *The Journal of biological chemistry* 275, 29794-29799.

Montana, C.L., Lawrence, K.A., Williams, N.L., Tran, N.M., Peng, G.H., Chen, S., and Corbo, J.C. (2011). Transcriptional regulation of neural retina leucine zipper (Nrl), a photoreceptor cell fate determinant. *The Journal of biological chemistry* 286, 36921-36931.

Montell, C., Jones, K., Zuker, C., and Rubin, G. (1987). A second opsin gene expressed in the ultraviolet-sensitive R7 photoreceptor cells of *Drosophila melanogaster*. *The Journal of neuroscience : the official journal of the Society for Neuroscience* 7, 1558-1566.

Morey, M., Yee, S.K., Herman, T., Nern, A., Blanco, E., and Zipursky, S.L. (2008). Coordinate control of synaptic-layer specificity and rhodopsins in photoreceptor neurons. *Nature* 456, 795-799.

Mori, M., Ghyselinck, N.B., Chambon, P., and Mark, M. (2001). Systematic immunolocalization of retinoid receptors in developing and adult mouse eyes. *Investigative ophthalmology & visual science* 42, 1312-1318.

Morris, V.B. (1982). An afoveate area centralis in the chick retina. *J Comp Neurol* 210, 198-203.

Moses, K., Ellis, M.C., and Rubin, G.M. (1989). The glass gene encodes a zinc-finger protein required by *Drosophila* photoreceptor cells. *Nature* 340, 531-536.

Muranishi, Y., Terada, K., Inoue, T., Katoh, K., Tsujii, T., Sanuki, R., Kurokawa, D., Aizawa, S., Tamaki, Y., and Furukawa, T. (2011). An essential role for RAX homeoprotein and NOTCH-HES signaling in *Otx2* expression in embryonic retinal photoreceptor cell fate determination. *The Journal of neuroscience : the official journal of the Society for Neuroscience* 31, 16792-16807.

Mustafi, D., Engel, A.H., and Palczewski, K. (2009). Structure of cone photoreceptors. *Progress in retinal and eye research* 28, 289-302.

Nagle, B.B.a.B.W. (1983). Retinomotor movements of photoreceptors and retinal pigment epithelium: Mechanisms and regulation. . In *Progress in Retinal Research*, N.O.a.G. Chader, ed. (Oxford: Pergamon), pp. 67-109.

Nakano, T., Ando, S., Takata, N., Kawada, M., Muguruma, K., Sekiguchi, K., Saito, K., Yonemura, S., Eiraku, M., and Sasai, Y. (2012). Self-formation of optic cups and storable stratified neural retina from human ESCs. *Cell stem cell* 10, 771-785.

Nathans, J. (1999). The Evolution and Physiology of Human Color Vision: Insights from Molecular Genetic Studies of Visual Pigments. *Neuron* 24, 299-312.

Nathans, J., Davenport, C.M., Maumenee, I.H., Lewis, R.A., Hejtmancik, J.F., Litt, M., Lovrien, E., Weleber, R., Bachynski, B., Zwas, F., *et al.* (1989). Molecular genetics of human blue cone monochromacy. *Science* 245, 831-838.

- Nathans, J., Thomas, D., and Hogness, D. (1986). Molecular Genetics of Human Color Vision: The Genes Encoding Blue, Green, and Red Pigments. *Science* 232, 193-202.
- Nawrocki, L., BreMiller, R., Streisinger, G., and Kaplan, M. (1985). Larval and adult visual pigments of the zebrafish, *Brachydanio rerio*. *Vision research* 25, 1569-1576.
- Nelson, S.M., Frey, R.A., Wardwell, S.L., and Stenkamp, D.L. (2008). The developmental sequence of gene expression within the rod photoreceptor lineage in embryonic zebrafish. *Developmental dynamics : an official publication of the American Association of Anatomists* 237, 2903-2917.
- Nelson, S.M., Park, L., and Stenkamp, D.L. (2009). Retinal homeobox 1 is required for retinal neurogenesis and photoreceptor differentiation in embryonic zebrafish. *Developmental biology* 328, 24-39.
- Neumann, C.J., and Nusslein-Volhard, C. (2000). Patterning of the zebrafish retina by a wave of sonic hedgehog activity. *Science (New York, NY)* 289, 2137-2139.
- Ng, L., Hurley, J.B., Dierks, B., Srinivas, M., Salto, C., Vennstrom, B., Reh, T.A., and Forrest, D. (2001). A thyroid hormone receptor that is required for the development of green cone photoreceptors. *Nature genetics* 27, 94-98.
- Ng, L., Lu, A., Swaroop, A., Sharlin, D.S., Swaroop, A., and Forrest, D. (2011). Two transcription factors can direct three photoreceptor outcomes from rod precursor cells in mouse retinal development. *The Journal of neuroscience : the official journal of the Society for Neuroscience* 31, 11118-11125.
- Ng, L., Lyubarsky, A., Nikonov, S.S., Ma, M., Srinivas, M., Kefas, B., St Germain, D.L., Hernandez, A., Pugh, E.N., Jr., and Forrest, D. (2010). Type 3 deiodinase, a thyroid-hormone-inactivating enzyme, controls survival and maturation of cone photoreceptors. *The Journal of neuroscience : the official journal of the Society for Neuroscience* 30, 3347-3357.
- Nicotra, C.M., Gueli, M.C., de Luca, G., Bono, A., Pintaudi, A.M., and Paganini, A. (1994). Retinoid dynamics in chicken eye during pre- and postnatal development. *Molecular and cellular biochemistry* 132, 45-55.
- Niederreither, K., McCaffery, P., Drager, U.C., Chambon, P., and Dolle, P. (1997). Restricted expression and retinoic acid-induced downregulation of the retinaldehyde dehydrogenase type 2 (RALDH-2) gene during mouse development. *Mechanisms of development* 62, 67-78.

Nishida, A., Furukawa, A., Koike, C., Tano, Y., Aizawa, S., Matsuo, I., and Furukawa, T. (2003). *Otx2* homeobox gene controls retinal photoreceptor cell fate and pineal gland development. *Nature neuroscience* 6, 1255-1263.

Nishiguchi, K.M., Friedman, J.S., Sandberg, M.A., Swaroop, A., Berson, E.L., and Dryja, T.P. (2004). Recessive *NRL* mutations in patients with clumped pigmented retinal degeneration and relative preservation of blue cone function. *Proceedings of the National Academy of Sciences of the United States of America* 101, 17819-17824.

O'Tousa, J.E., Baehr, W., Martin, R.L., Hirsh, J., Pak, W.L., and Applebury, M.L. (1985). The *Drosophila ninaE* gene encodes an opsin. *Cell* 40, 839-850.

Ochi, H., Sakagami, K., Ishii, A., Morita, N., Nishiuchi, M., Ogino, H., and Yasuda, K. (2004). Temporal expression of *L-Maf* and *RaxL* in developing chicken retina are arranged into mosaic pattern. *Gene expression patterns : GEP* 4, 489-494.

Ogawa, N., Hatsuda, T., Mochizuki, A., and Tachikawa, M. (2017). Dynamical pattern selection of growing cellular mosaic in fish retina. *Phys Rev E* 96, 032416.

Ogawa, Y., Shiraki, T., Kojima, D., and Fukada, Y. (2015). Homeobox transcription factor *Six7* governs expression of green opsin genes in zebrafish. *Proceedings Biological sciences / The Royal Society* 282, 20150659.

Ogilvie, J.M., Speck, J.D., and Lett, J.M. (2000). Growth factors in combination, but not individually, rescue rd mouse photoreceptors in organ culture. *Experimental neurology* 161, 676-685.

Oh, E.C., Cheng, H., Hao, H., Jia, L., Khan, N.W., and Swaroop, A. (2008). Rod differentiation factor *NRL* activates the expression of nuclear receptor *NR2E3* to suppress the development of cone photoreceptors. *Brain research* 1236, 16-29.

Oh, E.C., Khan, N., Novelli, E., Khanna, H., Strettoi, E., and Swaroop, A. (2007). Transformation of cone precursors to functional rod photoreceptors by *bZIP* transcription factor *NRL*. *Proceedings of the National Academy of Sciences of the United States of America* 104, 1679-1684.

Olariu, V., and Peterson, C. (2019). Kinetic models of hematopoietic differentiation. *Wiley interdisciplinary reviews Systems biology and medicine* 11, e1424.

Olsson, A., Venkatasubramanian, M., Chaudhri, V.K., Aronow, B.J., Salomonis, N., Singh, H., and Grimes, H.L. (2016). Single-cell analysis of mixed-lineage states leading to a binary cell fate choice. *Nature* 537, 698-702.

Omori, Y., Katoh, K., Sato, S., Muranishi, Y., Chaya, T., Onishi, A., Minami, T., Fujikado, T., and Furukawa, T. (2011). Analysis of transcriptional regulatory pathways of photoreceptor genes by expression profiling of the Otx2-deficient retina. *PloS one* 6, e19685.

Onishi, A., Peng, G.H., Chen, S., and Blackshaw, S. (2010). Pias3-dependent SUMOylation controls mammalian cone photoreceptor differentiation. *Nature neuroscience* 13, 1059-1065.

Onishi, A., Peng, G.H., Hsu, C., Alexis, U., Chen, S., and Blackshaw, S. (2009). Pias3-dependent SUMOylation directs rod photoreceptor development. *Neuron* 61, 234-246.

Osorio, D., and Vorobyev, M. (2005). Photoreceptor spectral sensitivities in terrestrial animals: adaptations for luminance and colour vision. *Proceedings Biological sciences / The Royal Society* 272, 1745-1752.

Osorio, D., and Vorobyev, M. (2008). A review of the evolution of animal colour vision and visual communication signals. *Vision research* 48, 2042-2051.

Otake, S., Gowdy, P.D., and Cicerone, C.M. (2000). The spatial arrangement of L and M cones in the peripheral human retina. *Vision research* 40, 677-693.

Packer, O., Hendrickson, A.E., and Curcio, C.A. (1990). Development redistribution of photoreceptors across the *Macaca nemestrina* (pigtail macaque) retina. *J Comp Neurol* 298, 472-493.

Papatsenko, D., Sheng, G., and Desplan, C. (1997). A new rhodopsin in R8 photoreceptors of *Drosophila*: evidence for coordinate expression with Rh3 in R7 cells. *Development* 124, 1665-1673.

Patterson, E.J., Wilk, M., Langlo, C.S., Kasilian, M., Ring, M., Hufnagel, R.B., Dubis, A.M., Tee, J.J., Kalitzeos, A., Gardner, J.C., *et al.* (2016). Cone Photoreceptor Structure in Patients With X-Linked Cone Dysfunction and Red-Green Color Vision Deficiency. *Investigative ophthalmology & visual science* 57, 3853-3863.

Pearson, R.A., Barber, A.C., Rizzi, M., Hippert, C., Xue, T., West, E.L., Duran, Y., Smith, A.J., Chuang, J.Z., Azam, S.A., *et al.* (2012). Restoration of vision after transplantation of photoreceptors. *Nature* 485, 99-103.

Peng, G.H., and Chen, S. (2011). Active opsin loci adopt intrachromosomal loops that depend on the photoreceptor transcription factor network. *Proceedings of the National Academy of Sciences of the United States of America* 108, 17821-17826.

Perz-Edwards, A., Hardison, N.L., and Linney, E. (2001). Retinoic acid-mediated gene expression in transgenic reporter zebrafish. *Developmental biology* 229, 89-101.

Pessoa, C.N., Santiago, L.A., Santiago, D.A., Machado, D.S., Rocha, F.A., Ventura, D.F., Hokoc, J.N., Pazos-Moura, C.C., Wondisford, F.E., Gardino, P.F., *et al.* (2008). Thyroid hormone action is required for normal cone opsin expression during mouse retinal development. *Investigative ophthalmology & visual science* 49, 2039-2045.

Phillips, M.J., Jiang, P., Howden, S., Barney, P., Min, J., York, N.W., Chu, L.F., Capowski, E.E., Cash, A., Jain, S., *et al.* (2018). A Novel Approach to Single Cell RNA-Sequence Analysis Facilitates In Silico Gene Reporting of Human Pluripotent Stem Cell-Derived Retinal Cell Types. *Stem cells* (Dayton, Ohio) 36, 313-324.

Pichaud, F. (2014). Transcriptional regulation of tissue organization and cell morphogenesis: the fly retina as a case study. *Developmental biology* 385, 168-178.

Prabhudesai, S.N., Cameron, D.A., and Stenkamp, D.L. (2005). Targeted effects of retinoic acid signaling upon photoreceptor development in zebrafish. *Developmental biology* 287, 157-167.

Quan, X.J., Ramaekers, A., and Hassan, B.A. (2012). Transcriptional control of cell fate specification: lessons from the fly retina. *Current topics in developmental biology* 98, 259-276.

Ragge, N.K., Brown, A.G., Poloschek, C.M., Lorenz, B., Henderson, R.A., Clarke, M.P., Russell-Eggitt, I., Fielder, A., Gerrelli, D., Martinez-Barbera, J.P., *et al.* (2005). Heterozygous mutations of OTX2 cause severe ocular malformations. *American journal of human genetics* 76, 1008-1022.

Raymond, P.A. (1995a). Development and morphological organization of photoreceptors In *Neurobiology and clinical Aspects of the Outer Retina*, S.N.A. M.B.A. Djamgoz, S. Vallergera, ed. (London: Chapman & Hall), pp. 1-23.

Raymond, P.A., and Barthel, L.K. (2004). A moving wave patterns the cone photoreceptor mosaic array in the zebrafish retina. *The International journal of developmental biology* 48, 935-945.

Raymond, P.A., Barthel, L.K., Rounsifer, M.E., Sullivan, S.A., and Knight, J.K. (1993). Expression of rod and cone visual pigments in goldfish and zebrafish: a rhodopsin-like gene is expressed in cones. *Neuron* 10, 1161-1174.

Raymond, P.A., Colvin, S.M., Jabeen, Z., Nagashima, M., Barthel, L.K., Hadidjojo, J., Popova, L., Pejaver, V.R., and Lubensky, D.K. (2014). Patterning the cone mosaic array in zebrafish retina requires specification of ultraviolet-sensitive cones. *PloS one* 9, e85325.

Raymond, P.B., Linda; Curran, Gary (1995b). Developmental Patterning of Rod and Cone Photoreceptors in Embryonic Zebrafish. *The Journal of Comparative Neurology* 395, 537-550.

Ready, D.F., Hanson, T.E., and Benzer, S. (1976). Development of the *Drosophila* retina, a neurocrystalline lattice. *Developmental biology* 53, 217-240.

Ready, T.W.a.D.F. (1993). Pattern formation in the *Drosophila* retina. In *The Development of Drosophila melanogaster* (Cold Spring Harbor Laboratory Press), pp. 1277-1325.

Reh, T.A. (2016). Photoreceptor Transplantation in Late Stage Retinal Degeneration. *Investigative ophthalmology & visual science* 57, ORSFg1-7.

Rehmtulla, A., Warwar, R., Kumar, R., Ji, X., Zack, D.J., and Swaroop, A. (1996). The basic motif-leucine zipper transcription factor Nrl can positively regulate rhodopsin gene expression. *Proceedings of the National Academy of Sciences of the United States of America* 93, 191-195.

Rivolta, C., Berson, E.L., and Dryja, T.P. (2001). Dominant Leber congenital amaurosis, cone-rod degeneration, and retinitis pigmentosa caused by mutant versions of the transcription factor CRX. *Human mutation* 18, 488-498.

Roberts, E., Stone, J.E., and Luthey-Schulten, Z. (2013). Lattice Microbes: high-performance stochastic simulation method for the reaction-diffusion master equation. *J Comput Chem* 34, 245-255.

Roberts, M.R., Hendrickson, A., McGuire, C.R., and Reh, T.A. (2005). Retinoid X receptor (γ) is necessary to establish the S-opsin gradient in cone photoreceptors of the developing mouse retina. *Investigative ophthalmology & visual science* 46, 2897-2904.

Roberts, M.R., Srinivas, M., Forrest, D., Morreale de Escobar, G., and Reh, T.A. (2006). Making the gradient: thyroid hormone regulates cone opsin expression in the developing mouse retina. *Proceedings of the National Academy of Sciences of the United States of America* 103, 6218-6223.

Roger, J.E., Nellissery, J., Kim, D.S., and Swaroop, A. (2010). Sumoylation of bZIP transcription factor NRL modulates target gene expression during photoreceptor differentiation. *The Journal of biological chemistry* 285, 25637-25644.

- Rohlich, P., van Veen, T., and Szel, A. (1994). Two different visual pigments in one retinal cone cell. *Neuron* 13, 1159-1166.
- Roorda, A., Metha, A.B., Lennie, P., and Williams, D.R. (2001). Packing arrangement of the three cone classes in primate retina. *Vision research* 41, 1291-1306.
- Roorda, A., and Williams, D.R. (1999). The arrangement of the three cone classes in the living human eye. *Nature* 397, 520-522.
- Rossi, E.A., Chung, M., Dubra, A., Hunter, J.J., Merigan, W.H., and Williams, D.R. (2011). Imaging retinal mosaics in the living eye. *Eye (London, England)* 25, 301-308.
- Rothenberg, E.V. (2019). Causal Gene Regulatory Network Modeling and Genomics: Second-Generation Challenges. *J Comput Biol.*
- Rothermel, A., and Layer, P.G. (2003). GDNF regulates chicken rod photoreceptor development and survival in reaggregated histotypic retinal spheres. *Investigative ophthalmology & visual science* 44, 2221-2228.
- Rovet, J., and Simic, N. (2008). The role of transient hypothyroxinemia of prematurity in development of visual abilities. *Semin Perinatol* 32, 431-437.
- Sakai, Y., Luo, T., McCaffery, P., Hamada, H., and Drager, U.C. (2004). CYP26A1 and CYP26C1 cooperate in degrading retinoic acid within the equatorial retina during later eye development. *Developmental biology* 276, 143-157.
- Samuels, H.H., Tsai, J.S., Casanova, J., and Stanley, F. (1974). Thyroid hormone action: in vitro characterization of solubilized nuclear receptors from rat liver and cultured GH1 cells. *The Journal of clinical investigation* 54, 853-865.
- Santiago Ramon, C. (2000). *Texture of the Nervous System of Man and the Vertebrates, Vol II and III*, English edition edn (New York: Springer-Verlag/Wein).
- Satoh, S., Tang, K., Iida, A., Inoue, M., Kodama, T., Tsai, S.Y., Tsai, M.J., Furuta, Y., and Watanabe, S. (2009). The spatial patterning of mouse cone opsin expression is regulated by bone morphogenetic protein signaling through downstream effector COUP-TF nuclear receptors. *The Journal of neuroscience : the official journal of the Society for Neuroscience* 29, 12401-12411.

- Schmitt, E.A., and Dowling, J.E. (1996). Comparison of topographical patterns of ganglion and photoreceptor cell differentiation in the retina of the zebrafish, *Danio rerio*. *The Journal of comparative neurology* 371, 222-234.
- Schroeder, A., Jimenez, R., Young, B., and Privalsky, M.L. (2014). The ability of thyroid hormone receptors to sense t4 as an agonist depends on receptor isoform and on cellular cofactors. *Molecular endocrinology* 28, 745-757.
- Setty, M., Kiseliovas, V., Levine, J., Gayoso, A., Mazutis, L., and Pe'er, D. (2019). Characterization of cell fate probabilities in single-cell data with Palantir. *Nat Biotechnol* 37, 451-460.
- Sharlin, D.S., Visser, T.J., and Forrest, D. (2011). Developmental and cell-specific expression of thyroid hormone transporters in the mouse cochlea. *Endocrinology* 152, 5053-5064.
- Shen, Y.C., and Raymond, P.A. (2004). Zebrafish cone-rod (*crx*) homeobox gene promotes retinogenesis. *Developmental biology* 269, 237-251.
- Shibusawa, N., Hashimoto, K., Nikrodhanond, A.A., Liberman, M.C., Applebury, M.L., Liao, X.H., Robbins, J.T., Refetoff, S., Cohen, R.N., and Wondisford, F.E. (2003). Thyroid hormone action in the absence of thyroid hormone receptor DNA-binding in vivo. *The Journal of clinical investigation* 112, 588-597.
- Simic, N., Westall, C., Astzalos, E.V., and Rovet, J. (2010). Visual abilities at 6 months in preterm infants: impact of thyroid hormone deficiency and neonatal medical morbidity. *Thyroid* 20, 309-315.
- Sjoberg, M., Vennstrom, B., and Forrest, D. (1992). Thyroid hormone receptors in chick retinal development: differential expression of mRNAs for alpha and N-terminal variant beta receptors. *Development* 114, 39-47.
- Slavotinek, A.M., Garcia, S.T., Chandratillake, G., Bardakjian, T., Ullah, E., Wu, D., Umeda, K., Lao, R., Tang, P.L., Wan, E., *et al.* (2015). Exome sequencing in 32 patients with anophthalmia/microphthalmia and developmental eye defects. *Clinical genetics* 88, 468-473.
- Sluch, V.M., Chamling, X., Liu, M.M., Berlinicke, C.A., Cheng, J., Mitchell, K.L., Welsbie, D.S., and Zack, D.J. (2017). Enhanced Stem Cell Differentiation and Immunopurification of Genome Engineered Human Retinal Ganglion Cells. *Stem Cells Transl Med* 6, 1972-1986.

Smallwood, P.M., Wang, Y., and Nathans, J. (2002). Role of a locus control region in the mutually exclusive expression of human red and green cone pigment genes. *Proceedings of the National Academy of Sciences of the United States of America* 99, 1008-1011.

Sohocki, M.M., Sullivan, L.S., Mintz-Hittner, H.A., Birch, D., Heckenlively, J.R., Freund, C.L., McInnes, R.R., and Daiger, S.P. (1998). A range of clinical phenotypes associated with mutations in CRX, a photoreceptor transcription-factor gene. *American journal of human genetics* 63, 1307-1315.

Sowden, J.C., Holt, J.K., Meins, M., Smith, H.K., and Bhattacharya, S.S. (2001). Expression of Drosophila omb-related T-box genes in the developing human and mouse neural retina. *Investigative ophthalmology & visual science* 42, 3095-3102.

Srinivas, M., Ng, L., Liu, H., Jia, L., and Forrest, D. (2006). Activation of the blue opsin gene in cone photoreceptor development by retinoid-related orphan receptor beta. *Molecular endocrinology* 20, 1728-1741.

Stenkamp, D.L., Frey, R.A., Mallory, D.E., and Shupe, E.E. (2002). Embryonic retinal gene expression in sonic-you mutant zebrafish. *Developmental dynamics : an official publication of the American Association of Anatomists* 225, 344-350.

Stenkamp, D.L., Gregory, J.K., and Adler, R. (1993). Retinoid effects in purified cultures of chick embryo retina neurons and photoreceptors. *Investigative ophthalmology & visual science* 34, 2425-2436.

Stevens, C.B., Cameron, D.A., and Stenkamp, D.L. (2011). Plasticity of photoreceptor-generating retinal progenitors revealed by prolonged retinoic acid exposure. *BMC developmental biology* 11, 51.

Straznicky, C., and Chehade, M. (1987). The formation of the area centralis of the retinal ganglion cell layer in the chick. *Development* 100, 411-420.

Suzuki, S.C., Bleckert, A., Williams, P.R., Takechi, M., Kawamura, S., and Wong, R.O. (2013). Cone photoreceptor types in zebrafish are generated by symmetric terminal divisions of dedicated precursors. *Proceedings of the National Academy of Sciences of the United States of America* 110, 15109-15114.

Swain, P.K., Chen, S., Wang, Q.L., Affatigato, L.M., Coats, C.L., Brady, K.D., Fishman, G.A., Jacobson, S.G., Swaroop, A., Stone, E., *et al.* (1997). Mutations in the cone-rod homeobox gene are associated with the cone-rod dystrophy photoreceptor degeneration. *Neuron* 19, 1329-1336.

Swain, P.K., Hicks, D., Mears, A.J., Apel, I.J., Smith, J.E., John, S.K., Hendrickson, A., Milam, A.H., and Swaroop, A. (2001). Multiple phosphorylated isoforms of NRL are expressed in rod photoreceptors. *The Journal of biological chemistry* 276, 36824-36830.

Szel, A., Csorba, G., Caffè, A.R., Szel, G., Rohlich, P., and van Veen, T. (1994). Different patterns of retinal cone topography in two genera of rodents, *Mus* and *Apodemus*. *Cell and tissue research* 276, 143-150.

Szel, A., Rohlich, P., Caffè, A.R., and van Veen, T. (1996). Distribution of cone photoreceptors in the mammalian retina. *Microscopy research and technique* 35, 445-462.

Tahayato, A., Sonnevile, R., Pichaud, F., Wernet, M.F., Papatsenko, D., Beaufils, P., Cook, T., and Desplan, C. (2003). *Otd/Crx*, a dual regulator for the specification of ommatidia subtypes in the *Drosophila* retina. *Developmental cell* 5, 391-402.

Takagi, M., Nagasaki, K., Fujiwara, I., Ishii, T., Amano, N., Asakura, Y., Muroya, K., Hasegawa, Y., Adachi, M., and Hasegawa, T. (2015). Heterozygous defects in *PAX6* gene and congenital hypopituitarism. *European journal of endocrinology / European Federation of Endocrine Societies* 172, 37-45.

Takechi, M., and Kawamura, S. (2005). Temporal and spatial changes in the expression pattern of multiple red and green subtype opsin genes during zebrafish development. *J Exp Biol* 208, 1337-1345.

Tarboush, R., Novales Flamarique, I., Chapman, G.B., and Connaughton, V.P. (2014). Variability in mitochondria of zebrafish photoreceptor ellipsoids. *Visual neuroscience* 31, 11-23.

Teles, J., Pina, C., Eden, P., Ohlsson, M., Enver, T., and Peterson, C. (2013). Transcriptional regulation of lineage commitment--a stochastic model of cell fate decisions. *PLoS Comput Biol* 9, e1003197.

Thanawala, S.U., Rister, J., Goldberg, G.W., Zuskov, A., Olesnicky, E.C., Flowers, J.M., Jukam, D., Purugganan, M.D., Gavis, E.R., Desplan, C., *et al.* (2013). Regional modulation of a stochastically expressed factor determines photoreceptor subtypes in the *Drosophila* retina. *Developmental cell* 25, 93-105.

Thisse, C., Degraeve, A., Kryukov, G.V., Gladyshev, V.N., Obrecht-Pflumio, S., Krol, A., Thisse, B., and Lescure, A. (2003). Spatial and temporal expression patterns of selenoprotein genes during embryogenesis in zebrafish. *Gene expression patterns : GEP* 3, 525-532.

Tio, M., Ma, C., and Moses, K. (1994). *spitz*, a *Drosophila* homolog of transforming growth factor- α , is required in the founding photoreceptor cells of the compound eye facets. *Mechanisms of development* 48, 13-23.

Tomlinson, A. (2003). Patterning the peripheral retina of the fly: decoding a gradient. *Developmental cell* 5, 799-809.

Tomlinson, A., and Ready, D.F. (1987). Neuronal differentiation in *Drosophila* ommatidium. *Developmental biology* 120, 366-376.

Treisman, J.E. (2013). Retinal differentiation in *Drosophila*. *Wiley interdisciplinary reviews Developmental biology* 2, 545-557.

Trezise, A.E., and Collin, S.P. (2005). Opsins: evolution in waiting. *Current biology : CB* 15, R794-796.

Trimarchi, J.M., Harpavat, S., Billings, N.A., and Cepko, C.L. (2008). Thyroid hormone components are expressed in three sequential waves during development of the chick retina. *BMC developmental biology* 8, 101.

Troutt, L.L., and Burnside, B. (1988). Microtubule polarity and distribution in teleost photoreceptors. *The Journal of neuroscience : the official journal of the Society for Neuroscience* 8, 2371-2380.

Tsujimura, T., Chinen, A., and Kawamura, S. (2007). Identification of a locus control region for quadruplicated green-sensitive opsin genes in zebrafish. *Proceedings of the National Academy of Sciences of the United States of America* 104, 12813-12818.

Tsujimura, T., Hosoya, T., and Kawamura, S. (2010). A single enhancer regulating the differential expression of duplicated red-sensitive opsin genes in zebrafish. *PLoS genetics* 6, e1001245.

Tsujimura, T., Masuda, R., Ashino, R., and Kawamura, S. (2015). Spatially differentiated expression of quadruplicated green-sensitive RH2 opsin genes in zebrafish is determined by proximal regulatory regions and gene order to the locus control region. *BMC genetics* 16, 130.

Tucker, B.A., Park, I.H., Qi, S.D., Klassen, H.J., Jiang, C., Yao, J., Redenti, S., Daley, G.Q., and Young, M.J. (2011). Transplantation of adult mouse iPS cell-derived photoreceptor precursors restores retinal structure and function in degenerative mice. *PloS one* 6, e18992.

Tyler, M.J., Carney, L.H., and Cameron, D.A. (2005). Control of cellular pattern formation in the vertebrate inner retina by homotypic regulation of cell-fate decisions. *The Journal of neuroscience : the official journal of the Society for Neuroscience* 25, 4565-4576.

v. Campenhausen, M., and Kirschfeld, K. Spectral sensitivity of the accessory optic system of the pigeon. *Journal of Comparative Physiology A* 183, 1-6.

Viets, K., Eldred, K.C., and Johnston, R.J., Jr. (2016a). Mechanisms of Photoreceptor Patterning in Vertebrates and Invertebrates. *Trends in genetics : TIG* 32, 638-659.

Viets, K., Eldred, K.C., and Johnston, R.J., Jr. (2016b). Mechanisms of Photoreceptor Patterning in Vertebrates and Invertebrates. *Trends in genetics : TIG*.

Vihtelic, T.S., Doro, C.J., and Hyde, D.R. (1999). Cloning and characterization of six zebrafish photoreceptor opsin cDNAs and immunolocalization of their corresponding proteins. *Visual neuroscience* 16, 571-585.

Vincent, A., Forster, N., Maynes, J.T., Paton, T.A., Billingsley, G., Roslin, N.M., Ali, A., Sutherland, J., Wright, T., Westall, C.A., *et al.* (2014). OTX2 mutations cause autosomal dominant pattern dystrophy of the retinal pigment epithelium. *Journal of medical genetics* 51, 797-805.

Vollrath, D., Nathans, J., and Davis, R.W. (1988). Tandem array of human visual pigment genes at Xq28. *Science* 240, 1669-1672.

Volpert, K.N., Rothermel, A., and Layer, P.G. (2007). GDNF stimulates rod photoreceptors and dopaminergic amacrine cells in chicken retinal reagggregates. *Investigative ophthalmology & visual science* 48, 5306-5314.

Wahlin, K.J., Maruotti, J.A., Sripathi, S.R., Ball, J., Angueyra, J.M., Kim, C., Grebe, R., Li, W., Jones, B.W., and Zack, D.J. (2017). Photoreceptor Outer Segment-like Structures in Long-Term 3D Retinas from Human Pluripotent Stem Cells. *Sci Rep* 7, 766.

Wai, M.S., Lorke, D.E., Kung, L.S., and Yew, D.T. (2006). Morphogenesis of the different types of photoreceptors of the chicken (*Gallus domesticus*) retina and the effect of amblyopia in neonatal chicken. *Microscopy research and technique* 69, 99-107.

Wang, J., Zhang, K., Xu, L., and Wang, E. (2011a). Quantifying the Waddington landscape and biological paths for development and differentiation. *Proceedings of the National Academy of Sciences of the United States of America* 108, 8257-8262.

Wang, S., Sengel, C., Emerson, M.M., and Cepko, C.L. (2014). A gene regulatory network controls the binary fate decision of rod and bipolar cells in the vertebrate retina. *Developmental cell* 30, 513-527.

Wang, Y., Macke, J.P., Merbs, S.L., Zack, D.J., Klaunberg, B., Bennett, J., Gearhart, J., and Nathans, J. (1992). A locus control region adjacent to the human red and green visual pigment genes. *Neuron* 9, 429-440.

Wang, Y., Smallwood, P.M., Cowan, M., Blesh, D., Lawler, A., and Nathans, J. (1999). Mutually exclusive expression of human red and green visual pigment-reporter transgenes occurs at high frequency in murine cone photoreceptors. *Proceedings of the National Academy of Sciences of the United States of America* 96, 5251-5256.

Wang, Y.V., Weick, M., and Demb, J.B. (2011b). Spectral and temporal sensitivity of cone-mediated responses in mouse retinal ganglion cells. *The Journal of neuroscience : the official journal of the Society for Neuroscience* 31, 7670-7681.

Weir, P.T., and Dickinson, M.H. (2012). Flying *Drosophila* orient to sky polarization. *Current biology : CB* 22, 21-27.

Weiss, A.H., Kelly, J.P., Bisset, D., and Deeb, S.S. (2012). Reduced L- and M- and increased S-cone functions in an infant with thyroid hormone resistance due to mutations in the *THRbeta2* gene. *Ophthalmic genetics* 33, 187-195.

Wernet, M.F., Labhart, T., Baumann, F., Mazzoni, E.O., Pichaud, F., and Desplan, C. (2003). Homothorax switches function of *Drosophila* photoreceptors from color to polarized light sensors. *Cell* 115, 267-279.

Wernet, M.F., Mazzoni, E.O., Celik, A., Duncan, D.M., Duncan, I., and Desplan, C. (2006). Stochastic spineless expression creates the retinal mosaic for colour vision. *Nature* 440, 174-180.

Wernet, M.F., Velez, M.M., Clark, D.A., Baumann-Klausener, F., Brown, J.R., Klovstad, M., Labhart, T., and Clandinin, T.R. (2012). Genetic dissection reveals two separate retinal substrates for polarization vision in *Drosophila*. *Current biology : CB* 22, 12-20.

Wheeler, T.G. (1982). Color vision and retinal chromatic information processing in teleost: a review. *Brain research* 257, 177-235.

Wilby, D., Toomey, M.B., Olsson, P., Frederiksen, R., Cornwall, M.C., Oulton, R., Kelber, A., Corbo, J.C., and Roberts, N.W. (2015). Optics of cone photoreceptors in the chicken (*Gallus gallus domesticus*). *Journal of the Royal Society, Interface / the Royal Society* 12, 20150591.

- Williams, D.R. (2011). Imaging single cells in the living retina. *Vision research* 51, 1379-1396.
- Williams, R.W. (1991). The human retina has a cone-enriched rim. *Visual neuroscience* 6, 403-406.
- Wolff, T., and Ready, D.F. (1991). The beginning of pattern formation in the *Drosophila* compound eye: the morphogenetic furrow and the second mitotic wave. *Development* 113, 841-850.
- Wright, A.F., Reddick, A.C., Schwartz, S.B., Ferguson, J.S., Aleman, T.S., Kellner, U., Jurklies, B., Schuster, A., Zrenner, E., Wissinger, B., *et al.* (2004). Mutation analysis of NR2E3 and NRL genes in Enhanced S Cone Syndrome. *Human mutation* 24, 439.
- Xiao, M., and Hendrickson, A. (2000). Spatial and temporal expression of short, long/medium, or both opsins in human fetal cones. *The Journal of Comparative Neurology* 425, 545-559.
- Xie, B., Charlton-Perkins, M., McDonald, E., Gebelein, B., and Cook, T. (2007). Senseless functions as a molecular switch for color photoreceptor differentiation in *Drosophila*. *Development* 134, 4243-4253.
- Yanagi, Y., Takezawa, S., and Kato, S. (2002). Distinct functions of photoreceptor cell-specific nuclear receptor, thyroid hormone receptor beta2 and CRX in one photoreceptor development. *Investigative ophthalmology & visual science* 43, 3489-3494.
- Yaron, O., Farhy, C., Marquardt, T., Applebury, M., and Ashery-Padan, R. (2006). Notch1 functions to suppress cone-photoreceptor fate specification in the developing mouse retina. *Development* 133, 1367-1378.
- Yassin, S.A., Al-Dawood, A.J., Al-Zamil, W.M., Al-Ghamdi, M.A., and Al-Khudairy, Z.N. (2018). Comparative study of visual dysfunctions in 6-10-year-old very preterm- and full-term-born children. *Int Ophthalmol*.
- Yoshida, S., Mears, A.J., Friedman, J.S., Carter, T., He, S., Oh, E., Jing, Y., Farjo, R., Fleury, G., Barlow, C., *et al.* (2004). Expression profiling of the developing and mature *Nrl*^{-/-} mouse retina: identification of retinal disease candidates and transcriptional regulatory targets of *Nrl*. *Human molecular genetics* 13, 1487-1503.
- Young, R.W. (1985). Cell differentiation in the retina of the mouse. *The Anatomical record* 212, 199-205.

Zhang, B., and Wolynes, P.G. (2014). Stem cell differentiation as a many-body problem. *Proceedings of the National Academy of Sciences of the United States of America* *111*, 10185-10190.

Zhong, X., Gutierrez, C., Xue, T., Hampton, C., Vergara, M.N., Cao, L.H., Peters, A., Park, T.S., Zambidis, E.T., Meyer, J.S., *et al.* (2014). Generation of three-dimensional retinal tissue with functional photoreceptors from human iPSCs. *Nature communications* *5*, 4047.

Zhou, J.X., Aliyu, M.D., Aurell, E., and Huang, S. (2012). Quasi-potential landscape in complex multi-stable systems. *Journal of the Royal Society, Interface / the Royal Society* *9*, 3539-3553.

Zhou, S., Flamier, A., Abdouh, M., Tetreault, N., Barabino, A., Wadhwa, S., and Bernier, G. (2015). Differentiation of human embryonic stem cells into cone photoreceptors through simultaneous inhibition of BMP, TGFbeta and Wnt signaling. *Development* *142*, 3294-3306.

Zuker, C.S., Cowman, A.F., and Rubin, G.M. (1985). Isolation and structure of a rhodopsin gene from *D. melanogaster*. *Cell* *40*, 851-858.

Zuker, C.S., Montell, C., Jones, K., Laverly, T., and Rubin, G.M. (1987). A rhodopsin gene expressed in photoreceptor cell R7 of the *Drosophila* eye: homologies with other signal-transducing molecules. *The Journal of neuroscience : the official journal of the Society for Neuroscience* *7*, 1550-1557.

Curriculum Vitae

Kiara C. Eldred

Department of Biology, Johns Hopkins University
3400 N. Charles St.
Mudd Hall Room 314
Baltimore, MD 21218

Phone (lab): (410) 516-9908
Phone (cell): (206) 947-8755
Email: keldred1@jhu.edu

Education

- 2020 Ph.D., Cell, Molecular, Developmental Biology and Biophysics
 Johns Hopkins University, Baltimore, MD
- 2012 B.S., Biochemistry
 University of Washington, Seattle, WA
- 2012 Minor, Environmental Studies
 University of Washington, Seattle, WA

Honors and Awards

- 2019 Harold M. Weintraub Graduate Student Award
- 2019 Stephen and Carolyn Oppenheimer Graduate Thesis Award
- 2019 Science Outreach Award
- 2017 XSEDE Startup Allocation
- 2015 Johns Hopkins Biology Department Annual Retreat Poster Award
- 2015 National Science Foundation Graduate Research Fellowship
- 2015 Howard Hughes Medical Institute Gilliam Fellow for Advanced Study
- 2013 Owens Scholar Fellowship, Johns Hopkins University
- 2011-2013 Dean's List, University of Washington
- 2008-2012 National Elks Scholarship
- 2008 Regional Elks Scholarship
- 2008 Ballard Rotary Scholarship

Research Experience

- 2013-2020 Doctoral Thesis Research
 Department of Biology, Johns Hopkins University
 Advisors: Dr. Robert J. Johnston and Dr. Samer Hattar
 Mechanisms controlling photoreceptor patterning in the human eye

- 2008-2013 Research Assistant
 Department of Biochemistry
 University of Washington
 Advisor: Dr. Richard Palmiter
Role of NMDA receptors in medium spiny neurons of the striatum in learning
- 2011-2013 Research Assistant/Data Coordinator
 NOAA Northwest Fisheries Science Center
 Advisor: Dr. Stephanie Moore
Factors regulating excystment of Alexandrium in Puget Sound, WA, USA
- 2009 Research Assistant
 Department of Environmental Science
 University of Washington
 Advisor: Dr. Ursula Valdez
Ecological examination of Amazon rainforest
- 2007-2008 Research Assistant
 ZymoGenetics
 Advisor: Dr. Pallavur Sivakumar
Role of VEGF signaling in tumor angiogenesis

Publications

8. **Eldred KC**, Avelis C, Johnston RJ. Jr., Roberts E. (2019)
 Modeling binary and graded cone cell fate patterning in the mouse retina.
 bioRxiv, 650606 (In revision at PLOS Comp. Bio.)
7. **Eldred KC**, Hadyniak SE, Hussey K, Brennerman B, Zhang PW, Chamling X, Sluch V, Welsbie D.S, Hattar S, Taylor J, Wahlin K, Zack D, and Johnston, RJ. Jr. (2018)
 Thyroid hormone signaling specifies cone subtypes in human retinal organoids.
Science, Vol 362, Issue 6411, pg. 200.

Featured in (selected from 140 media outlets from 18 countries):

Articles [TIME](#), [Forbes](#), [Washington Post](#), [Scientific American](#), [Vice](#), [Live Science](#), [Axios](#)

Radio interviews [NPR](#)

Video profile [The Hub JHU](#)

6. Duboué ER, Hong E, **Eldred KC**, and Halpern ME. (2017)
 Left Habenular Activity Attenuates Fear Responses in Larval Zebrafish.
Current Biology, Vol. 27, Issue 14, pg. 2154-2162.e3

5. Viets K*, **Eldred KC***, Johnston RJ. Jr. (2016)
Mechanisms of photoreceptor patterning in vertebrates and invertebrates.
Trends in Genetics, Vol. 32, Issue 10, pg. 638-659
denotes equal contribution 1 authors.
4. Megill A, Tran T, **Eldred KC**, Lee NJ, Wong PC, Hoe HS, Kirkwood A, Lee HK. (2015)
Defective age-dependent metaplasticity in a mouse model of Alzheimer's disease.
J Neuroscience, Vol. 35, Issue 32, pg. 11346-11357
3. Moore SK, Brian BD, Hay LR, Emenegger J, **Eldred KC**, Greengrove CL, Masura JE, Anderson DM. (2015)
Factors regulating excystment of *Alexandrium* in Puget Sound, WA, USA.
Harmful Algae, Vol. 43, pg. 103-110.
2. **Eldred KC**, Palmiter, RD. (2013)
Amphetamine-induced sensitization has little effect on multiple learning paradigms and fails to rescue mice with a striatal learning defect.
PLOS One, Vol. 8, Issue 4, pg. e59964
1. Beutler LR, **Eldred KC**, Quintana A, Keene CD, Rose SE, Postupna N, Montine TJ, Palmiter RD. (2011)
Severely impaired learning and altered neuronal morphology in mice lacking NMDA receptors in medium spiny neurons.
PLoS One, Vol. 6, Issue 11, pg. e28168

Manuscripts in Preparation

2. Hussey* K, **Eldred* KC**, Hadyniak SE, Santiago C, Blackshaw S, Johnston, RJ. Jr.
Temporal action of thyroid hormone and retinoic acid in patterning the human fovea.
Planned submission date: June 2020.
denotes equal contribution 1 authors.
1. Hadyniak SE, **Eldred KC**, Brenerman B, Hussey K, Neitz J, Neitz M, Taylor J, and Johnston, RJ. Jr.
Retinoic acid signaling controls temporal specification of green and red cones in human retinal organoids.
Planned submission date: February 2020.

Presentations

12. Thyroid Hormone action in Retinal Development (2020)
International Thyroid Congress, Xi'an, China.

11. Photoreceptor specification in the human eye (2019)
Onassis Foundation Science Lectures in Biology and Chemistry, Heraklion, Crete
10. Photoreceptor specification in the human eye (2019)
Harold M. Weintraub Graduate Student Award Symposium, Seattle, WA
9. Photoreceptor specification in the human eye (2018)
Johns Hopkins University Annual Biology retreat, Cumberland, MD
8. Photoreceptor specification in the human eye (2018)
SMBE Meeting: Molecular Evolution and the Cell, Park City, UT
7. Photoreceptor specification in the human eye (2018)
Retinal Journal Club, NIH/NIMH, Bethesda, MD
6. Photoreceptor specification in the human eye (2017)
HHMI Gilliam Annual Meeting, Bethesda, MD
5. Analysis of photoreceptor mosaics (2017)
Mid-Atlantic Regional Chromosome Pairing Conference, Baltimore, MD
4. Mechanisms governing stochastic patterning of photoreceptors in the human eye (2016)
Mid-Atlantic Regional Chromosome Pairing Conference, Baltimore, MD
3. Mechanisms governing stochastic patterning of photoreceptors in the human eye (2015)
Northeast Regional Chromosome Pairing Conference, Boston, MA
2. Learning by amphetamine sensitized mice (2012)
University of Washington Undergraduate Research Symposium, Seattle, WA
1. Characterization of mice lacking NMDA Receptors in the Striatum (2011)
University of Washington Undergraduate Research Symposium, Seattle, WA

Posters

11. Eldred KC, Karl Wahlin, Don Zack, Samer Hattar, Robert Johnston. (2018).
Mechanisms Governing Opsin Expression in the Human Eye
Gordon Conference: Visual Systems Development
10. Eldred KC, Karl Wahlin, Don Zack, Samer Hattar, Robert Johnston. (2017).
Photoreceptor Specification in the Human Eye
Johns Hopkins University Annual Biology Department Retreat

9. Eldred KC, Karl Wahlin, Don Zack, Samer Hattar, Robert Johnston. (2016).
Mechanisms Governing Cone Subtype Fate in the Human Eye
Johns Hopkins University Annual Biology Department Retreat
8. Eldred KC, Karl Wahlin, Don Zack, Samer Hattar, Robert Johnston. (2016).
Mechanisms Governing Cone Subtype Fate in the Human Eye
From Stem Cells to Human Development Conference
7. Eldred KC, Karl Wahlin, Don Zack, Samer Hattar, Robert Johnston. (2016).
Mechanisms Governing Opsin Expression in the Human Eye
Gordon Conference: Visual Systems Development
6. Eldred KC, Karl Wahlin, Don Zack, Samer Hattar, Robert Johnston. (2016).
Mechanisms Governing Opsin Expression in the Human Eye
ABRCMS
5. Eldred KC, Karl Wahlin, Don Zack, Samer Hattar, Robert Johnston. (2015).
Mechanisms Governing Opsin Expression in the Human Eye
Johns Hopkins University Annual Biology Department Retreat
Won Best Poster Award
4. Eldred KC, Samer Hattar, Robert Johnston. (2014).
Mechanisms Governing Opsin Expression in the Human Eye
Johns Hopkins University Annual Biology Department Retreat
3. Eldred KC, Duboue E, Halpern M. (2013).
Lesioning of the Fasciculus Retroflexi Prolongs Freezing Post-shock
Johns Hopkins University Annual Biology Department Retreat
2. Eldred KC, Palmiter R. (2009).
Effects of Environmental Enrichment Against Neurodegeneration and Loss of Motor Performance in DIR Cre; NRI lox/lox Mice
University of Washington Undergraduate Research Symposium
1. Eldred KC, Palmiter R., (2010).
Characterization of Mice Lacking NMDA Receptors in the Striatum
University of Washington Undergraduate Research Symposium

Supervisory Experience

2018 – 2020	1 laboratory technician
2015 – 2020	3 undergraduate students (2 received fellowships)
2015 – 2020	6 rotation students (2 joined the lab)

Teaching Experience/Science Outreach

2019	Collaborative Science Art Project at Empty Galleries in Hong Kong Grow and display retinal organoids for the public to observe
2014 – 2019 (SABES)	Mentor for STEM Achievement in Baltimore Elementary Schools After-school STEM learning program for inner-city students
2016-2018	Advisory board for Career Fridays, organized for graduate students Provides diverse career opportunities to PhD candidates
2015	Teaching Assistant for Intro Biology
2014	Teaching Assistant for Genetics
2013 - 2015	BioEYES Volunteer and guest lecturer Provides zebrafish development curriculum and materials to K-12 classes

Environmental Outreach

2017 - 2019	Laboratory Sustainability Founder, Coordinator, and Administrative Liaison Coordinating laboratory recycling in the Department of Biology at Johns Hopkins
-------------	---